# Changes to the NCEP Meso Eta Runs: Extended range, added input, added output, convective changes

*Geoffrey Manikin, *Michael Baldwin, William Collins,
Joseph Gerrity, Dennis Keyser, Ying Lin, Kenneth Mitchell, and Eric Rogers

Mesoscale Modeling Branch and *General Sciences Corporation
Environmental Modeling Center, National Centers for Environmental Prediction

## I. Introduction

A package of changes will be described for the 32-km 45-layer Mesoscale Eta model (also known as the "Early" Eta at 00z and 12z and hereafter referred to as simply the Meso Eta). While it had been running there since November, the Meso Eta was officially implemented on the new NCEP IBM SP supercomputer in January 2000. The model is run 4 times per day at 00Z, 06Z, 12Z, and 18Z with identical resolution. Each run now goes out to 48 hours and each run is initialized from the fully cycled Eta Data Assimilation System (EDAS) of 12 hour duration. AWIPS output for the off-time (06 and 18Z) runs is only available out to 33 and 30 hours, respectively, due to the previous time format of those runs. (The Eta was run at 29 km/45 level resolution at 03Z and 18Z out to 33 and 30 hours, respectively, and those runs were uniquely referred to as the "Meso Eta."). An overview of the Meso Eta can be found here.

## II. Description of and rationale for changes

This implementation will consist of five changes. They are 1) an extension of the 00z and 12z runs of the Meso Eta out to 60 hours and 06z and 18z runs to 48 hours; 2) changes to the model output, featuring more and higher resolution output via the AWIPS SBN, an alternate computation of the sea level pressure, and an improved computation of storm motion; 3) changes to the convective scheme, 4) a return to using the WSR-88D VAD winds with a new quality control code for them and 5) adding the computation of the precise location of each level of radiosonde data taking into account balloon drift.

The basis for each of these changes is the following: 1) Numerous requests for extended Meso Eta guidance to cover the "day 2" period in the on-time runs and a 48-hour update for the off-time runs have been received from the field and NCEP centers. 2) with all 4 daily runs of the Meso Eta uniform in their resolution, it is desirable to unify the guidance provided for AWIPS over the SBN and especially to improve the resolution of that guidance that is available from the 00z and 12z runs (now limited to 80 km grid #211). Also, the Shuell technique for computing sea level pressure has been requested by the field as an alternate option for viewing forecasts of sea level pressure, and SPC has requested switching the storm motion computation to the Bunkers et al (1998) dynamic method to produce superior forecasts of helicity 3) there are two

well-known Meso Eta convective scheme precipitation biases - a high bias along the southeast U.S. coasts of the Gulf of Mexico and Atlantic Ocean and a low bias over elevated terrain of the western U.S. 4) the VAD winds represent a large data set that regrettably had to be turned off in January 1999 due to occasional bad data problems and contamination by migratory birds but can now again be used with the addition of a new quality control program 5) it is desirable to compute the drift of the radiosonde balloon and produce a unique latitude/longitude location for each level of the ascent as opposed to the prior inaccurate treatment of the data as a vertical ascent directly above the radiosonde release location.

## III. Extension of Eta-32 forecast to 60 hours (Rogers)

In June 1998, all operational Eta model runs at NCEP were "unified", i.e. the Eta-29, which was run at 03Z and 15Z out to 33-h, was replaced by an Eta-32 run at 03Z and 18Z out to 33-h and 30-h, respectively. This matched the resolution of the on-time 00z and 12z (so called "early") runs which both run to 48 hours. Each run was initialized using the Eta Data Assimilation System (EDAS) with full cycling of atmospheric and soil variables (Rogers et al., 1998). At that time the 03Z run could not be moved to 06Z as had been intended due to computing constraints at NCEP and its conflict with the MRF. When the EDAS / Eta-32 was converted to run on the NCEP IBM-SP computer in November 1999, the 03Z run was moved to 06Z and the forecast was run to 48-h for all four cycle times (00Z, 06Z, 12Z, 18Z). Each Eta-32 forecast is initialized by a 12-h EDAS run. However, the 06Z and 18Z runs are only processed out to 33-h and 30-h, respectively for distribution via AWIPS SBN, reflecting the forecast lengths of the pre-IBM-SP off-time Eta forecasts. With this implementation, processing of the off-time run out to 48-h will be done and the forecasts will be disseminated to AWIPS via the SBN. Additionally, the on-time Eta runs at 00Z and 12Z will be extended from 48-h to 60-h, and these forecasts will also be disseminated.

## IV. New output (Manikin)

Currently, the off-time Meso Eta output sent to the AWIPS SBN is sent on high- resolution grids 212 (40-km resolution) and 215 (20-km resolution). These output grids will now be made available for the on-time runs as well, but there will be no changes to the on-time availability of lower resolution output. For all Eta output grids, octet 6 of the GRIB Product Generation Section (PDS), the model generating ID number, will be changed from 85 to 84 for the 06Z and 18Z runs and from 89 to 84 for the 00Z and 12Z runs. All grids outputted to the SBN will now contain the sea level pressure computed with the Shuell reduction in addition to the value computed with the Eta Mesinger reduction. Precipitation buckets for the higher resolution grids (212 and 215) at the on-times will now be 3-hourly like those at the off-times. The low resolution grids (211, 104) will continue to contain the current 12-hour buckets (to maintain connectivity to legacy systems and software).

The Bunkers et al. (1998) dynamic method is now used to compute the storm motion vectors. This replaces the Davies and Johns (1993) method for predicting the motion of supercell

thunderstorms which was based on a climatology of central and eastern U.S. supercells. The dynamic method is a more physically-based computation and uses two components to predict storm motion:
1) the influence of the mean wind on initial cell motion and 2) the interactions of the updraft with the sheared environment. The dynamic method tends to perform as well or better than the previous method in "classic" severe weather cases marked by upper right-quadrant hodographs and tends to perform much better than the older method in cases marked by non-classic hodographs such as northwest-flow severe events.

## V. Changes to the Betts-Miller-Janjic convective scheme (Mitchell, Baldwin, Gerrity, Lin, Manikin)

Two well-acknowledged regional precipitation biases have been noted for several years in the Eta model. The model tends to produce too little precipitation over the higher terrain of the western United States (Baldwin and Black, 1996) and too much precipitation over the coastal regions of the Gulf and south Atlantic states (Manikin et al., 1998), and both problems are related to the model's convective parameterization. A complete discussion of the problems and corrections is given below in Section X; a more brief description is given here.

The Eta model uses the Betts-Miller-Janjic convective scheme (Betts and Miller, 1986, Janjic, 1994). Many changes to this scheme designed to correct these two mentioned major biases have been tested over the last several years with varying results; those changes determined to have a positive impact have been adopted into the newest version of the scheme. The changes will impact all grid points, but the impacts will vary by region. Specifically, to attack the low bias in the west:

- the minimum cloud depth required for deep convective processes (which generate precipitation) to occur at a grid point (as opposed to shallow processes which also redistribute heat and moisture but do not generate precipitation) is changed from a fixed value of 290 mb to 200 * (surface pressure / 1000) mb. Over higher terrain, observed precipitating convective clouds often have high bases and therefore fail to meet the scheme's 290 mb depth requirement which is probably best suited for locations at or near sea level.

- at a given grid point the reference humidity profile to which the scheme attempts to adjust the ambient humidity is too moist in the case where the ambient freezing level occurs near the cloud base. If the scheme must adjust the humidity to an unreasonably moist profile in order to generate precipitation, little or no precipitation will be produced at that grid point. Tests have indicated that the base of western U.S. convective clouds is often near the freezing level. The scheme is changed to make the humidity reference profile drier in this scenario.

- the search for the most buoyant layer at a grid point is changed from examining the lowest 130 mb at all point to looking over the lowest 200 * (psfc/1000) mb. This aids convective development in situations of elevated instability.

To address the high bias along the southeast coasts:

- The distinction of drier reference humidity profiles in the convective scheme at land points and more moist profiles at water points is removed, and the choice of profiles is unified to the sea profiles at all points. The discontinuity in profiles along the coast becomes a problem in situations where low-level air parcels with a long trajectory over the water have the opportunity to achieve a state of convective quasi-equilibrium consistent with the more moist sea profiles. Once they reach the land and "sense" the drier profiles, the excess moisture is removed in the form of heavy convective precipitation right on the coast. Not only does this model-generated precipitation often fail to verify, but it also frequently prevents the model from generating sufficient verifying precipitation further inland due to less moisture being available. It should be noted that the original version of the convective scheme used unified profiles; the land-sea difference was introduced several years later in an attempt to generate more convective precipitation over the land. The unification of the profiles does not always entirely eliminate the coastal precipitation but usually at the least significantly reduces the amounts.

This new version of the convective scheme was tested in the summer of 1999 in a real-time parallel version of the model run at 80-km horizontal resolution with a continuously cycled EDAS. This parallel, called the "ETAY" was compared to the same 80-km Eta set-up without the convective changes, called the "ETAV." (These tests were run at a lower resolution due to limited computer resources.) Statistics are examined for the 3 May 1999 to 31 August 1999 time period for all verifying forecast times. The equitable threat and bias scores for the entire U.S. domain are shown in Fig. 1. In general, there is slight improvement in the threat scores and a decrease in the bias, but the greatest reduction in bias (between 0.25" and 0.75" is actually accompanied by an increase in the threat scores). We need, however, to examine the impacts on the regions targeted for improvement. The results for the western U.S. in Fig. 2 shows a modest improvement in the threat scores but a somewhat large positive bias at lower amounts. The forecasting community generally feels that if a modest bias in unavoidable, a positive bias is more desirable than a negative one. The southeast results in Fig. 3 show a slight improvement in the threat scores and a very noticeable improvement in the bias at amounts of one inch or less. It is very difficult to accompany a drastic reduction in bias with a rise in the threat scores; this likely indicates the value of reducing the bogus heavy coastal convection. An example of the reduction in coastal convection is shown in Figs. 4-6. Fig. 4 shows the observed precipitation in the 24 hours ending at12Z 28 June 1999. Fig. 5 shows the control ETAV forecast, and Fig. 6 shows the ETAY forecast with the changes to the convective scheme. The successful reduction in forecast precipitation along the Gulf coast is quite evident. A more complete examination of verification results, including monthly statistics, is given in Section X.

## VI. Quality Control of Vertical Azimuth Display (VAD) winds from the WSR-88D Radars (Collins)

The processing of VAD winds into PREPBUFR format began at NCEP in July, 1995 and began to be assimilated by the operational RUC-2 system in June, 1997. The VAD winds were then assimilated operationally by the Eta's 3-dimension variational assimilation system in July, 1997

and by the Global SSI assimilation system in February, 1998. However, when the many problems with the data became evident, all operational use of the VAD winds ended in January, 1999. As an example, Fig. 7 is a display of the low level VAD winds on the morning of 24 January 2000 and Fig. 8 is a display of the upper level VAD winds. These data were not available to the Eta analysis at the time.

Since being turned off last year, there has been extensive diagnosis at NCEP and elsewhere to determine the source of the problems. As a result of those investigations, a quality control (qc) technique was developed that specifically identifies errors with different characteristics, and marks them for non-use. Following will be a description of the four different error types and a description of the techniques to diagnose the errors.
The first error type is characterized as random, normally distributed errors, with measurable mean and standard deviation. When other sources of error have been eliminated, these are the ones that remain. They have a mean near zero and small standard deviation (about 2.0 ms-1). Engineering estimates of VAD wind error standard deviations, which are included in this first error type, are on the order of 1 ms-1. Any errors of this type are not diagnosed, unless they are large, as they are within acceptable limits.
The second error type is characterized by winds with very small magnitude, and may be located at any altitude. The source of these wind values is unknown, but they are clearly in error, and are all marked as bad. They make up about 8% of all winds.

Third, there are winds that are clearly outliers, both with respect to the first guess wind and to winds at near-by heights and times for the same station. These winds with 'rough' errors may be of almost any magnitude, and are assumed to have a uniform distribution within a given, large, range. The source of error for these winds is unknown. They are dealt with specifically in the quality control procedure. They make up about 7% of all observations.
And fourth, there are winds that are modified by radar signals returned from migrating birds. This problem, as applied to Doppler wind profilers, was recognized by FSL and is accounted for by their quality control for those winds. There is no such quality control presently applied to the VAD winds at the sites where they are generated, and so the method used for the Doppler wind profilers is adapted for use for the VAD winds in the present VAD wind qc program. The problem shows as a southerly wind component that is too strong from the north in the spring and too strong from the south in the fall. There are preferred altitudes and temperatures, as described a little later in this note. In late February, the winds affected by birds are diagnosed to be about 5% of the total winds during bird migration times.

The quality control of VAD winds is performed by a complex quality control (cqc) technique, whereby independent measures of the error are first computed before any error determination is made. In broad outline, the qc is similar to that already used for Doppler wind profilers at NCEP (Collins, 1993, 1994). For VAD cqc, the error measures, called residuals, are: 1) the difference between the measured wind components and the 6-hour forecast wind components at the observation locations, and 2) the difference between the observed wind components and the value at the observation location obtained with optimal interpolation from values at near-by locations in the vertical and in time. The optimal interpolation in the z-t plane uses a generalized

distance and covariance modeling determined from VAD wind data. In addition, the magnitude of the wind itself is used to diagnose errors of small magnitude (< 1 ms-1).
Decisions on data quality are made by the Decision Making Algorithm which makes specific use of the assumptions regarding the various data types as enumerated above. The determination of winds of small magnitude is trivial and they are marked for rejection. The determination of rough errors makes use of the assumption that they are combined with random distribution of small, acceptable, errors. A weight is computed using residuals 1) and 2) from above which, when small enough, indicates the likely presence of a rough error. Bird contamination is looked for only from 15 February to 15 June and 15 August to 15 November. The wind magnitude must not be small, the forecast temperature must be above -3 C, and the southerly wind increment (observation - 6-hour forecast) must be greater the 8 ms-1 for the first time period and less than -8 ms-1 for the second time period for the data to be marked as containing bird contamination. Generally, bird contamination occurs only in limited height bands, sometimes even above 10,000 ft. The geographical and vertical climatology of bird contamination of VAD winds is under investigation for possible future use in better bird contamination discrimination. As a final check, any data with wind component increment magnitudes greater than 12 ms-1 are also marked as bad.

## VII. Radiosonde and PIBAL Balloon Drift: Calculation of Latitude, Longitude, & Time (Keyser)

The balloon drift calculation involves estimating an updated latitude, longitude and observation time on each reported level as the radiosonde or PIBAL balloon ascends through the atmosphere. The horizontal drift is calculated on each valid wind and height level based on the mean wind vector in the layer beneath and the estimated time over which the balloon traversed this layer. The bottom level of this layer is the previous valid wind and height level in the profile. The drift time is calculated from the layer thickness and an assumed constant balloon ascent rate of 5 meters per second.

The horizontal drift calculation is performed on all levels with valid wind and height, where both have passed all quality control checks to this point. In order to generate a smooth profile of drift latitude/longitude, radiosonde heights are integrated from reported height and temperature levels to levels where no height information was reported (e.g., significant temperature and winds-by-pressure levels) and likewise radiosonde and PIBAL winds are interpolated to levels where no wind data were reported (e.g., significant temperature levels). For PIBAL reports, the U.S. Standard Atmosphere height is used on missing height levels. If any of the reported data used in either the height integration or the wind interpolation have failed quality control checks, then the generated data are also considered to be of bad quality and the generated data levels will not be used in the horizontal drift calculation. In addition, if the pressure difference between bracketing wind levels exceeds 150 mb, then no wind interpolation is done onto levels in between and these levels not be used in the horizontal drift calculation.

Several checks are applied to the horizontal drift calculation on each level. If any check fails, no

calculation is done and the drift latitude/longitude from the level beneath is transferred to the current level. These checks include: a valid height and wind, a positive calculated drift time interval in the layer below, a calculated drift time interval of less than one-hour in the layer below, and a calculated latitude and longitude change both less than one degree from the level beneath. In addition, if, on any level, the pressure difference in the layer below is greater than 150 mb, then the drift latitude/longitude from the level beneath is transferred to all levels above. Finally, the horizontal balloon drift cannot be calculated at the South Pole station, 89009. Here, the station's latitude and longitude are transferred to all levels. Fig. 9 shows an example of the tracks of rawinsondes with the underlying grid points being those of grid #212 the 40 km AWIPS display grid used for Meso Eta output.

## VIII. Results from 32-km parallel test

A parallel test of the full package of changes to the Eta-32 system (designated ETAX) was started at 00Z 2/12/2000. Charts with quantitative verification statistics for this test can be found at http://sgi62.wwb.noaa.gov:8080/ETA32PARA/ . One caveat: given the small sample size, the results may be regime-dependent and therefore not representative of performance over an entire cool season. Highlights from this page are described below.

**a) Fit to rawinsonde data**

Root-mean-square (RMS) errors of 12-h and 36-h operational Eta-32 and ETAX forecasts versus rawinsondes over the CONUS at mandatory pressure levels have been computed for heights (Fig 10), temperature (Fig 11), vector wind (Fig 12) and relative humidity (Fig 13) for the period 12Z 2/13/2000 - 12Z 2/23/2000. Overall, there are generally small differences between in the RMS errors of the operational Eta-32 and the ETAX forecasts. Temperature RMS errors are slightly lower below 500 mb and slightly higher above 500 mb in the ETAX forecasts. The RMS vector wind errors of the ETAX forecasts are slightly higher (< 1 ms-1). This may be due to 1) small sample size; 2) assimilation of VAD winds which may lead to a slightly worse fit to other wind observations, and 3) although the drift of the rawinsonde balloon is accounted for in the 3DVAR analysis, it is not accounted for in the verification software.

Also included in these figures are the RMS errors of the 60-h forecasts from the ETAX system and the Aviation (AVN) run of the NCEP Global Spectral Model. For all four variables the ETAX tends to have lower RMS errors then the AVN, with the biggest difference seen in upper tropospheric heights, mid-tropospheric winds, and relative humidity.

**b. 24-h accumulated precipitation skill scores**

Fig. 14 shows the 24-h accumulated precipitation bias and equitable threat score (ETS) for all Eta-32 and ETAX forecasts over the CONUS from 12Z 2/13/2000 - 12Z 2/23/2000. There is an increase in ETS in the ETAX forecasts for all thresholds below 2 inches, up to 20% higher at the 0.75" and 1.00" thresholds, without the notable increase in negative bias which was seen at the highest thresholds in the warm season 80 km tests. The eastern (Fig 15) and western (Fig 16) U.S. scores show a similar signal to the overall CONUS scores. Evidence from examination of

selected cases shows the new convective scheme in the ETAX forecast is decreasing convective precipitation in frontal rainbands. However, there is a corresponding increase in grid-scale precipitation which compensates for the drop in convective precipitation. An example of this is seen in Fig 17, which shows the 36-h Eta-32 and ETAX 24-h accumulated precipitation forecasts valid at 12Z 2/26/2000. Although there is little difference in total precipitation along the north-south frontal band extending from Arkansas to Wisconsin, there is less convective precipitation in the ETAX in Missouri and Arkansas. The verification (Fig 18) will be added when it is available.

Fig 19 shows the 24-h accumulated precipitation bias score and ETS for 60-h ETAX and AVN forecasts for 12Z 2/13/2000 - 12Z 2/23/2000. The ETAX ETS scores are higher than those from the AVN at all thresholds above 0.1" and at 3.00". The ETAX bias score is lower at all thresholds below 2.00", staying close to 1.0 between the 0.1" and 1.00" thresholds. The scores for the 24, 36, and 48-h Eta-32, ETAX and AVN forecasts for the same period (Fig 20) show that the Eta-32 had higher ETS then the AVN at all thresholds except 1.00", while the ETAX had higher ETS than both the Eta-32 and AVN at all thresholds but 0.01" It appears that the new convective scheme in the ETAX led to the enhanced the modest improvement in ETS seen in the operational Eta-32 over the AVN, and that this enhancement was carried over into the 60-h forecasts.

## IX. Conclusion

A package of changes to the 32-km 45-layer Meso Eta model has been described. The model is run 4 times per day (at 00Z, 06Z. 12Z, and 18Z) out to 48 hours. The 00Z and 12Z runs will be extended to 60 hours in response to a numerous requests for extended "day 2" guidance. In addition, the output available for AWIPS over the SBN is unified so that the 40-km grid #212 and 20-km grid #215 output is available for all 4 forecast cycles and is available for the full length of each run. The Shuell method of computing sea level pressure is added to the AWIPS output for the SBN, and the model computation of storm motion is changed from a method based on climatology to one more physically-based.

The data assimilation for the model is improved in two ways. First, the quality control program is updated to include a check for migratory birds in the processing of Vertical Azimuth Display (VAD) winds. This permits the inclusion of this data set, which had been turned off in January 1999, into the assimilation. Second, the drift of radiosondes is now accounted for in the processing of that data. A updated latitude, longitude, and time are computed for each reported level of data.

Finally, the convective scheme is modified to reduce two well-known precipitation biases in the Eta model: a dry bias over the higher terrain of the west and a moist bias in the southeast, especially along the Gulf and Atlantic coastal areas. The required depth for a deep (precipitating) convective cloud is changed from a fixed value to one scaled by a factor based on surface pressure to account for the higher- based convective clouds in the west. Also, the situation where the cloud base is located near the freezing level constructs a humidity reference profile that

makes deep convection too difficult; the profile in that situation is now constructed to render precipitating convection more likely. Lastly, the distinction between reference profiles at land and sea points is removed to eliminate the discontinuity in profiles at the coast that causes incorrect forecasts of heavy convective precipitation there. The profiles are changed to the sea version at all grid points. Verification of the new scheme shows a slight improvement to the threat scores with a decrease in bias when the entire domain is considered. Inspection of individual regions, however, shows that the changes are having significant positive effects in the southeast and west.

The date of the operational implementation of the 60 hour range extension and addition of higher resolution gridded output 212 & 215 to AWIPS SBN has been advertised for 21 March 2000 through the DRG. If CAFTI approves, that date would be our target date for implementation of the package.

Special thanks go to Ying Lin and Perry Shafran for their efforts in producing the figures, graphics and webpages and Geoff DiMego for his editing and linking skills all of which greatly enhanced this presentation.

## X. Context, Content and Detailed Impacts of Changes to the Eta Convective Parameterization Scheme (Mitchell, Baldwin, Gerrity, Lin, Manikin)

Since around the mid 1990's, there have been two pronounced, generally acknowledged regional biases in Eta model convective precipitation amounts; namely 1) a low bias over the high mountains of the western U.S. and 2) a high bias in coastal regions of Gulf and southern Atlantic states (Baldwin and Black, 1996; Gartner et al., 1996; Staudenmaier, 1996; Manikin et al., 1998). These convective biases are most pronounced during the warm season as expected (although the southern coastal bias is evident to some extent throughout the year). These systematic warm season Eta biases are cited periodically in daily QPF discussions issued by NCEP/HPC and have been highlighted in COMET Eta model training materials in recent years (1998-1999), such as those available online here1.

Extensive sensitivity tests were undertaken by NCEP/EMC to pinpoint the primary causes of these regional biases. For example, some of the earliest tests by Baldwin and Black (1996) demonstrated that the low convective precipitation bias in the West was not eliminated merely by a marked increase in model resolution, which in turn improved the definition of orography. Further testing focusing on these regional biases (e.g. Manikin et al., 1998, for the coastal bias) identified the primary causes to be several specific aspects of the Eta convective parameterization scheme.

We first describe the changes to the Eta convective parameterization scheme that were identified as substantially reducing the cited regional biases and ultimately chosen for operational implementation. Then we present forecast fields and verification scores from an extensive realtime parallel test over the period May-September 1999 to demonstrate both the original bias

problems and the substantial positive impact of the convection scheme changes.

Before proceeding, it must be emphasized that the aforementioned regional convection biases, which are of opposite sign, are in addition to the broader, more generic Eta model bias of underforecasting very heavy convective precipitation events exceeding say 1.5 inch per day, such as those associated with long-lived mesoscale convective complexes (MCCs). This latter bias is a more difficult generic problem shared by the vast majority of operational NWP models. The convection scheme changes presented and implemented here do not solve this broader problem. NCEP/EMC and collaborators continue to explore this problem by testing more extensive changes, including a) additional changes to the existing convection scheme, b) alternative convection schemes (Manikin et al, 1996, Kain et al, 1998), and c) improved initialization techniques (Lin et al, 1998; Stensrud et al, 1999).

### X.1Description of changes to the convection scheme

#### X.1.aSummary of scheme before the changes

There are over a dozen well-known convective parameterization schemes. An excellent overview of convective parameterization schemes, including the Eta model convective scheme, is provided online by the COMET NWP lesson available here2. Virtually all convection schemes can be classified as one of two broad types: a) adjustment schemes and b) mass flux schemes. The present Eta model convection parameterization scheme is generally referred to as the Betts-Miller-Janjic scheme (hereafter BMJ scheme). This scheme, which is an adjustment scheme, originated with the work of Betts (1986) and Betts and Miller (1986), and was further modified for use in the NCEP Eta model by Janjic (1990,) and more extensively by Janjic (1994). Readers may augment these detailed BMJ references with the summaries provided online by Black (1999, COMET COMAP Symposium, here3) and Staudenmaier (1996, WR-TA-96-23, here4). We will not present a complete description of the BMJ scheme here, but will emphasize mostly those aspects affected by the changes tested here, as described in Sections X.1.b and X.1.c.

Adjustment schemes simulate the effects of convection at a given model grid point by nudging the vertical profiles of temperature and moisture at that grid point toward specified reference profiles. A central characteristic of the BMJ scheme is its separate deep convection and shallow convection components. At a given grid point at a given time step, if the BMJ scheme is invoked in response to convective instability criteria, the BMJ scheme invokes either the deep convection component or the shallow convection component, but not both. The model first checks for deep convection and then shallow convection. Only the deep convection component will produce precipitation. The two components differently compute the a) reference profiles for temperature and moisture and b) the rates at which the model profiles are adjusted to the reference profiles.

To determine if either component is invoked at all, the model first determines if a convective cloud can form (i.e. will a lifted parcel result in buoyancy) and if so, what is the base and depth of that cloud, as follows. The scheme identifies the most unstable model level (largest saturated

equivalent potential temperature) within 130 mb of the model surface, and the LCL of a parcel lifted from that level. Cloud base is set as the model level just below this LCL. The temperature profile (Tmad) of the moist adiabat above this cloud base is computed and cloud top is set as the highest model level where Tmad is first colder than the existing (ambient) temperature. If this convective cloud depth is greater than 10 mb and at least two model layers deep, then the scheme proceeds, otherwise no deep or shallow convection is invoked.

If the cloud depth is greater than a deep convection threshold of 290 mb, the scheme proceeds to the deep convection branch. Here the deep convection scheme computes Tref, the temperature reference profile (defined from cloud base to cloud top), to be 90 percent of the slope of the moist adiabat between cloud base and the ambient freezing level and linear between the temperature this yields at the freezing level and the temperature at cloud top. This reference profile is generally cooler (warmer) then the ambient temperature in the lower (upper) cloud column, hence the deep convection adjustment cools near cloud bottom and warms near cloud top (stabilizes).

The humidity reference profile is specified in terms of a humidity variable known as "saturation pressure deficit" and denoted as "DSP". (DSP is defined as the upward vertical displacement in pressure units-- zero or negative by definition -- that a given parcel of pressure P and temperature T would have to be lifted to reach saturation.) From a parcel's given P, T, and DSP, any of the other familiar humidity variables such as specific humidity or dew point can be uniquely derived. The humidity reference profile of DSP is prescribed by giving DSP values at cloud base (DSPB), freezing level (DSP0), and cloud top (DSPT), and applying linear variation in between. Typical values of these DSPs are of order -40 mb at cloud base, -60 mb at freezing level, and -20 mb at cloud top. From the profiles of Tref and DSP, the reference profile of specific humidity is derived. These temperature and moisture profiles are then modified to ensure that the enthalpy in the cloud column is conserved during the adjustment. This enthalpy check enforces a balance between the net latent heat release and the net moisture change due to condensation. Between cloud base and cloud top, the deep convection scheme then nudges the ambient temperature and humidity profiles to these reference profiles using a specified relaxation time-constant (of order 40 minutes). The vertical integral of the difference between the adjusted and original moisture profiles of specific humidity yields the precipitation amount. Also, a net change in entropy is calculated from the change in the temperature profile. If either the entropy change is negative (implying an undesired net cooling) or the calculated precipitation is negative (implying an undesired net moistening) at a given grid point at a given time step, then the deep convection adjustment is aborted and the scheme logic "swaps" instead to the shallow convection branch. We do not discuss the shallow convection scheme further here, as no changes to the shallow convection scheme physics were included in the tests.

The original forms of the temperature and humidity reference profiles described above were determined empirically by Betts (1986) from observed thermodynamic profiles in many post-convective environments. The precipitation amounts and rates turn out to be very sensitive to the specified DSP profiles. Therefore, NCEP introduced two additional degrees of freedom for the DSP profiles in the deep convection branch.

First, Janjic (1994) introduced a temporally varying cloud efficiency factor E, computed dynamically as a ratio of the net water vapor change in the cloud column arising from a) the entropy change versus that arising from b) the precipitation. During a deep convection episode in this revised scheme, E varies from a high efficiency value of 1.0 (a faster, less mature convective system that is predominantly in the stage of mixing heat and moisture upward, while producing only modest rainfall) to a low efficiency value of 0.20 (a slower, more mature convective system that is in a predominantly rain producing stage). The efficiency factor E is used to a) increase the nudging relaxation time, thereby slowing the convective adjustment, for decreasing efficiency (about a 40 percent increase at lowest efficiency) and b) impose smaller (more moist) DSP magnitudes for low efficiency. Hence, so-called "DRY" baseline values of DSPB, DSP0, and DSPT are specified for E=1.0. The actual DSPs applied at any given time vary between these values for E=1.0 and a factor FS=.85 times these values for E=0.20. The factor FS is a tuneable parameter, as are the values of DSPB, DSP0, and DSPT. In the special case of cloud base being close to the freezing level (namely, higher than 150 mb below the freezing level) the scheme imposes DSPB=DSP0=DSPT = -30 mb.

Secondly, Mesinger (1991, personal communication) adopted different "land" and "sea" values for the DRY baseline values of DSPB, DSP0, and DSPT. He chose drier values of these baseline values over land than over sea. Other conditions being the same, the BMJ deep convection scheme will initiate convective precipitation sooner if the DSP magnitudes are larger (drier). The original rationale for drier DSPs over land was to emulate the perception that a greater variety and frequency of deep convection trigger mechanisms occur over the land mass, owing to the greater surface heterogeneity present from gradients in orography, soil moisture, vegetation, albedo, surface roughness, etc. Thus, the Eta model has been executing operationally with the following different land and sea values for the "DRY" DSPs (in mb units):

| Dry Limits (mb) | Land Limits | Sea Limits |
|---|---|---|
| DSPB | -22.50 | -18.75 |
| DSP0 | -70.50 | -58.75 |
| DSPT | -48.44 | -38.75 |

In conclusion, both lower values of the efficiency parameter E and the "sea-mode" choice of the DRY DSP reference values will result in more moist humidity reference profiles in the BMJ scheme, thereby reducing deep convection precipitation amounts.

**X.1.bPreface to BMJ changes**

Convective parameterization schemes in general are well known to be replete with parameters and decision thresholds that can be optimized or tuned in a specific model. The BMJ scheme is no exception. Such optimization is periodically called for as the parent model undergoes changes to its resolution, explicit grid-scale microphysics, PBL parameterization, land-surface parameterization, or initialization, analysis, and data assimilation methods.

Over the last several years, EMC has tested many modest BMJ scheme changes (some individually, some in combination) in a large set of Eta model case study runs. Some results were mostly positive, some mixed, and some clearly negative. From this large set of candidate changes, we ultimately chose the ones described below to execute in combination in the long term parallel testing presented in Sec. X.2, the results of which convinced us to recommend implementation. These changes are described with respect to the "control" BMJ scheme summarized above in Section X.1.a.

The adopted changes are grouped and discussed below as those targeted to improve a) the high precipitation bias over the southeast and b) the low precipitation bias over the high terrain of the west. In practice, however, given the ultra sensitivity of convection schemes of all kinds to even tiny changes in decision thresholds and other parameters, each of the changes described below can have some impact anywhere throughout the model domain.

**X.1.cChanges aimed at coastal precipitation high bias**

In warm season months, as the Bermuda high amplifies and migrates northward, persistent prevailing southerly and southeasterly flow (originating from the warm ocean waters of the Gulf, Caribbean, and tropical Atlantic) sets up in lower troposphere over the Gulf and south Atlantic states. Trajectories of low-level air parcels reaching these coastal regions from off-shore have typically experienced a longstanding upstream fetch over warm seas for 2 days or more and have typically achieved a quasi-equilibrium convective stability state consistent with the more moist "sea" values of the BMJ humidity reference profiles. As these trajectories first reach the land mass, in the Eta model physics they suddenly sense the drier BMJ reference profiles over land.

This discontinuity in sea versus land humidity reference profiles, we now realize, gives rise to a) much too frequent initiation of a deep convection response along the immediate coastline and b) a somewhat time lagged over response of deep convection further inland in southeast states. In the modified package, we drop use of separate land and sea humidity reference profiles in favor of using sea reference profiles universally over the entire model domain. More specifically, we use only the "sea" limits of the DSP parameters given at end of Section X.1.b.

**X.1.dChanges aimed at high terrain low bias**

As shown above, the control BMJ scheme uses a universal deep convective cloud threshold of 290 mb, wherein cloud base is the LCL of the most unstable layer in the lowest 130 mb above the model surface. Two factors in the western U.S. substantially reduce the chance that this deep cloud threshold will be satisfied; namely the high terrain (i.e. much lower surface pressure) and the generally dry low-level environment (high LCL values). Consequently, in the tests below, we replace the fixed deep cloud threshold depth of 290 mb with the following:

deep cloud threshold (mb) = 200 * (Psfc/1000)

where Psfc is the surface presssure (in mb) of the model surface. Hence the threshold is scaled by

surface pressure and decreases over higher terrain (lower surface pressure). Furthermore, the baseline value of 200 mb at Psfc=1000 mb is smaller than the universal value of 290 mb in the control scheme. The new threshold increases the frequency of the BMJ deep convection branch being invoked everywhere, but especially over high terrain areas.

We next recall that in the case of cloud base being near the freezing level (within 150 mb), the control scheme imposes a special case of DSPB=DSP0=DSPT= -30mb in the deep convection branch. This DSP magnitude is relatively small and implies a rather moist BMJ humidity reference profile, which greatly decreases the magnitude of the precipitation that the deep convection scheme will produce. Once again, both the high terrain (low surface pressure) and generally dry low levels (high LCL) characteristic of the western U.S. contribute to a higher likelihood that the cloud base will be close to the freezing level.

In the new approach tested below, the "cloud base near freezing level" case is invoked if the cloud base is higher than 150 * (Psfc/1000) mb. Hence, the cloud base threshold is now scaled by surface pressure and over higher terrain (lower surface pressure), the threshold is smaller and therefore not as easily satisfied. Furthermore, when the new threshold is satisfied, the imposed value of the DSPs is less severe, being given not by a fixed constant of -30 mb but rather DSP=DSP0 below the freezing level (typically between the -50 and -58 mb range) and DSP above the freezing level given as in all other deep convective clouds (i.e. linear interpolation between DSP0 and DSPT).

In the final change, the search for the most bouyant layer above the model surface was changed from looking over the lowest 130 mb to looking over the lowest 200 * (Psfc/1000) mb. This change is not so much targeted to help over high terrain, but rather is viewed as beneficial everywhere to enhance finding elevated instability.

**X.2Impact of convection scheme changes on Eta precipitation forecasts**

To extensively test the combined BMJ scheme changes described above, EMC conducted nearly five months of warm season, continuous, realtime, parallel tests of 0-48 hour Eta forecasts (twice daily from 00 UTC and 12 UTC) covering the period 03 May to 27 September 1999. Owing to the limited spare capacity of computer resources for realtime parallel tests, these tests were conducted at 80-km resolution. One parallel suite, hereafter designated as "ETAV" or "V", mimicked the operational Eta analysis/assimilation/forecast suite (designated "OPNL") in every way except the Eta forecast and analysis resolution was 80-km versus the operational 32-km. This ETAV operational clone included the same input observations, 3-D variational analysis scheme, model domain size, and *continuously cycled* Eta Data Assimilation System (EDAS), as the 32-km operational Eta suite, which was mostly recently described in TBP-447 by Rogers et al. (1998), available online here5. The second parallel suite, hereafter designated "ETAY" or "Y", mirrored ETAV, except for the inclusion of the BMJ scheme changes given in Sec. X.1. On 03 May 1999, the ETAV and ETAY initial conditions for all state variables (atmosphere and land) were derived in an identical manner (spatial interpolation) from the operational Eta/EDAS states.

Below, we present three types of results:
a) U.S. maps of total monthly observed and forecast precipitation (OBS, OPNL, ETAV, ETAY)
b) case study maps of 24-h observed and forecast precipitation (OBS, OPNL, ETAV, ETAY)
c) regional precipitation verification scores over the period 03 May - 31 Aug (ETAV, ETAY)
The precipitation maps of a) and b) will show that ETAV reproduces well (albeit somewhat smoother) the patterns, essential features, and systematic biases of the OPNL precipitation. This demonstrates that ETAV provides a viable reference as an "operational" surrogate, despite its lower resolution. Executing two 80-km parallel suites requires roughly 1/8 the computer time of executing one parallel suite at the 32-km resolution of current operations.

**X.2.aImpact on monthly patterns of precipitation forecast bias over CONUS**

To begin, we first broadly illustrate the systematic regional biases summarized earlier. We present in Fig. 21a (OPNL), 21b (ETAV), 21c (ETAY), and 21d (OBS) the U.S. maps of monthly summations of daily forecast and observed 24-h precipitation for July 1999. As companions, Figs. 22a (OPNL-OBS), 22b (ETAV-OBS), and 22c (ETAY-OBS) provide the corresponding monthly summations of daily "forecast-minus-observed" 24-h precipitation. The September 1999 counterparts to Figs. 1-2 are given in Figs. 23a, 23b, 23c, 23d and 24a, 24b, 24c. The forecast results in Figs. 1-4 represent the sum of all 0-24h Eta forecasts valid at 12 UTC in the given month. The analysis totals (OBS) are monthly summations of CPC's, 0.25-degree, gage-only, objective analysis of daily total precipitation over the interval 12 UTC to 12 UTC. Given this analysis interval, only 24-h forecast intervals ending at 12 UTC can be summed for comparison. (The CPC analysis is described more in the Note at the end of this section, or at the end of the online site here6.)

For those occasional days when the realtime ETAV and/or ETAY forecast runs were dropped, owing to operational production demands, those same days of precipitation were excluded from all forecast and observed accumulations, in order to maintain strict sampling consistency, and exclusion dates are listed at top of each monthly map.

While our discussion here will highlight the July and September results in Figs. 1-4, readers are urged to examine online, at the site designated here as MONTHLY, the full set of monthly maps for four months (Jun, Jul, Aug, Sep) and four Eta forecast periods (0-24h from 12 UTC, 12-36h from 00 UTC, 24-48h from 12 UTC, and sum of eight 3-h EDAS analysis/guess cycles). It is enlightening to examine more than one month, as the southeast U.S. positive bias patterns shift somewhat from month to month in response to a) changes in the prevailing Bermuda High circulation and b) the warm-up of ocean SSTs.

Fig. 21d (OBS) and Fig. 23d (OBS) show the total observed precipitation for July and September respectively. The CPC map of Jul 99 (Sep 99) anomalies from climatology is given in Fig. 25 (Fig. 26). We note that a) the below normal eastern seaboard of July becomes above normal in September owing to tropical storms Dennis and Floyd, b) the southwest U.S. monsoon in the Arizona/New Mexico region emerges in July stronger than normal and but wanes as usual in September, c) the wet anomaly of the upper Midwest in July becomes a dry anomaly in

September, and d) the northwest and south central U.S. are both below normal in both months.

We first consider the July forecast biases. Fig. 21a (OPNL) and Fig. 22a (OPNL-OBS), as well as Fig. 21b (ETAV) and Fig. 22b (ETAV-OBS) illustrate that the operational Eta and the 80-km operational surrogate both strikingly similar biases. Hence the ETAV parallel "control" suite faithfully reproduces the bias patterns of the operational suite. Most notably, both suites show a high precipitation bias throughout the southeast quadrant of the CONUS, with very large positive biases concentrated around the south Texas coast, south Carolina coast, and inland in the Gulf states of Mississippi and Alabama. Turning to the high terrain western states, north of the monsoon region we note a clear pattern of low bias in the Rocky Mountain regions of central Colorado, northern Utah, western Wyoming, and western Montana. Finally in the monsoon region, we see a positive monsoon bias, in both the larger spatial extent and amplitude of the monsoon rains.

The July impacts of the modified convection scheme are depicted in Fig. 21c (ETAY) and Fig. 22c (ETAY-OBS). Compared to the control-case bias in Fig. 22b, the modified convection case in Fig. 22c shows a striking and substantial reduction in the positive bias throughout the southeast. The large amplitude and widespread positive bias in the states of Mississippi, Alabama, Tennessee, and Kentucky are markedly reduced. Additionally, the area and amplitude of the very high positive bias centers in south Texas and S. Carolina have been substantially reduced, though not eliminated. Even the positive bias in the Northeast has improved, replaced with a mix of small bias of either sign.

Over the mountainous region of western Colorado, northern Utah, western Wyoming, and western Montana, the low bias has been vastly reduced with western Colorado actually becoming a modest high bias. The southwest monsoon region is a mixed bias impact, but we contend a better sense of this region is garnered from the full fields of Fig. 21b, 21c, and 21d, which show that the modified convection package yields a better spatial extent and shape to the monsoon rainfall pattern.

Finally we point out that in the upper Midwest, where the highest observed rainfall totals occurred, the negative bias in the modified convection case is somewhat worse, notably in the area of the absolute maximum of observed rainfall in west central Wisconsin (around 8-10 inches observed). An acknowledged negative feature of the modified convection scheme is a somewhat reduced ability to produce convective precipitation amounts for categories exceeding 1.5 inches per day, but the verification skill (threat score) of either version of the convection scheme for these heavy amounts is so low as to make the tiny loss of skill immaterial. Section X.2.c provides more on this issue.

The broad trends highlighted above for July (mountainous west, southeast) are also present in the other warm season months, illustrated next via the September results. Fig. 23a (OPNL) and Fig. 24a (OPNL-OBS), as well as Fig. 23b (ETAV) and Fig. 24b (ETAV-OBS) show again that the 80-km ETAV parallel control faithfully reproduces the monthly bias patterns of the 32-km OPNL. Both suites again reveal a widespread substantial positive bias throughout the southeast

region, still most notable along extensive coastal areas, but with some shift in the centers of most dramatic positive bias, wherein the S. Carolina and south Texas centers are now joined by southeastern Georgia and especially Florida (rather than say Alabama as in July). The positive coastal bias now includes several mid-Atlantic and southern New England states. Negative bias again prevails over the mountainous western states. Finally, a negative bias is again apparent in the areas of heaviest observed rainfall (eastern portions of Oklahoma and Kansas and eastern portion of N. Carolina where the tropical storm accumulations were the largest).

The September impacts of the modified convection scheme are depicted in Fig. 23c (ETAY) and Fig. 24c (ETAY-OBS). Compared to the control case in Fig. 23b (ETAV) and Fig. 24b (ETAV-OBS), the modified package still produces a vivid reduction of the positive bias across the southeast, and a dramatic reduction in very large positive biases across Florida, Georgia, S. Carolina, and south Texas. Additionally, the modified package reduces the coastal bias in the mid-Atlantic and southern New England states. In the western states, the impact is also positive with a reduction in the spatial extent of the negative bias. Given that the western state precipitation amounts are small in both forecast and observed (and hence the difference field amounts are small), the favorable western-state impact of the modifications is substantially more apparent by comparing the full fields of Fig. 23b (ETAV), Fig. 23c (ETAY), and Fig. 23d (OBS) wherein the ETAY case has clearly more precipitation across the broad four-corners region, northern Nevada, northeastern California, and northwest Washington.

Finally, over those centers of maximum observed heavy rainfall (eastern Oklahoma and Kansas, and eastern N. Carolina, the modified package again increases the negative monthly bias in these very heavy rain areas, but the synoptic event-by-event predictive skill of both convective packages is low for the these very heavy rain events.

**X.2.bImpact on specific forecast cases**

In this section we briefly examine 3 specific synoptic 36-h Eta forecast cases: 1) a Texas Gulf coast case on 28 Jun 99, b) a Carolinas coastal case of 14 Jul 99, and c) an inter-mountain western U.S. case of 08 Jul 99. Readers are encouraged to examine online a host of other daily precipitation forecast cases during the period May-Sep 99 at the site designated here as CASES. (wherein the link to a given day opens a left-hand column of various forecasts from different models such as AVN, NGM, 32-km Eta OPNL or "Early Eta", and 80-km ETAV and ETAY, accompanied by a right-hand column repeating the verifying gage-only precipitation analysis).

The 28 Jun case is presented in Fig. 27a (OPNL), Fig. 27b (ETAV), Fig. 27c (ETAY), and Fig. 27d (OBS). (In these case studies, with one exception noted later, the "OBS" analysis is a 14-km EMC objective analysis of the 24-h precipitation, again using the RFC gage observations.) The feature of interest is the long narrow coastal band of heavy forecast precipitation stretching across the entire 5-state northern boundary of the Gulf of Mexico in OPNL and ETAV (control). In contrast, the observed precipitation pattern (confirmed by radar, not shown) shows zero precipitation along this coastline, except in the Florida panhandle wherein amounts are still very light in the western panhandle. Rather, the observations show the locus of heavy precipitation is

interior Alabama, especially southern Alabama north of the Florida panhandle. The modified scheme in Fig. 27c (ETAY) yields a vastly improved pattern in this region, with negligible rainfall west of the Florida panhandle, and a shift of the heaviest rainfall in the panhandle region northward to southern Alabama, clearly in better agreement with observations. (Both schemes miss the heavy rainfall in northern Alabama.) This case is a classic example of where the operational Eta yields such an extensively long, multi-state, narrow band of heavy rainfall along the immediate coast as to render it impossible for the forecaster to surmise likely local centers of action from the model's QPF guidance.

A similar and dramatic case, from 27 Oct 97, involving the entire Texas coastline is presented in the Eta model sensitivity study of Manikin et al. (1998). This case study shows another example of 1) spurious Eta model heavy coastal convection suppressing convection from developing further inland where it is observed and 2) an Eta model rerun for this case wherein the universal application throughout the model domain of "sea-mode" moisture reference profiles in the BMJ scheme eliminates the coastal convection and yields heavy inland convective rainfall as observed.

The 14 Jul case of a coastal bias in the Carolinas is presented in Fig. 28a (OPNL), Fig. 28b (ETAV), Fig. 28c (ETAY), and Fig. 28d (OBS). Here for the "OBS" analysis we use EMC's multi-sensor, radar-dominated precipitation analysis (a national mosaic of radar umbrella "Stage II" analyses -- see Baldwin and Mitchell, 1997) in order to depict observed rainfall somewhat offshore. Along both Carolina coastlines, the OPNL and ETAV forecasts show a narrow band of heaviest precipitation just inland, whereas both OBS and the ETAY modified scheme show the narrow band of heaviest precipitation primarily just offshore.

In summary, the 28 Jun and 14 Jul cases indicate that the Eta model penchant for generating convective rainfall along the immediate inland coastal zone degrades the model's ability to distinguish coastal events that will be either somewhat off-shore or substantially further inland.

We complete our case studies with an 08 Jul case of widespread precipitation (albeit generally light to moderate), in the inter-mountain western states. This case is depicted in Fig. 29a (OPNL), Fig. 29b (ETAV), Fig. 29c (ETAY), and Fig. 29d (OBS). Compared to OBS, the OPNL and ETAV significantly under forecast the extensive spatial extent of rainfall in the four-corners region, Utah, western Colorado, and western Wyoming. The modified scheme in ETAY is clearly superior in this region, showing both greater spatial coverage and more grid points exceeding the smallest nonzero category (such were virtually non-existent in OPNL and ETAV in the west).

**X.2.cImpact on regional precipitation verification scores**

We refer the reader to ETScore for a description of the methods used for verifying 24 hour precipitation amounts and definitions of NCEP's preferred QPF skill scores of the Equitable Threat Score (ETS) and Bias. All scores in this section were from runs (ETAV and ETAY) and verification grids with 80 km resolution.

In this section we assess the impact of the modified convection scheme using objective verification scores. From the monthly forecast bias maps of Sec. X.2.a, we saw vividly that the bias characteristics of QPF vary substantially in magnitude from region to region across the CONUS. Thus it is imperative that we compute and evaluate regional verification scores. Fig. 30 shows a map of 13 CONUS sub-regions (3-letter labels) now routinely employed by EMC in model verifications. For the present verification, we merged these 13 sub-regions into six "super" regions, denoted in Fig. 30 as Southeast (SMW+SEC), Southern Plains (SPL), Northeast (NEC+APL), Northern Midwest (NPL+NMW), East (the former four combined), and West (non-East). For these six regions, respectively, Figs. 31, 32, 33, 34, 35,and 36 show the equitable threat score (top) and bias score (bottom), combined for all three Eta 24-h forecast periods (0-24, 12-36, and 24-48) and four parallel test months (03 May - 31 Aug) as a function of precipitation amount threshold (x-axis). In all six figures the solid line (dashed line) depicts the ETAV control (ETAY test). Note that the Y-axis in some figures begins at a nonzero value.

In the Southeast, Fig. 31 shows the ETAY threat score superior to the ETAV control for all categories of 1 inch and below, and virtually identical threat scores for the remaining larger categories. The ETAY bias score (recall a value of 1.0 is perfect) shows a striking improvement over ETAV for categories 1-inch and below. The improvement in threat score is especially noteworthy given the elimination of the positive bias, because it is generally agreed that moderate positive biases tend to unfairly inflate the threat score. For categories above 1-inch, the ETAY modifications yield a worse negative bias, but this did not further degrade already very low skill scores at these categories.

In the Southern Plains in Fig. 32, the ETAY threat score is notably superior to the ETAV control for all categories of 1.5 inch and below. Only at the highest category of 3 inches is the ETAV threat score superior. Inspecting the bias, the ETAY yields a notable reduction of positive bias in the first three categories. The negative bias for categories of .75 inch and above is clearly worse for the ETAY test, but yet the ETAY threat score is superior for 3 of these 5 largest categories. The net conclusion is that ETAY scores are superior in the Southern Plains.

In the Northeast in Fig. 33, the threat scores of ETAY and ETAV are virtually identical, while the bias of ETAY is clearly superior through all categories up to 1-inch, showing a marked reduction of the positive bias. Again, for heaviest thresholds of 1.5 and 2.0 inches, the ETAY yields a worse negative bias, but this does not further degrade the virtually zero threat score at these heaviest thresholds.

In the Northern Midwest in Fig. 34, the ETAY and ETAV threat scores at all categories are virtually identical. The ETAY bias score is somewhat degraded relative to ETAV in the first four categories, becoming modestly negative compared to ETAV. In the remaining categories there is no significant change in the typical negative bias at the higher categories.

The scores for the large CONUS region comprised of a merger of the previous four and designated here as "East" (i.e. eastward of the inter-mountain western states) are given in Fig. 35. Therein, the ETAY test yields slightly but consistently larger threat scores for all categories up to

and including 1-inch, virtually unchanged threat score at the 1- and 2-inch categories, and worse threat score only at the final 3-inch category.

Lastly, in the large inter-mountain region denoted here as West, Fig. 36 shows that the modified convection scheme of ETAY yields slightly better or unchanged threat scores for all categories up to and including 1-inch, slightly better but still very low threat score at 1.5 inch, and unchanged and still zero threat score for the heaviest categories of 2- and 3-inches. The bias scores of ETAY show that for the first three categories through 0.25 inch, the convection modifications have indeed eliminated the longstanding western negative bias, but at the expense of a now positive bias of somewhat larger magnitude. The general feeling from forecasters is that if a modest bias is unavoidable, they prefer a positive bias to a negative bias. For the remaining heavier categories, at .50 inch the modest negative bias is unchanged, and for categories of .75 inch and above, ETAY and ETAV biases are not meaningfully different.

**X.3Conclusion**

The preponderance of the subjective assessment of the precipitation maps of Sections X.2.a and X.2.b shows a significant improvement in QPF arising from the modified convection scheme, both in the east and in the west, and most notably in the overall southeast quadrant of the U.S. This subjective conclusion is further supported in the East by the objective verification scores of Section X.2.c. In the West, the objective verification reveals only a modest to marginal ETAY advantage. One caveat in the West is the unknown impact on the scores of the acknowledged sparseness of gage observations used in the verifying analysis. Ultimately in both the East and the West, we conclude in favor of the modified convection scheme on the weight of both the subjective and objective assessment.

**Note on the CPC daily precipitation analysis**: The plots designated OBS are a monthly summation of the daily, 0.25-degree, gage-only, objective precipitation analysis performed by CPC (Higgins, 1999, personal communication). This daily precipitation analysis is produced by a modified Cressman analysis of about 5000-5500 daily gage observations of 24-h total precipitation, received at NCEP in realtime from the NWS River Forecast Centers (RFC). The reporting period of these daily 24-h gage observations is nominally 12 UTC to 12 UTC, hence the daily analysis represents a 24-h sum from 12 UTC. More details on the CPC precipitation analysis are available at the bottom of the online site here6.

## XI. References

Baldwin, M. E., and T.L. Black, 1996: Precipitation forecasting experiments in the western U.S. NCEP's mesoscale Eta Model. Preprints, AMS 11th Conf. on Numerical Weather Prediction, 19-23 August 1996, Norfolk, VA, J109-J110.

Baldwin, M.E.., and K. E. Mitchell, 1997: The NCEP hourly multi-sensor U.S. precipitation analysis for operations and GCIP research. Preprints, AMS 13th Conf. on Hydrology, 2-7 February 1997, Long Beach, CA, 54-55.

Betts, A.K., 1986: A new convective adjustment scheme. Part I: Observational and theoretical basis. *Quart. J. Roy. Meteor*. Soc., 112, 677-691.

Betts, A.K., and M.J. Miller, 1986: A new convective adjustment scheme. Part II: Single column tests using GATE wave, BOMEX and arctic air-mass data sets. *Quart. J. Roy. Meteor*. Soc., 112, 693-709.

Bunkers, M. J., B. A. Klimowski, J.W. Zeitler, R. L. Thompson, and M. L. Weisman, 1998: Predicting Supercell Motion Using Hodograph Techniques,19th Conference on Severe Local Storms, Minneapolis, MN, Amer. Meteor. Soc., 611-614.

Collins, W. G., 1993: Complex quality control of Doppler wind profilers at the National Meteorological Center, 13th Conference on Weather Analysis and Forecasting, Aug. 2-6, 1993, Vienna, VA.
_____, 1994: Complex quality control of wind profiler data at the National Meteorological Center, Tenth Conference on Numerical Weather Prediction, July 18-22, 1994, Portland, OR.

Davies, J. M., and R. H. Johns, 1993: Some wind and instability parameters associated with strong and violent tornadoes. Part I:Wind shear and helicity. The Tornado: Its structure, Dynamics, Prediction, and Hazards. Geophys. Monogr., No. 79, Amer. Geophys. Union, 573-582.

Gartner, G.E., M.E. Baldwin, and N.W. Junker, 1996: Regional analysis of quantitative precipitation forecasts from NCEP's Early Eta and Meso-Eta Models. Preprints, AMS 15th Conf. on Weather Analysis and Forecasting, 19-23 August 1996, Norfolk, VA, 169-171.

Janjic, Z.I., 1990: The step-mountain coordinate: Physical package. Mon. Wea. Rev., 118, 1429-1443.

Janjic, Z.I., 1994: The step-mountain Eta coordinate model: Further developments of the convection, viscous sublayer, and turbulence closure schemes. Mon. Wea. Rev., 122, 927-945.

Kain, J.S., M.E. Baldwin, D.J. Stensrud, T.L. Black, and G.S. Manikin, 1998: Considerations for the implementation of a convective parameterization scheme in an operational mesoscale model. Preprints, AMS 12th Conf. on Numerical Weather Prediction, 11-16 January 1998, Phoenix, AZ, 103-106.

Lin., Y., K. Mitchell, E. Rogers and M. Baldwin, 1998: Assimilation of real-time, multi-sensor hourly precipitation observations into the NCEP Eta Model. Preprints, AMS 12th Conf. on Numerical Weather Prediction, 11-16 January 1998, Phoenix, AZ, 174-175.

Manikin, G.S., K.E. Mitchell, E. Rogers, and D.J. Stensrud, 1996: Severe weather forecasts using the Eta and Meso Eta Models. Preprints, AMS 15th Conf. on Weather Analysis and Forecasting, 19-23 August 1996, Norfolk, VA, 295-296.

Manikin, G.S., K.E. Mitchell, D.J. Stensrud, J.S. Kain, J.P. Gerrity, and M.E. Baldwin, 1998: Convective scheme tests on the coastal precipitation bias in the NCEP Eta Model. Preprints, AMS 12th Conf. on Numerical Weather Prediction, 11-16 January 1998, Phoenix, AZ, 107-110.

Rogers, E., M. Baldwin, T. Black, K. Brill, F. Chen, G. DiMego, J. Gerrity, G. Manikin, F. Mesinger, K. Mitchell, D. Parrish, and Q. Zhao, 1997 : Changes to the NCEP Operational "Early" Eta Analysis / Forecast System. NWS Technical Procedures Bulletin 447, NOAA/NWS. [Available at http://www.nws.noaa.gov/om/tpb/447.htm and from National Weather Service, Office of Meteorology, 1325 East-West Highway, Silver Spring, MD 20910 ]

Rogers, E., and coauthors, 1999: Changes to the NCEP operational Eta analysis. NWS Technical Procedures Bulletin No. 453, NOAA/NWS. Washington, DC. [ Available at http://www.nws.noaa.gov/om/tpb/3d-eta.htm and from National Weather Service, Office of Meteorology, 1325 East-West Highway, Silver Spring, MD 20910 ]

Staudenmaier, M., 1996: The convective parameterization scheme in the Meso-Eta Model. Western Region Technical Attachment No. 96-23, National Weather Service, 17 September 1996, Salt Lake City, UT, 6 pp.

Stensrud, D., G. Manikin, E. Rogers, and K. Mitchell, 1999: Importance of cold pools to NCEP Mesoscale Eta Model Forecasts. *Wea. Forecasting*, **14**, 650-670.

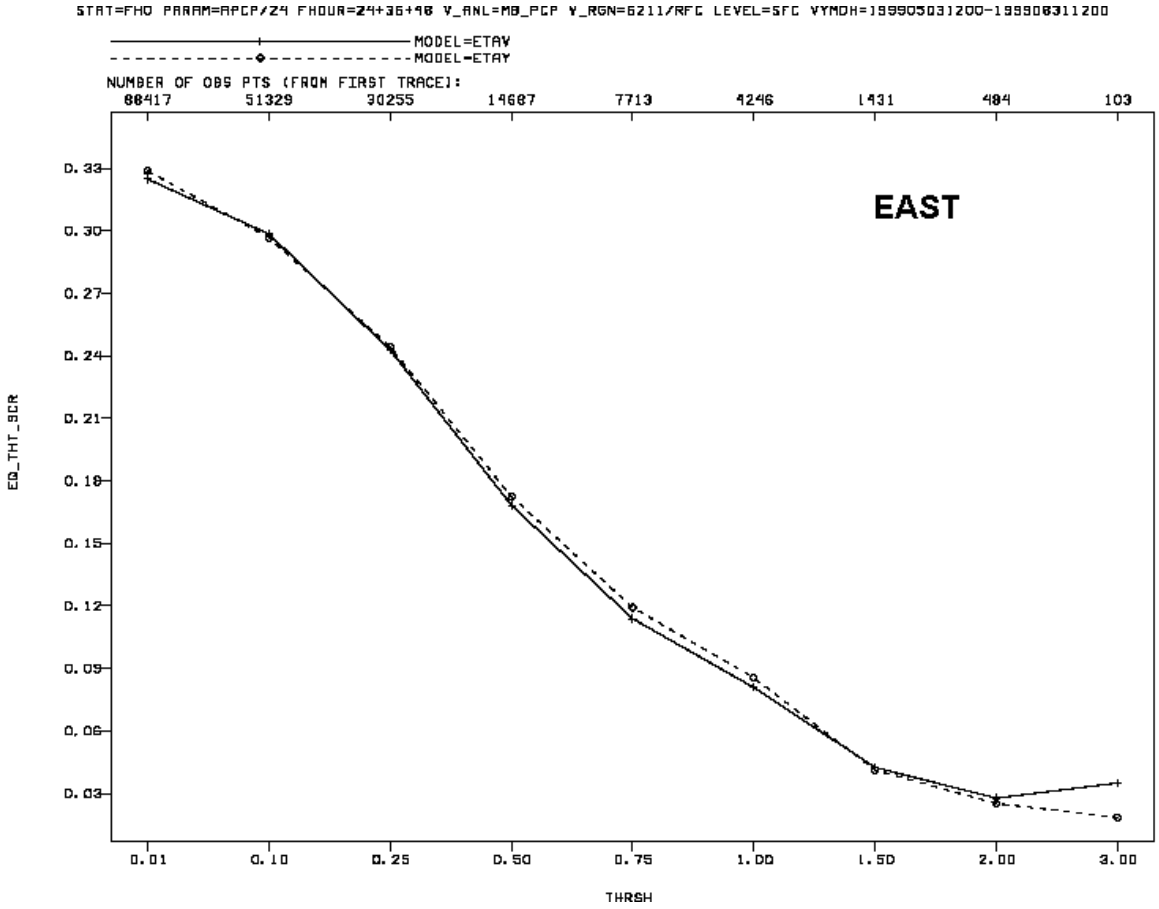
STAT=FHO PARAM=APCP/24 FHOUR=24+36+48 V_ANL=MB_PCP V_RGN=6211/RFC LEVEL=SFC VYMDH=19990503I200-19990831200
MODEL=ETAV
MODEL=ETAY
NUMBER OF OBS PTS (FROM FIRST TRACE):
88417
51329
30255
14687
7713
4246
1431
484
103
EAST
EQ_THT_SCR
0.33
0.30
0.27
0.24
0.21
0.18
0.15
0.12
0.09
0.06
0.03
0.01
0.10
0.25
0.50
0.75
1.00
1.50
2.00
3.00
THRSH

Figure 1

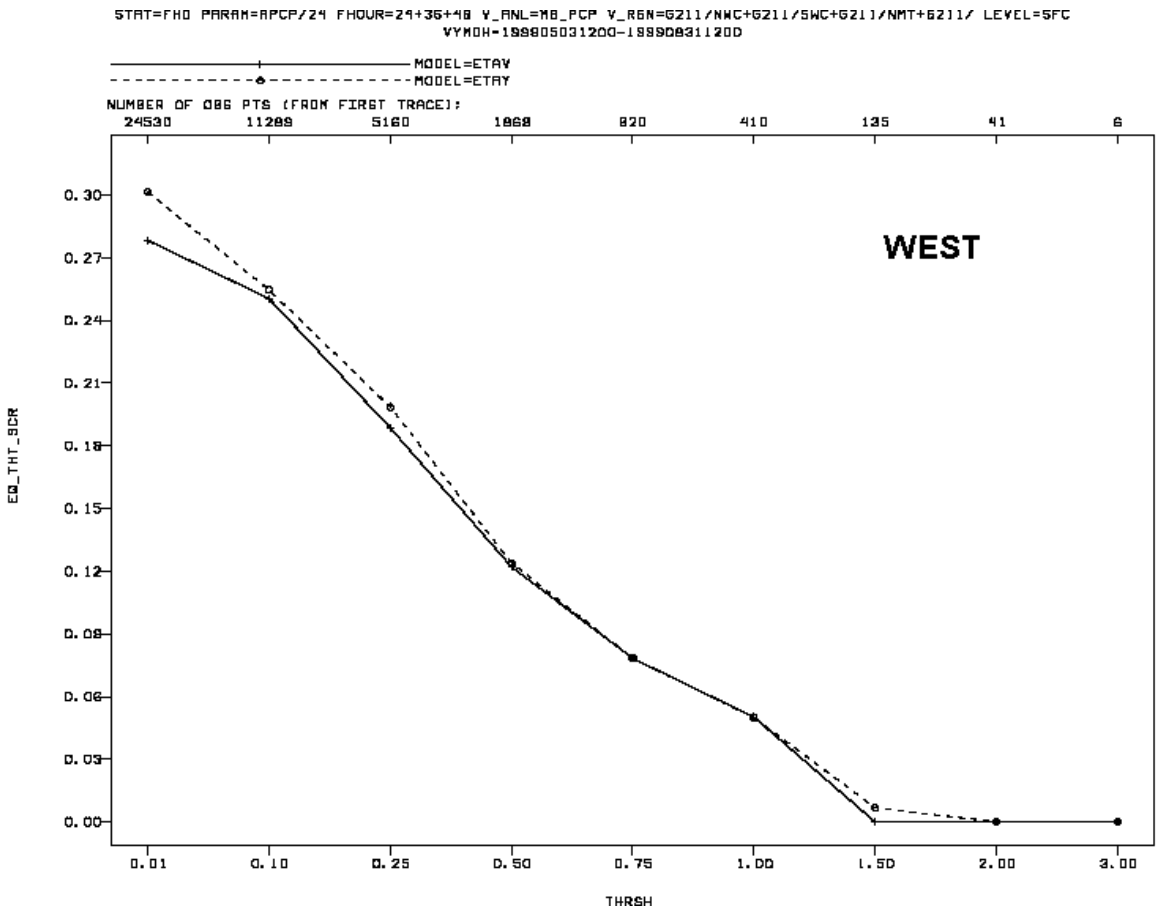
STAT=FHO PARAM=APCP/24 FHOUR=24+36+48 V_ANL=MB_PCP V_RGN=G211/NWC+G211/SWC+G211/NMT+G211/ LEVEL=SFC
VYMDH=1998050312DD-1998083112DD
MODEL=ETAV
MODEL=ETAY
NUMBER OF OBS PTS (FROM FIRST TRACE):
24530
11289
5160
1868
820
410
135
41
6
WEST
EQ_THT_SCR
0.30
0.27
0.24
0.21
0.18
0.15
0.12
0.09
0.06
0.03
0.00
0.01
0.10
0.25
0.50
0.75
1.00
1.50
2.00
3.00
THRSH

Figure 2

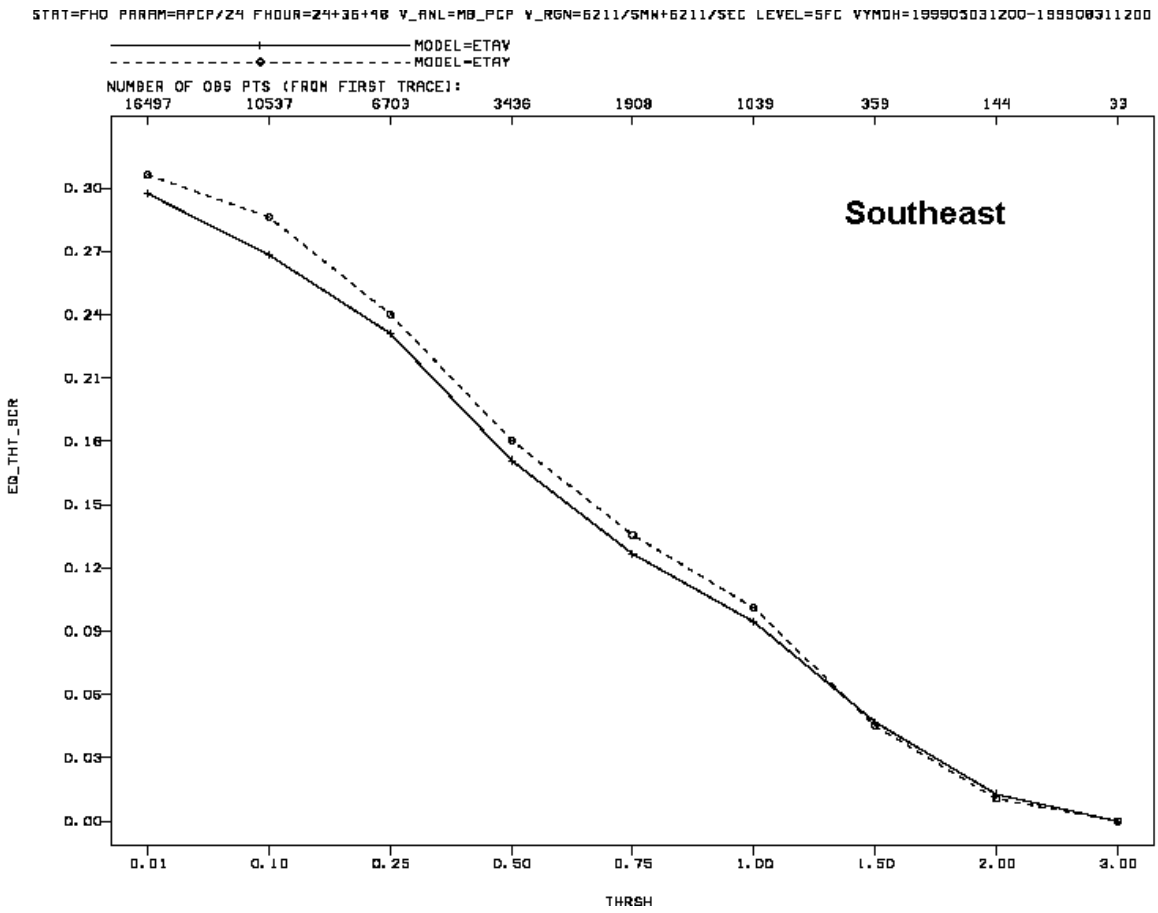
STAT=FHO PARAM=APCP/24 FHOUR=24+36+48 V_ANL=MB_PCP V_RGN=6211/SMN+6211/SEC LEVEL=SFC YYMDH=1999050312Z00-1999083112Z00
MODEL=ETAV
MODEL=ETAY
NUMBER OF OBS PTS (FROM FIRST TRACE):
16497
10537
6703
3436
1908
1039
359
144
33
Southeast
EQ_THT_SCR
0.30
0.27
0.24
0.21
0.18
0.15
0.12
0.09
0.06
0.03
0.00
0.01
0.10
0.25
0.50
0.75
1.00
1.50
2.00
3.00
THRSH

Figure 3

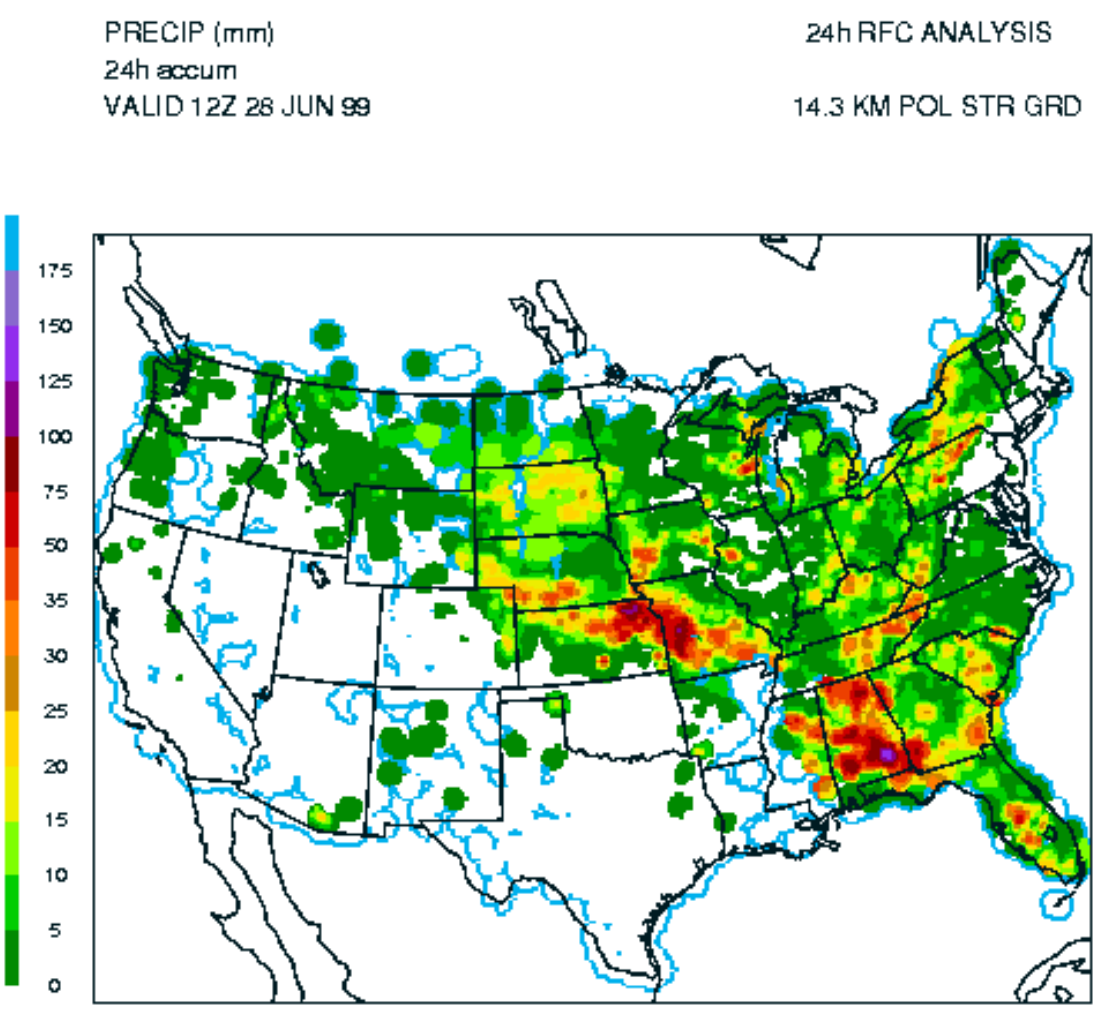
PRECIP (mm)
24h accum
VALID 12Z 28 JUN 99
24h RFC ANALYSIS
14.3 KM POL STR GRD
175
150
125
100
75
50
35
30
25
20
15
10
5
0

Figure 4

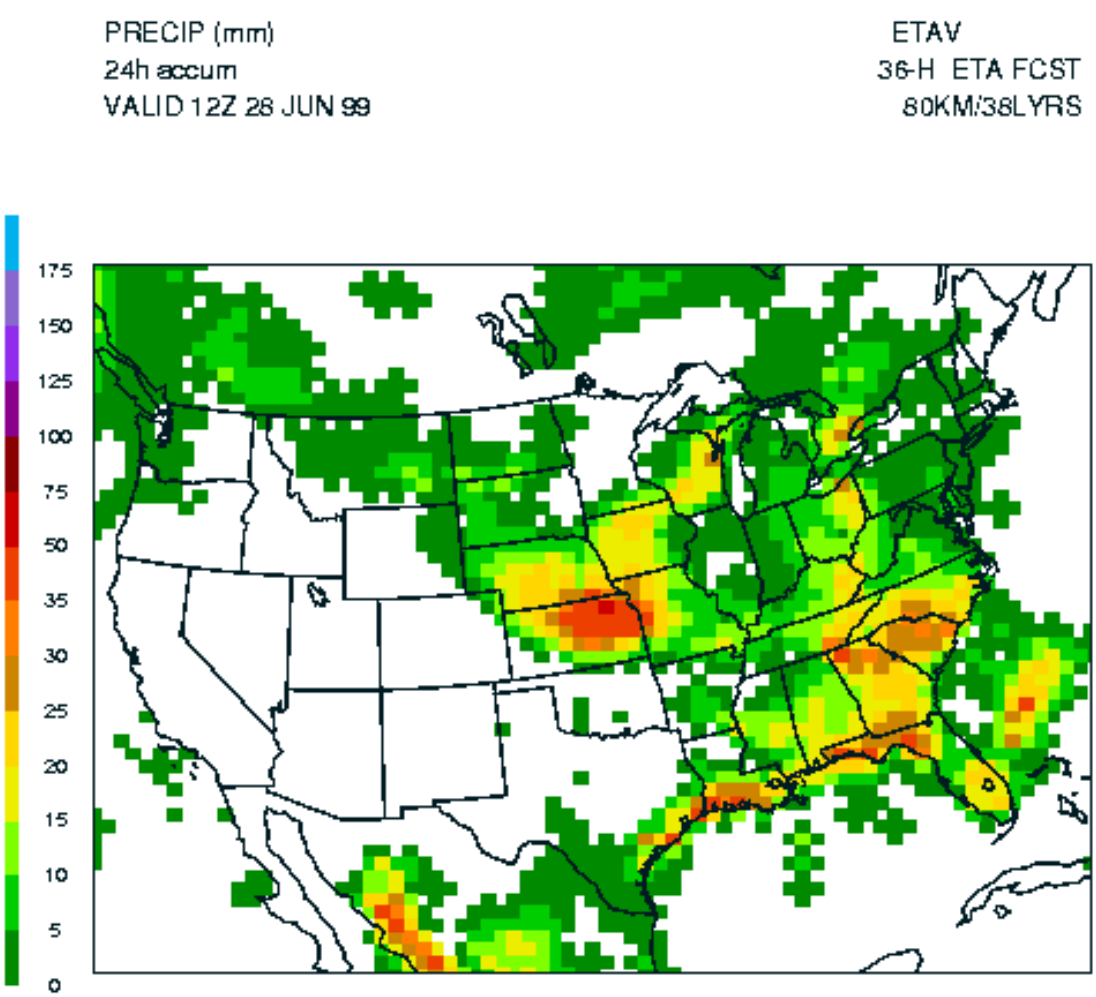
PRECIP (mm)
24h accum
VALID 12Z 28 JUN 99
ETAV
36-H ETA FCST
80KM/38LYRS
175
150
125
100
75
50
35
30
25
20
15
10
5
0

Figure 5

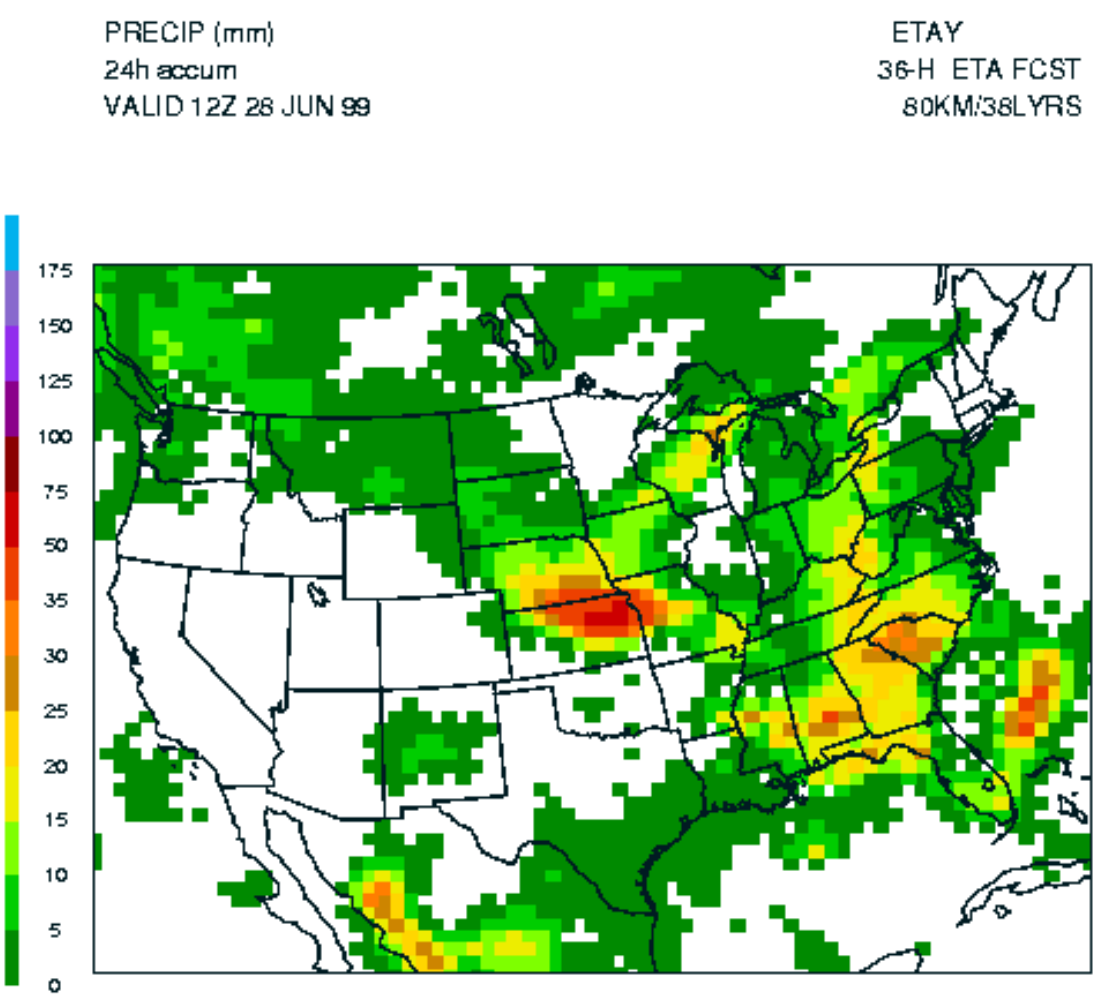
PRECIP (mm)
24h accum
VALID 12Z 28 JUN 99
ETAY
36-H ETA FCST
80KM/38LYRS
175
150
125
100
75
50
35
30
25
20
15
10
5
0

Figure 6

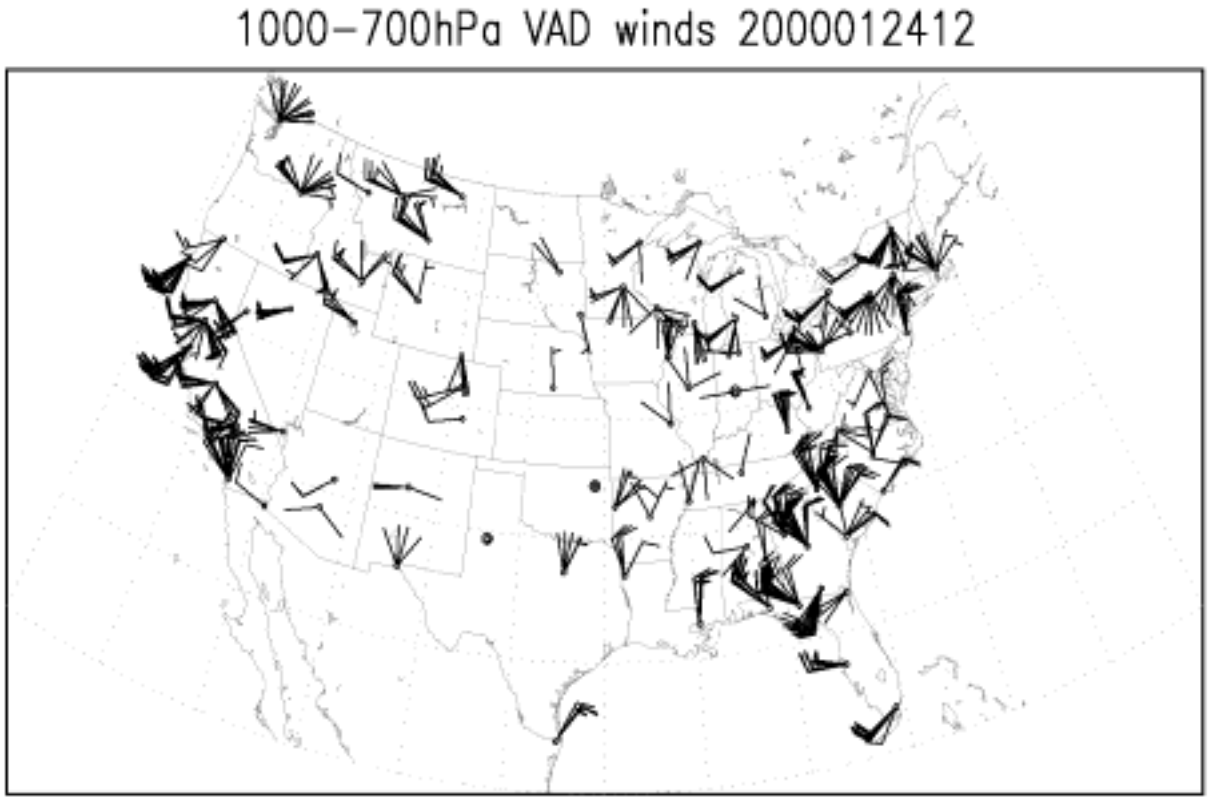


Figure 7

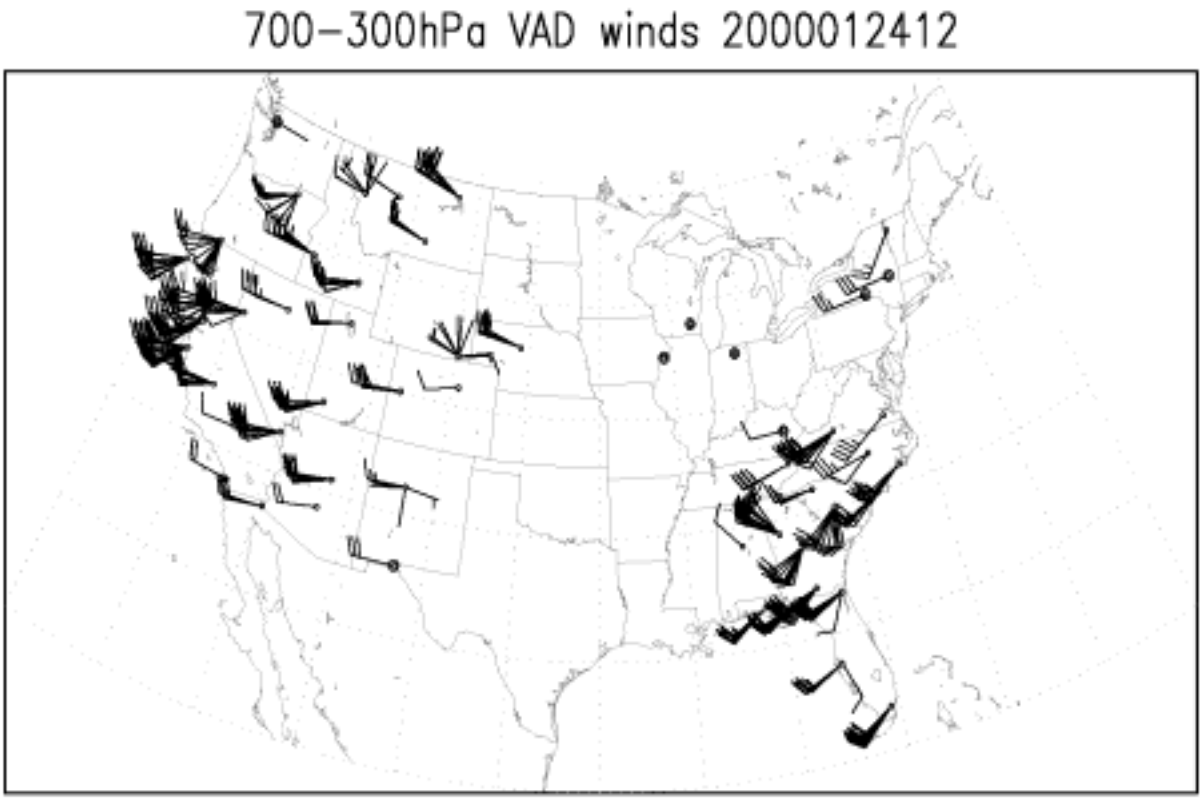


Figure 8

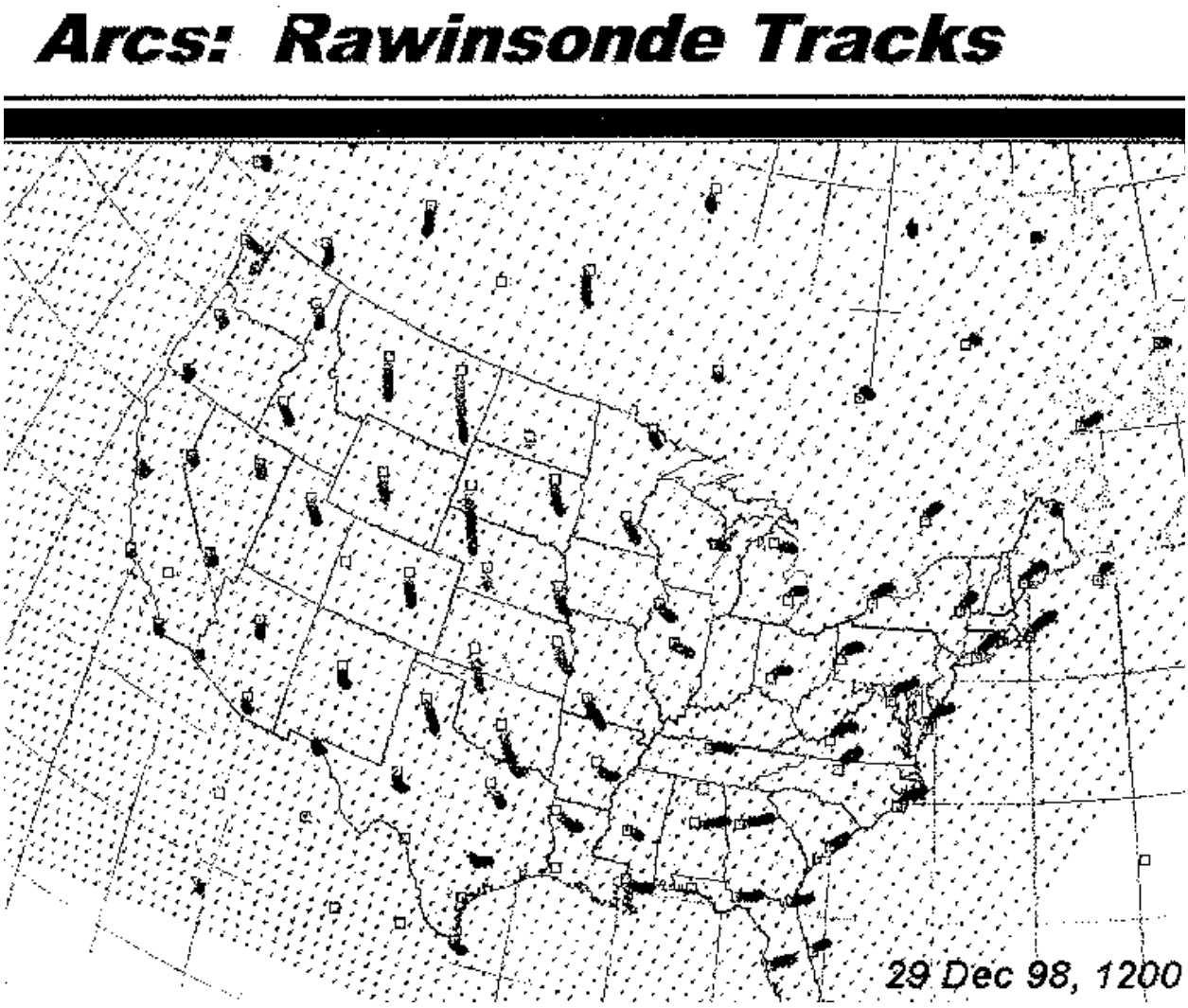


Figure 9

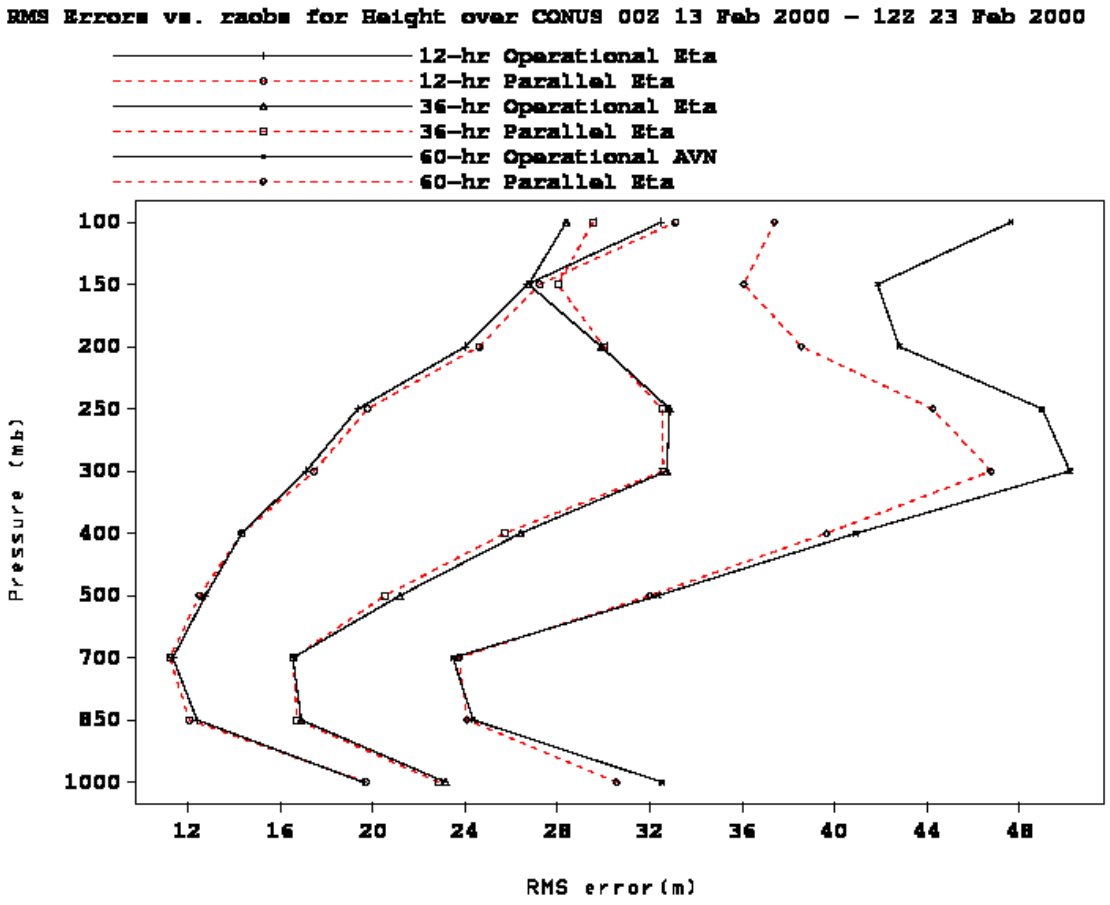
RMS Errors vs. raobs for Height over CONUS 00Z 13 Feb 2000 – 12Z 23 Feb 2000
12-hr Operational Eta
12-hr Parallel Eta
36-hr Operational Eta
36-hr Parallel Eta
60-hr Operational AVN
60-hr Parallel Eta
Pressure (mb)
100
150
200
250
300
400
500
700
850
1000
12
16
20
24
28
32
36
40
44
48
RMS error(m)

Figure 10

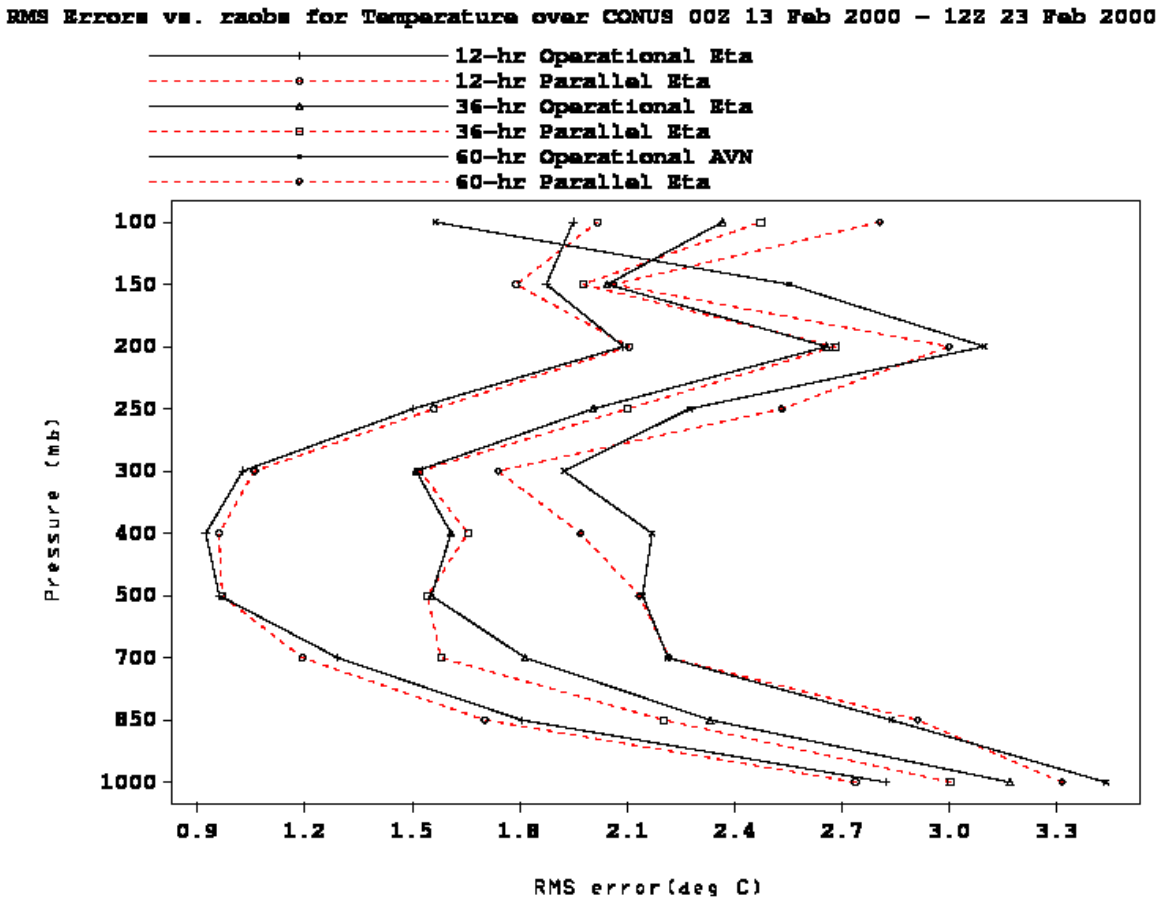
RMS Errors vs. raobs for Temperature over CONUS 00Z 13 Feb 2000 – 12Z 23 Feb 2000
12-hr Operational Eta
12-hr Parallel Eta
36-hr Operational Eta
36-hr Parallel Eta
60-hr Operational AVN
60-hr Parallel Eta
Pressure (mb)
100
150
200
250
300
400
500
700
850
1000
0.9
1.2
1.5
1.8
2.1
2.4
2.7
3.0
3.3
RMS error(deg C)

Figure 11

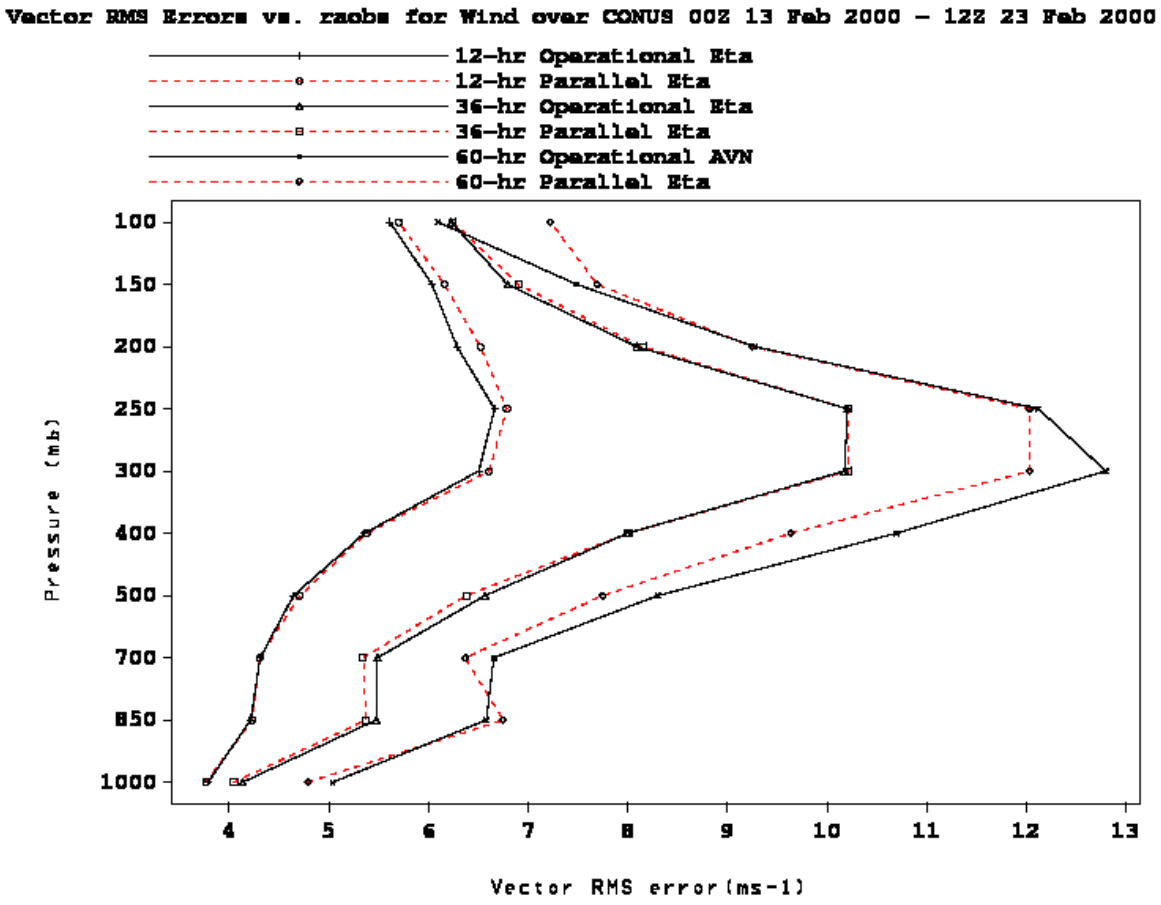
Vector RMS Errors vs. raobs for Wind over CONUS 00Z 13 Feb 2000 - 12Z 23 Feb 2000
12-hr Operational Eta
12-hr Parallel Eta
36-hr Operational Eta
36-hr Parallel Eta
60-hr Operational AVN
60-hr Parallel Eta
Pressure (mb)
100
150
200
250
300
400
500
700
850
1000
4
5
6
7
8
9
10
11
12
13
Vector RMS error(ms-1)

Figure 12

Figure 13

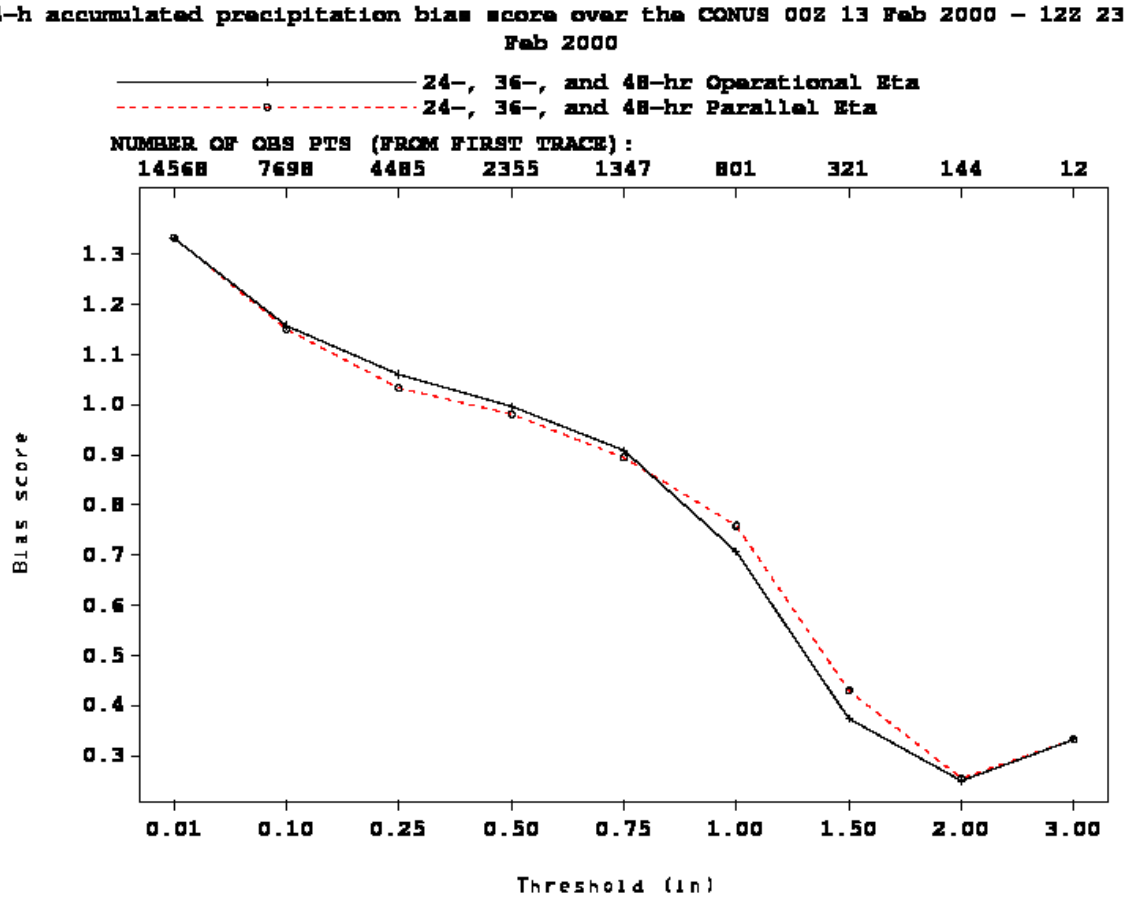
24-h accumulated precipitation bias score over the CONUS 00Z 13 Feb 2000 - 12Z 23 Feb 2000
24-, 36-, and 48-hr Operational Eta
24-, 36-, and 48-hr Parallel Eta
NUMBER OF OBS PTS (FROM FIRST TRACE):
14568 7698 4485 2355 1347 801 321 144 12
Bias score
1.3
1.2
1.1
1.0
0.9
0.8
0.7
0.6
0.5
0.4
0.3
0.01 0.10 0.25 0.50 0.75 1.00 1.50 2.00 3.00
Threshold (in)

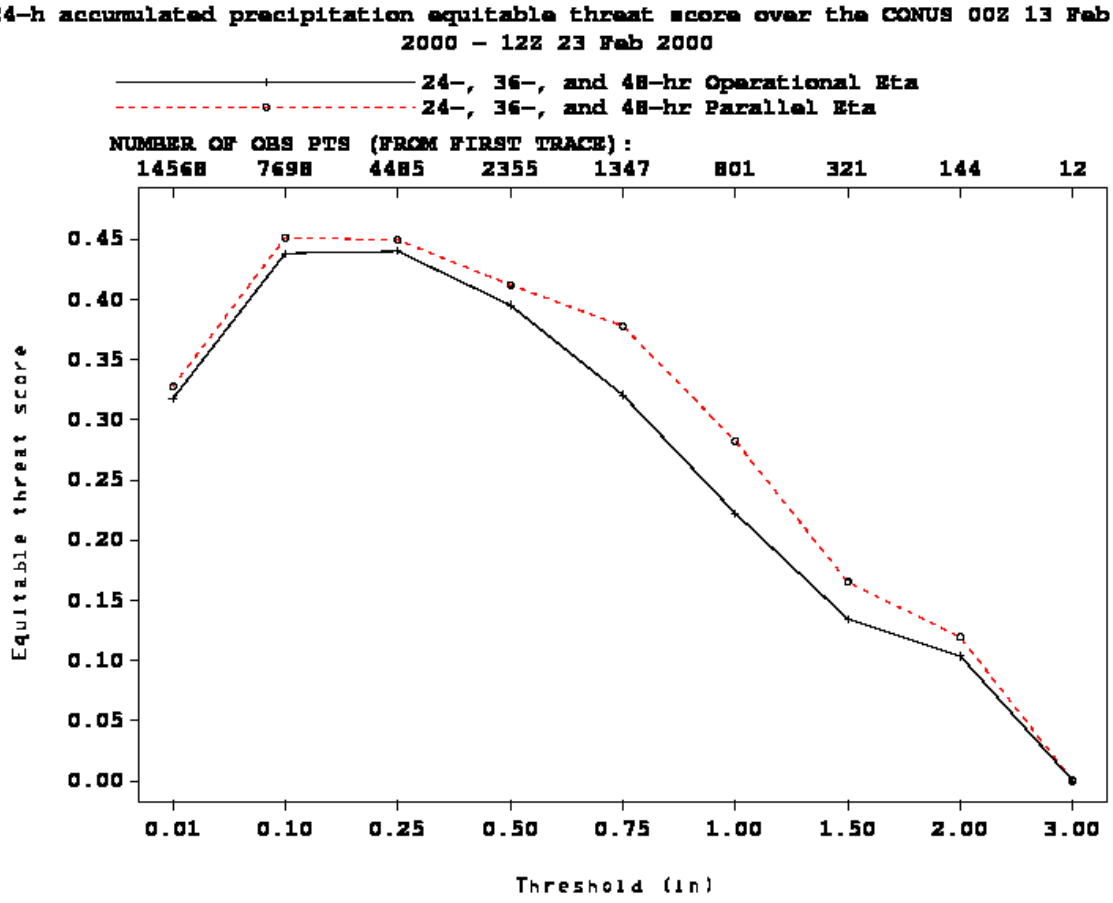
24-h accumulated precipitation equitable threat score over the CONUS 00Z 13 Feb 2000 - 12Z 23 Feb 2000
24-, 36-, and 48-hr Operational Eta
24-, 36-, and 48-hr Parallel Eta
NUMBER OF OBS PTS (FROM FIRST TRACE):
14568 7698 4485 2355 1347 801 321 144 12
Equitable threat score
0.45
0.40
0.35
0.30
0.25
0.20
0.15
0.10
0.05
0.00
0.01 0.10 0.25 0.50 0.75 1.00 1.50 2.00 3.00
Threshold (in)

Figure 14a

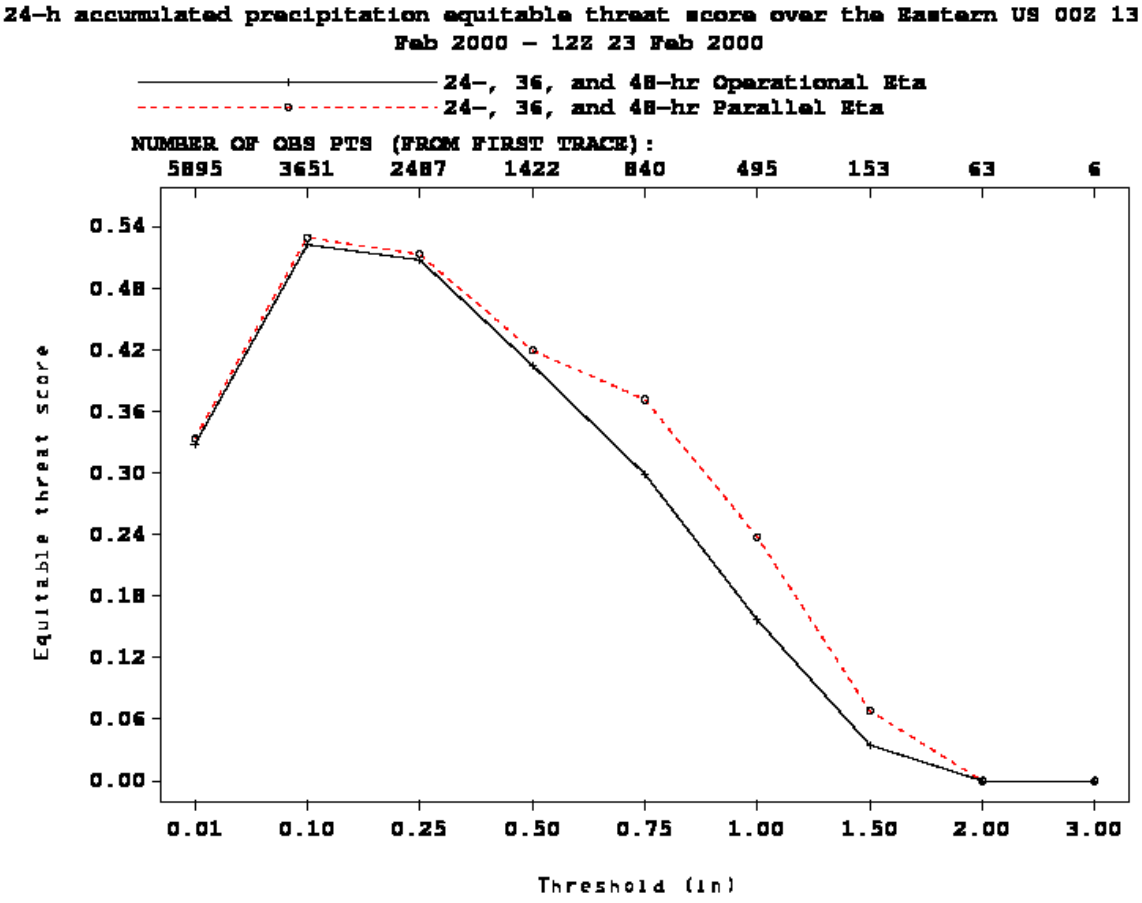
24-h accumulated precipitation equitable threat score over the Eastern US 00Z 13 Feb 2000 - 12Z 23 Feb 2000
24-, 36, and 48-hr Operational Eta
24-, 36, and 48-hr Parallel Eta
NUMBER OF OBS PTS (FROM FIRST TRACE):
5895 3651 2487 1422 840 495 153 63 6
Equitable threat score
0.54
0.48
0.42
0.36
0.30
0.24
0.18
0.12
0.06
0.00
0.01 0.10 0.25 0.50 0.75 1.00 1.50 2.00 3.00
Threshold (in)

Figure 14b

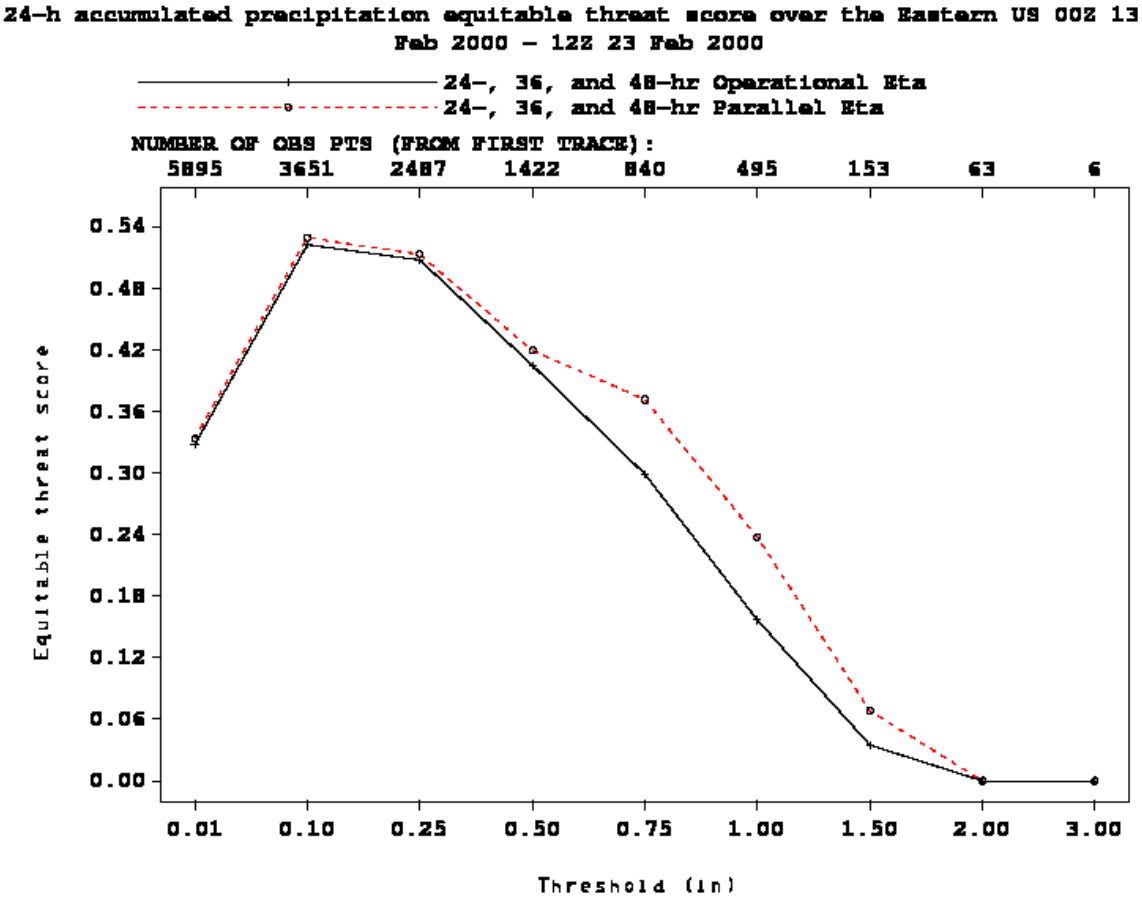
24-h accumulated precipitation equitable threat score over the Eastern US 00Z 13 Feb 2000 - 12Z 23 Feb 2000
24-, 36, and 48-hr Operational Eta
24-, 36, and 48-hr Parallel Eta
NUMBER OF OBS PTS (FROM FIRST TRACE):
5895 3651 2487 1422 840 495 153 63 6
Equitable threat score
0.54
0.48
0.42
0.36
0.30
0.24
0.18
0.12
0.06
0.00
0.01 0.10 0.25 0.50 0.75 1.00 1.50 2.00 3.00
Threshold (in)

Figure 15a

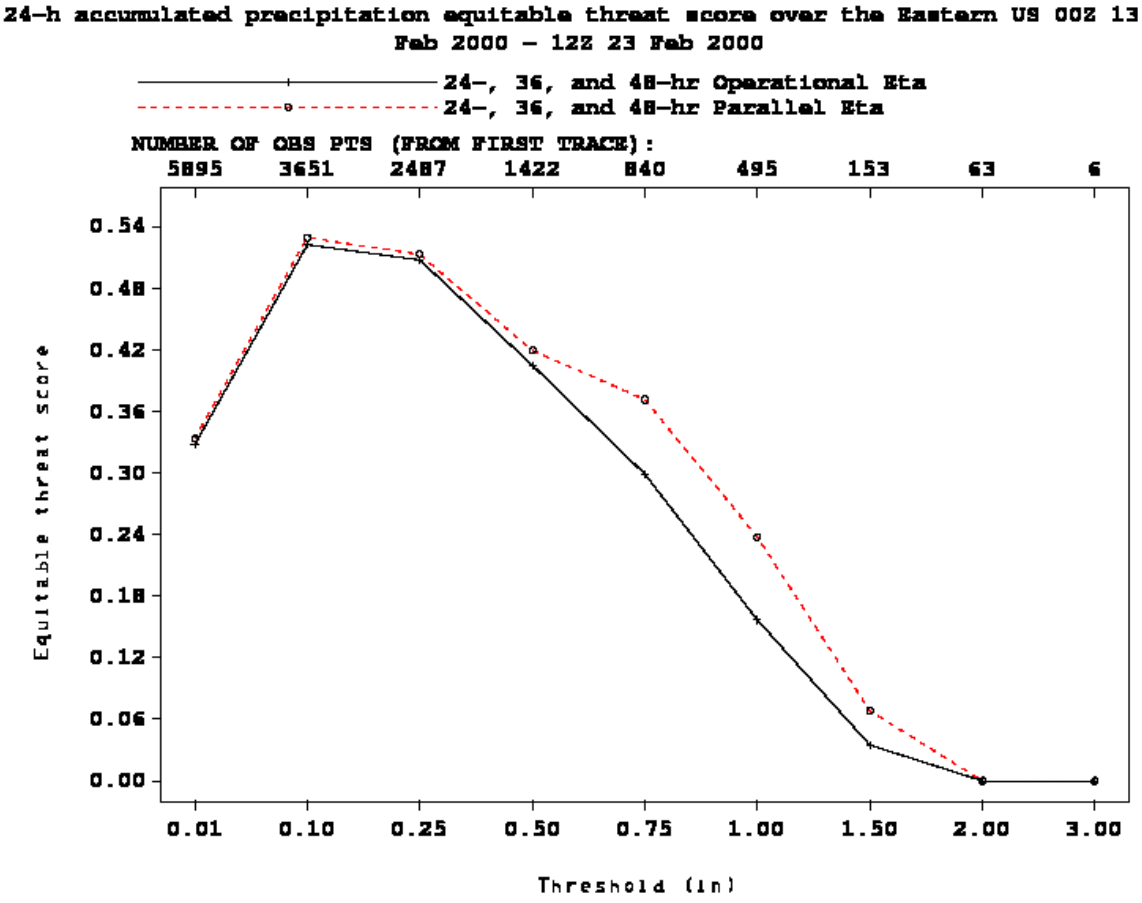
24-h accumulated precipitation equitable threat score over the Eastern US 00Z 13 Feb 2000 - 12Z 23 Feb 2000
24-, 36, and 48-hr Operational Eta
24-, 36, and 48-hr Parallel Eta
NUMBER OF OBS PTS (FROM FIRST TRACE):
5895 3651 2487 1422 840 495 153 63 6
Equitable threat score
0.54
0.48
0.42
0.36
0.30
0.24
0.18
0.12
0.06
0.00
0.01 0.10 0.25 0.50 0.75 1.00 1.50 2.00 3.00
Threshold (in)

Figure 15a

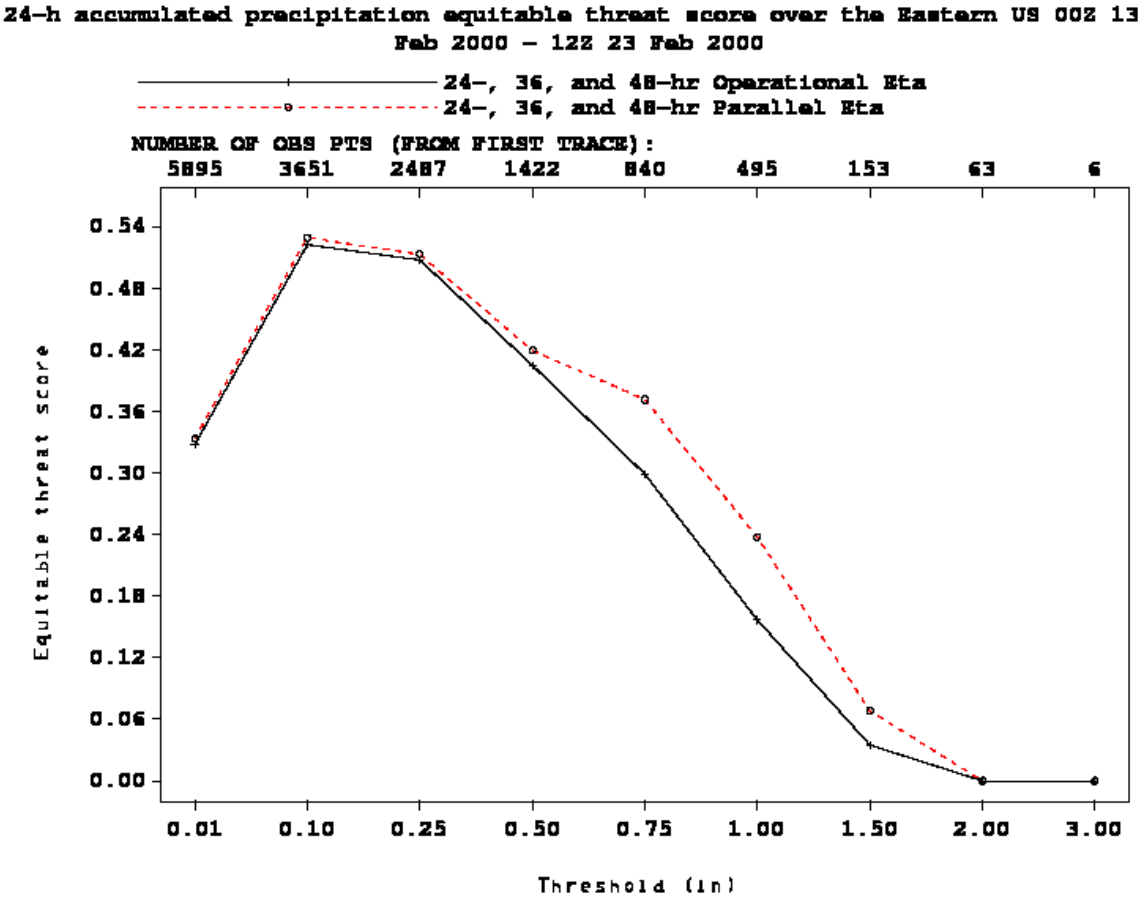
24-h accumulated precipitation equitable threat score over the Eastern US 00Z 13 Feb 2000 - 12Z 23 Feb 2000
24-, 36, and 48-hr Operational Eta
24-, 36, and 48-hr Parallel Eta
NUMBER OF OBS PTS (FROM FIRST TRACE):
5895 3651 2487 1422 840 495 153 63 6
Equitable threat score
0.54
0.48
0.42
0.36
0.30
0.24
0.18
0.12
0.06
0.00
0.01 0.10 0.25 0.50 0.75 1.00 1.50 2.00 3.00
Threshold (in)

Figure 15b

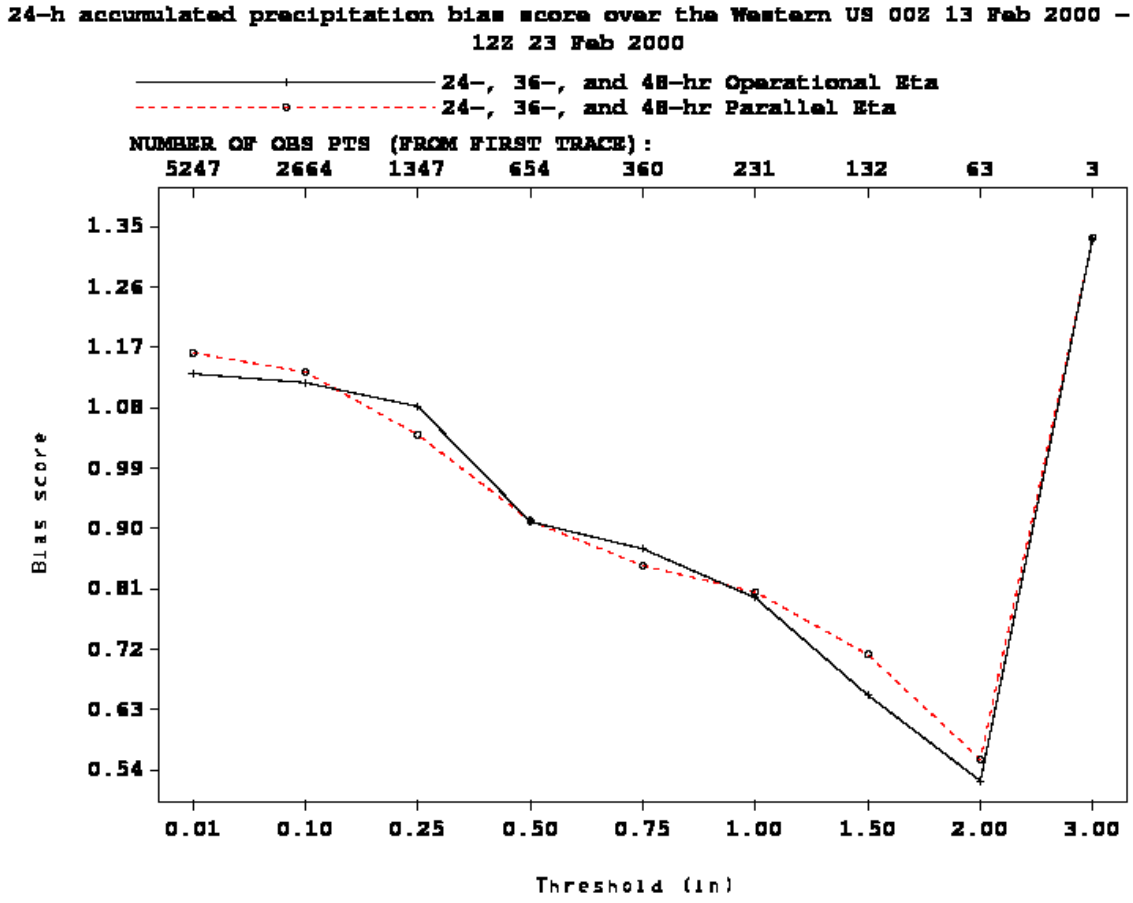
24-h accumulated precipitation bias score over the Western US 00Z 13 Feb 2000 - 12Z 23 Feb 2000
24-, 36-, and 48-hr Operational Eta
24-, 36-, and 48-hr Parallel Eta
NUMBER OF OBS PTS (FROM FIRST TRACE):
5247 2664 1347 654 360 231 132 63 3
1.35
1.26
1.17
1.08
0.99
0.90
0.81
0.72
0.63
0.54
Bias score
0.01 0.10 0.25 0.50 0.75 1.00 1.50 2.00 3.00
Threshold (in)

Figure 16a

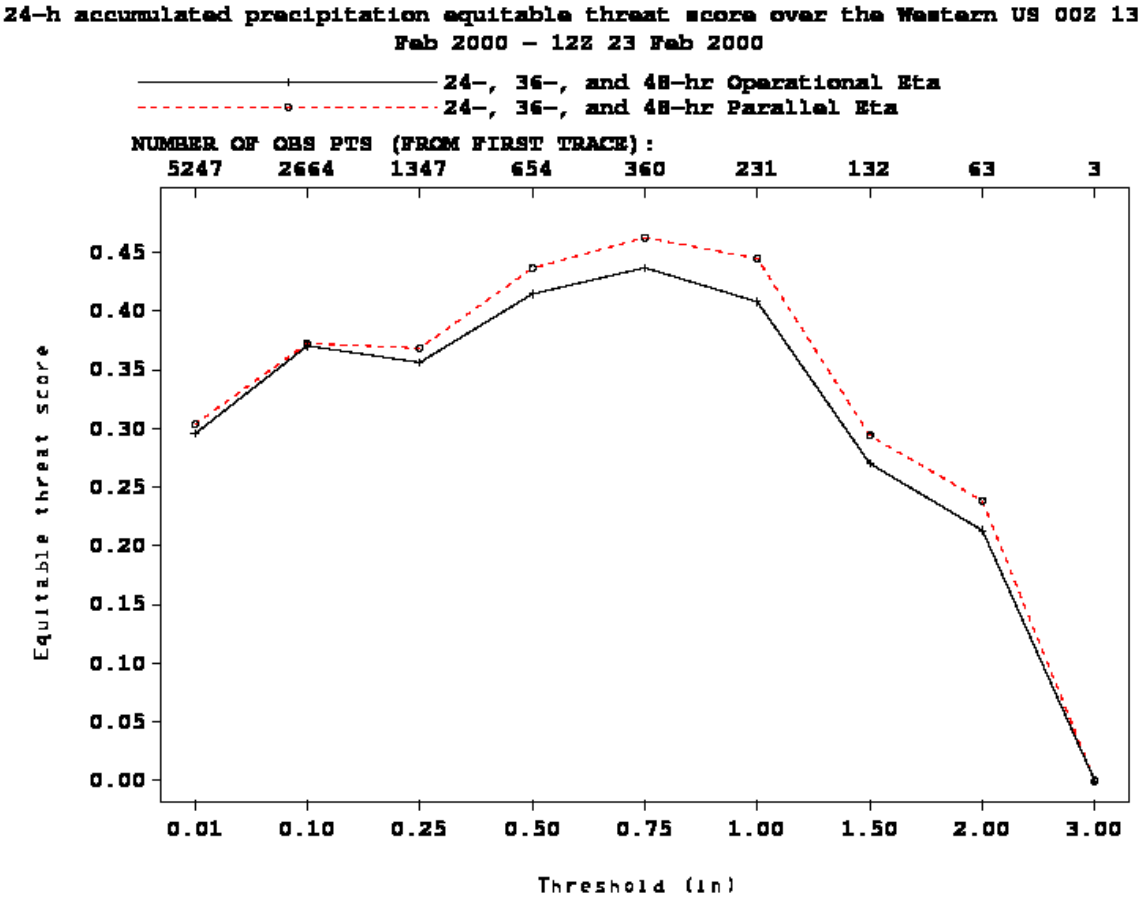
24-h accumulated precipitation equitable threat score over the Western US 00Z 13 Feb 2000 - 12Z 23 Feb 2000
24-, 36-, and 48-hr Operational Eta
24-, 36-, and 48-hr Parallel Eta
NUMBER OF OBS PTS (FROM FIRST TRACE):
5247 2664 1347 654 360 231 132 63 3
Equitable threat score
0.45
0.40
0.35
0.30
0.25
0.20
0.15
0.10
0.05
0.00
0.01 0.10 0.25 0.50 0.75 1.00 1.50 2.00 3.00
Threshold (in)

Figure 16b

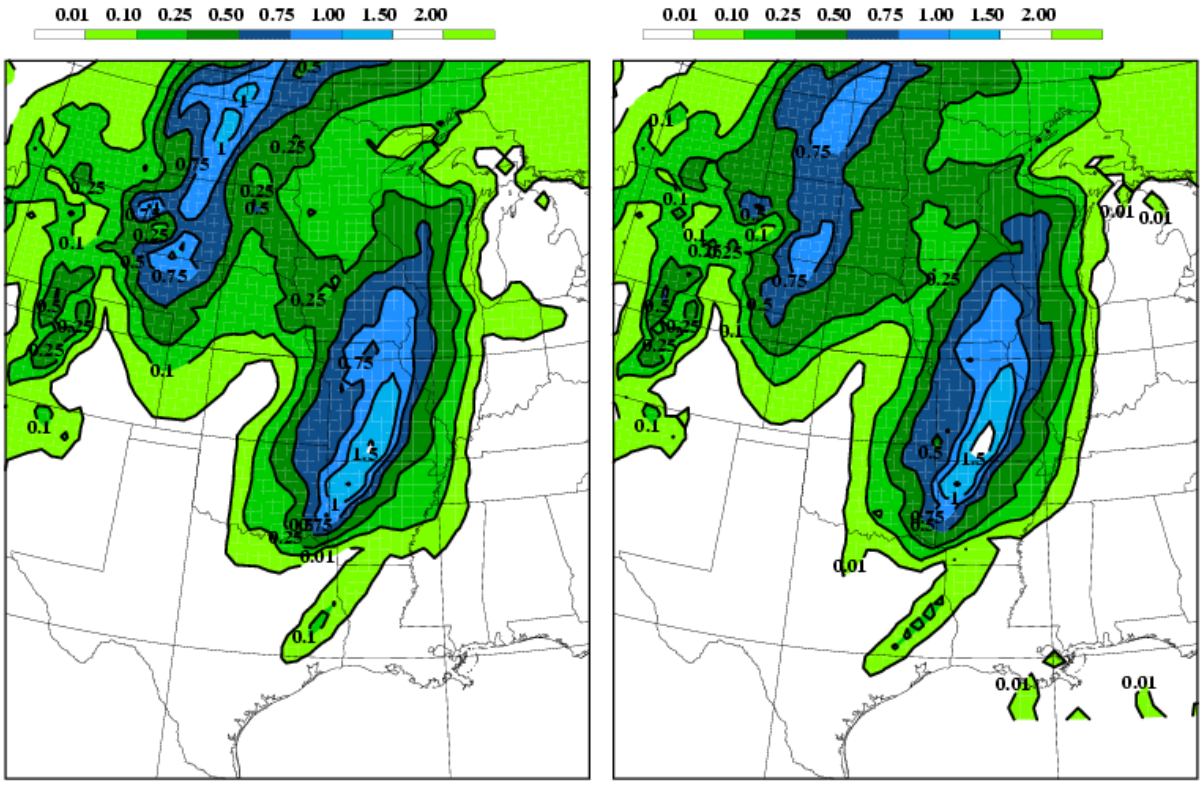
0.01 0.10 0.25 0.50 0.75 1.00 1.50 2.00
OPER ETA-32 36-H FCST : 24-H TOTAL PCP
0.01 0.10 0.25 0.50 0.75 1.00 1.50 2.00
PLL ETAX 36-H FCST : 24-H TOTAL PCP

Figure 17a

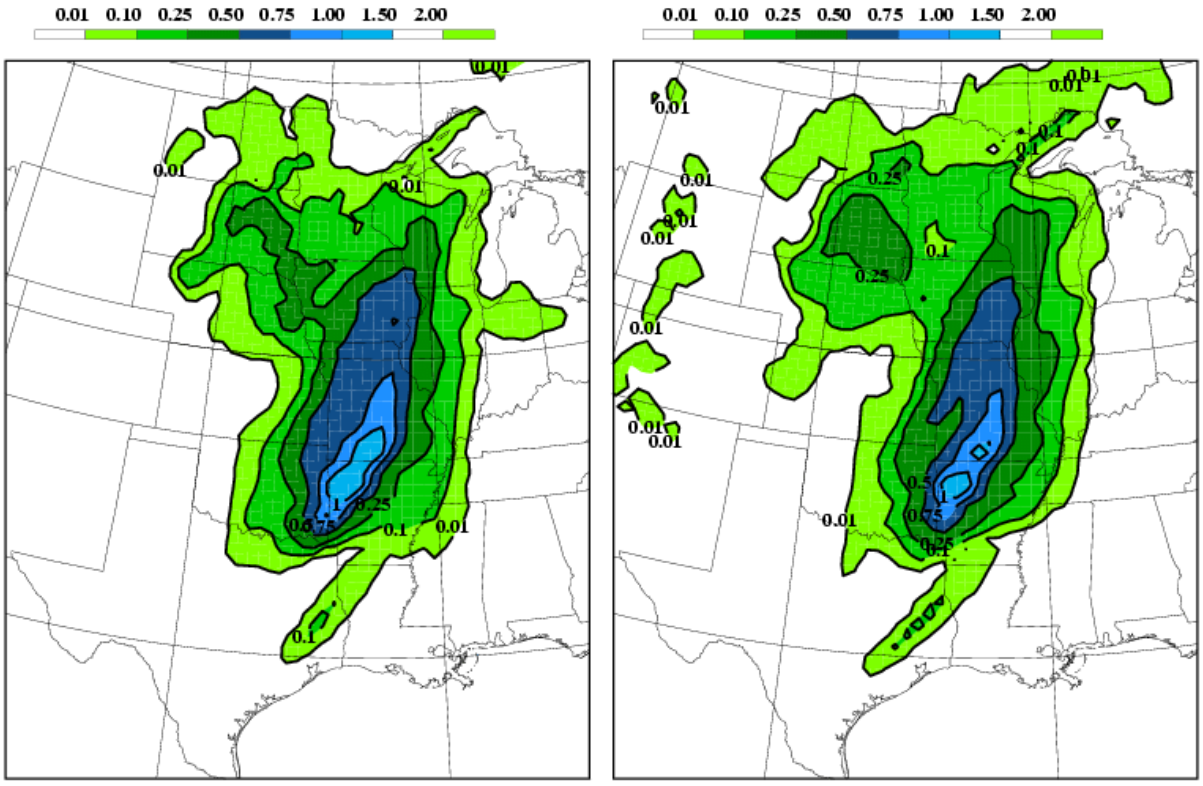
0.01 0.10 0.25 0.50 0.75 1.00 1.50 2.00
OPER ETA-32 36-H FCST : 24-H CONV PCP
0.01 0.10 0.25 0.50 0.75 1.00 1.50 2.00
PLL ETAX 36-H FCST : 24-H CONV PCP

Figure 17b

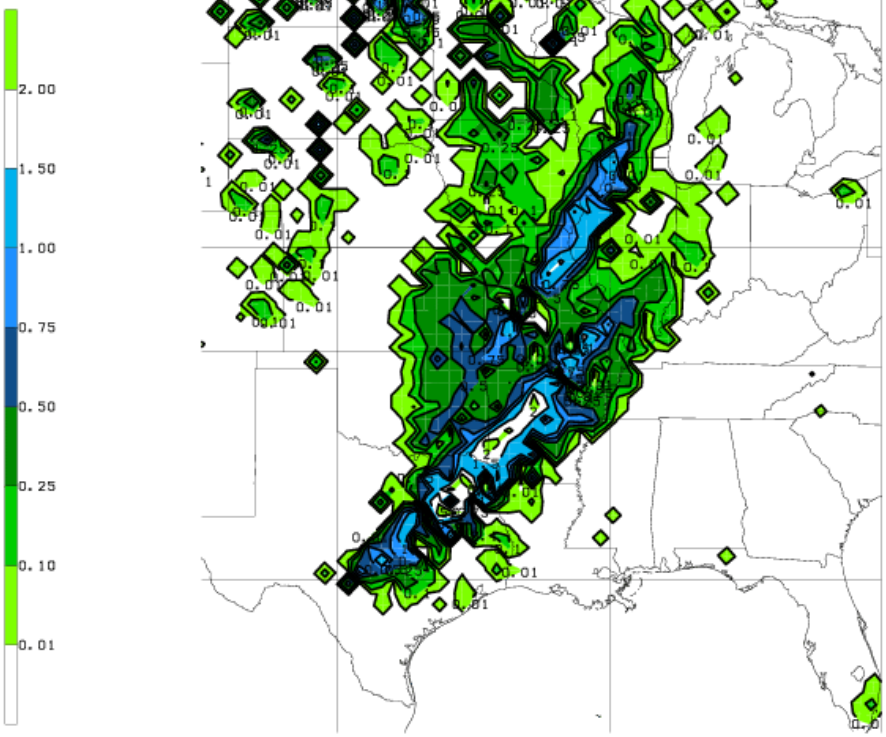
2.00
1.50
1.00
0.75
0.50
0.25
0.10
0.01
24H ACCUMULATED PRECIP - RFC ANALYSIS VALID 12Z 2/26/2000

Figure 18

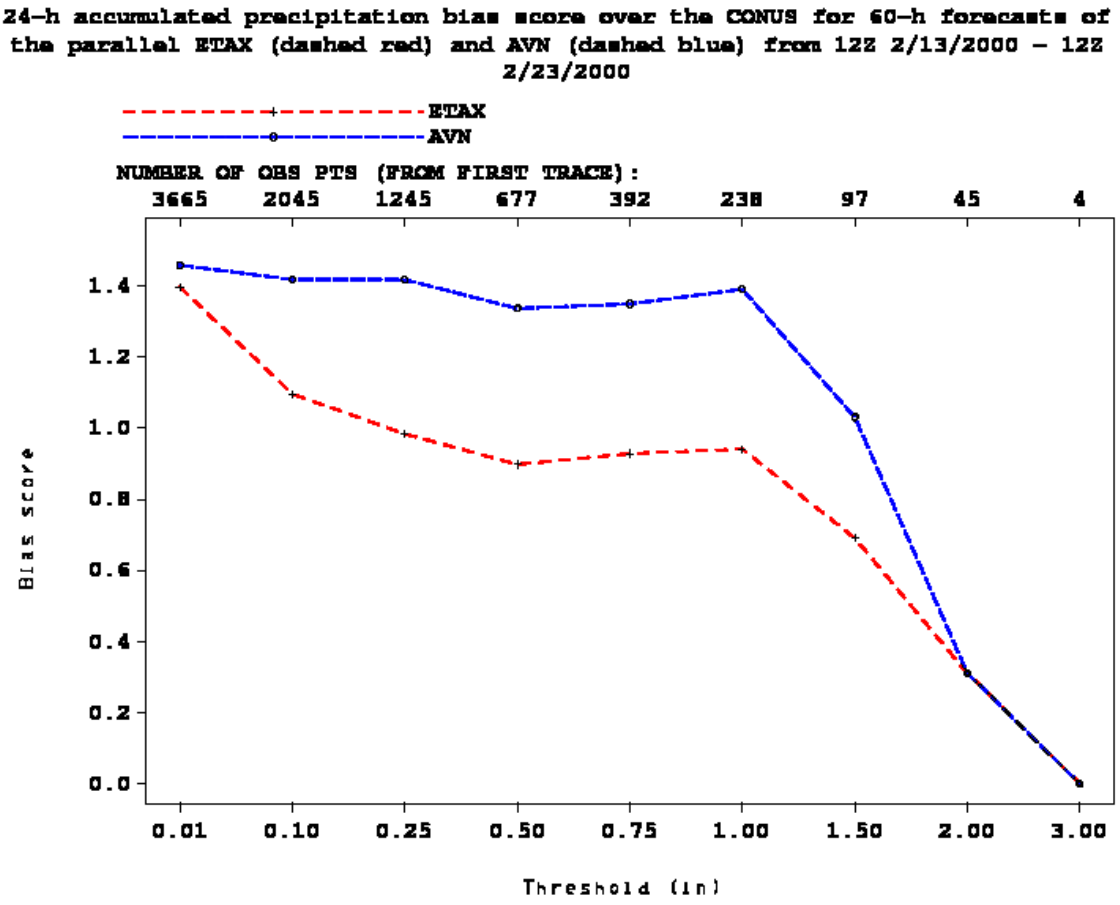
24-h accumulated precipitation bias score over the CONUS for 60-h forecasts of the parallel ETAX (dashed red) and AVN (dashed blue) from 12Z 2/13/2000 - 12Z 2/23/2000
ETAX
AVN
NUMBER OF OBS PTS (FROM FIRST TRACE):
3665 2045 1245 677 392 238 97 45 4
Bias score
1.4
1.2
1.0
0.8
0.6
0.4
0.2
0.0
0.01 0.10 0.25 0.50 0.75 1.00 1.50 2.00 3.00
Threshold (in)

Figure 19a

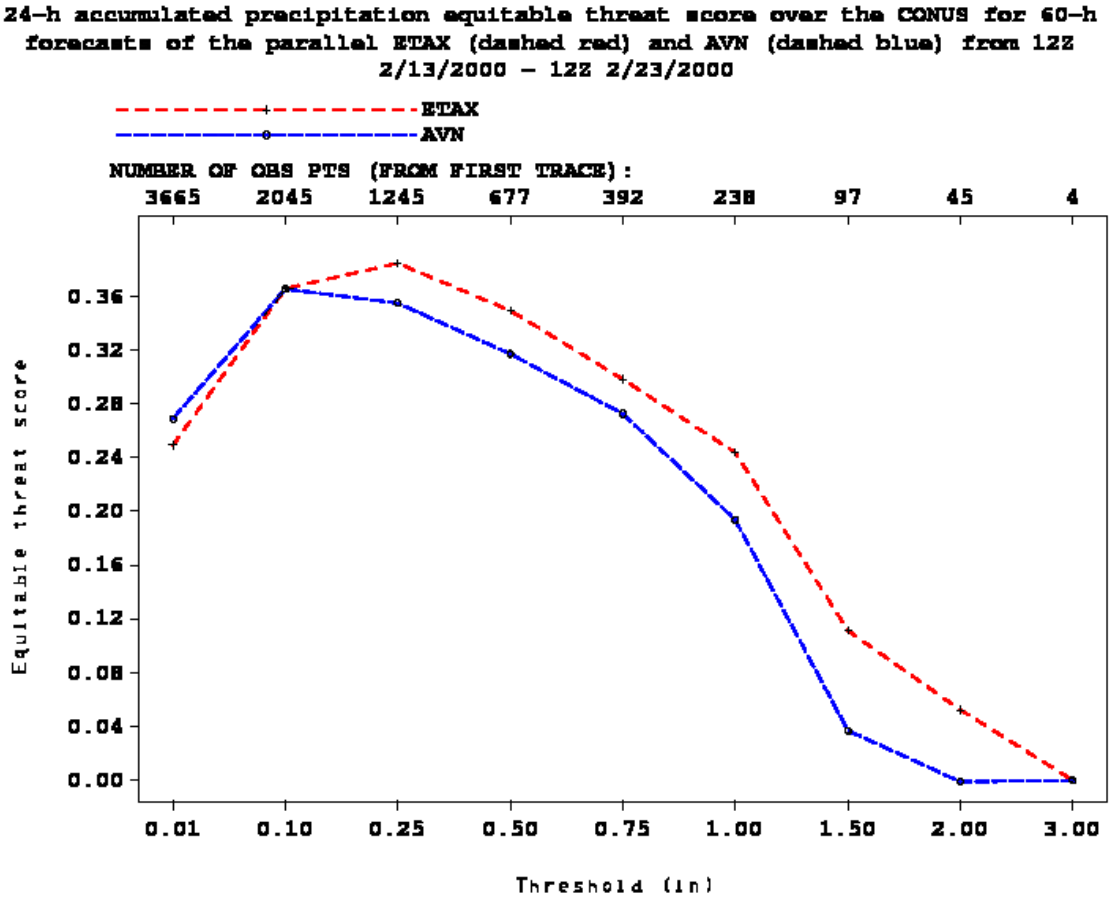
24-h accumulated precipitation equitable threat score over the CONUS for 60-h forecasts of the parallel ETAX (dashed red) and AVN (dashed blue) from 12Z 2/13/2000 - 12Z 2/23/2000
ETAX
AVN
NUMBER OF OBS PTS (FROM FIRST TRACE):
3665 2045 1245 677 392 238 97 45 4
Equitable threat score
0.36
0.32
0.28
0.24
0.20
0.16
0.12
0.08
0.04
0.00
0.01 0.10 0.25 0.50 0.75 1.00 1.50 2.00 3.00
Threshold (in)

Figure 19b

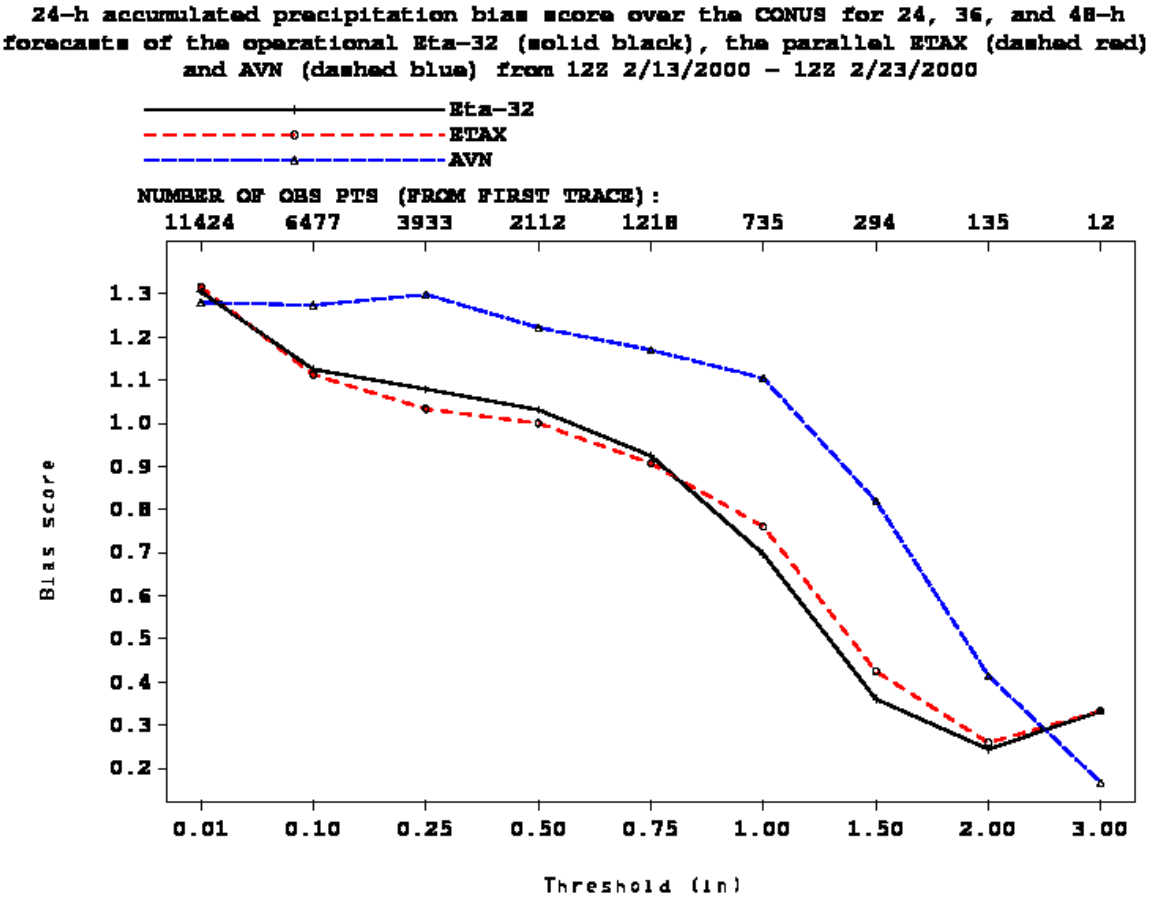
24-h accumulated precipitation bias score over the CONUS for 24, 36, and 48-h forecasts of the operational Eta-32 (solid black), the parallel ETAX (dashed red) and AVN (dashed blue) from 12Z 2/13/2000 - 12Z 2/23/2000
Eta-32
ETAX
AVN
NUMBER OF OBS PTS (FROM FIRST TRACE):
11424 6477 3933 2112 1218 735 294 135 12
Bias score
1.3
1.2
1.1
1.0
0.9
0.8
0.7
0.6
0.5
0.4
0.3
0.2
0.01 0.10 0.25 0.50 0.75 1.00 1.50 2.00 3.00
Threshold (in)

Figure 20a

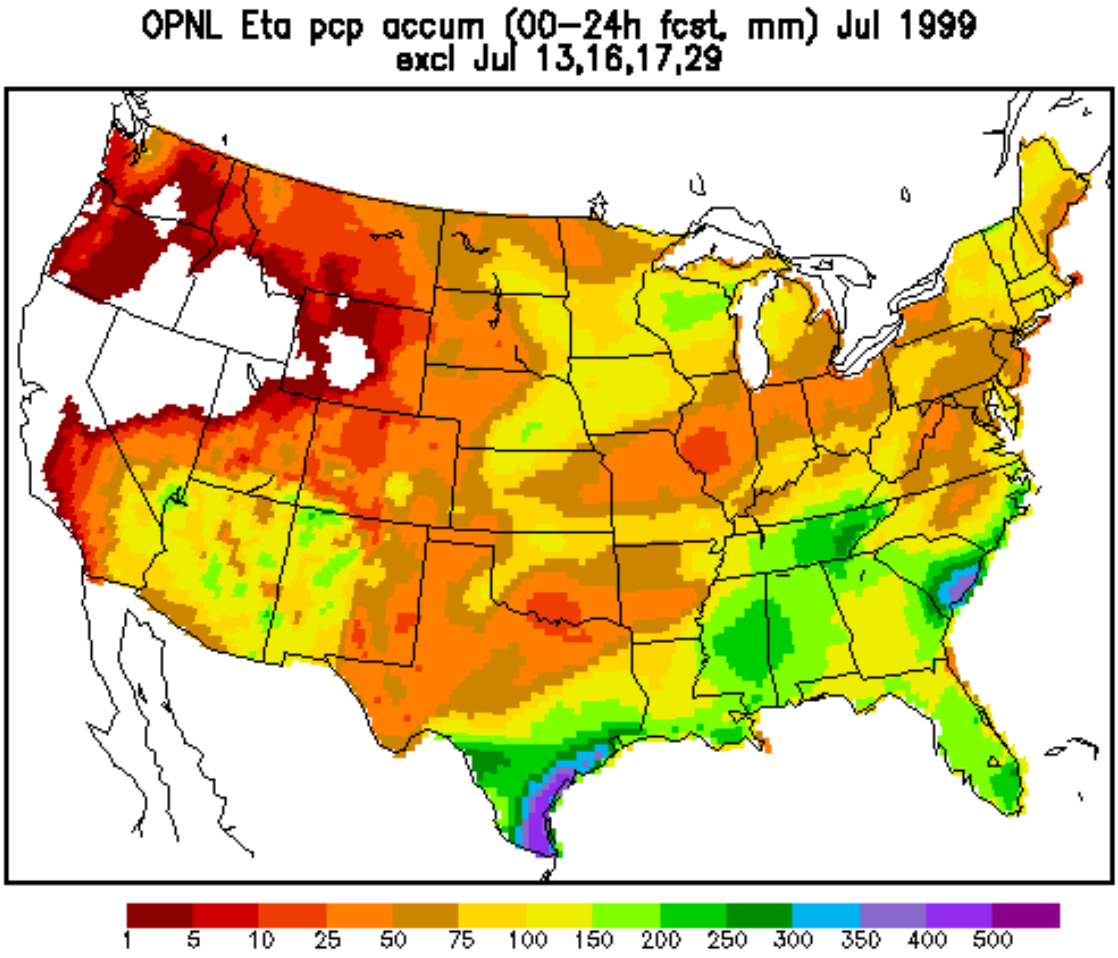
OPNL Eta pcp accum (00–24h fcst, mm) Jul 1999
excl Jul 13,16,17,29
1
5
10
25
50
75
100
150
200
250
300
350
400
500

Figure 20b

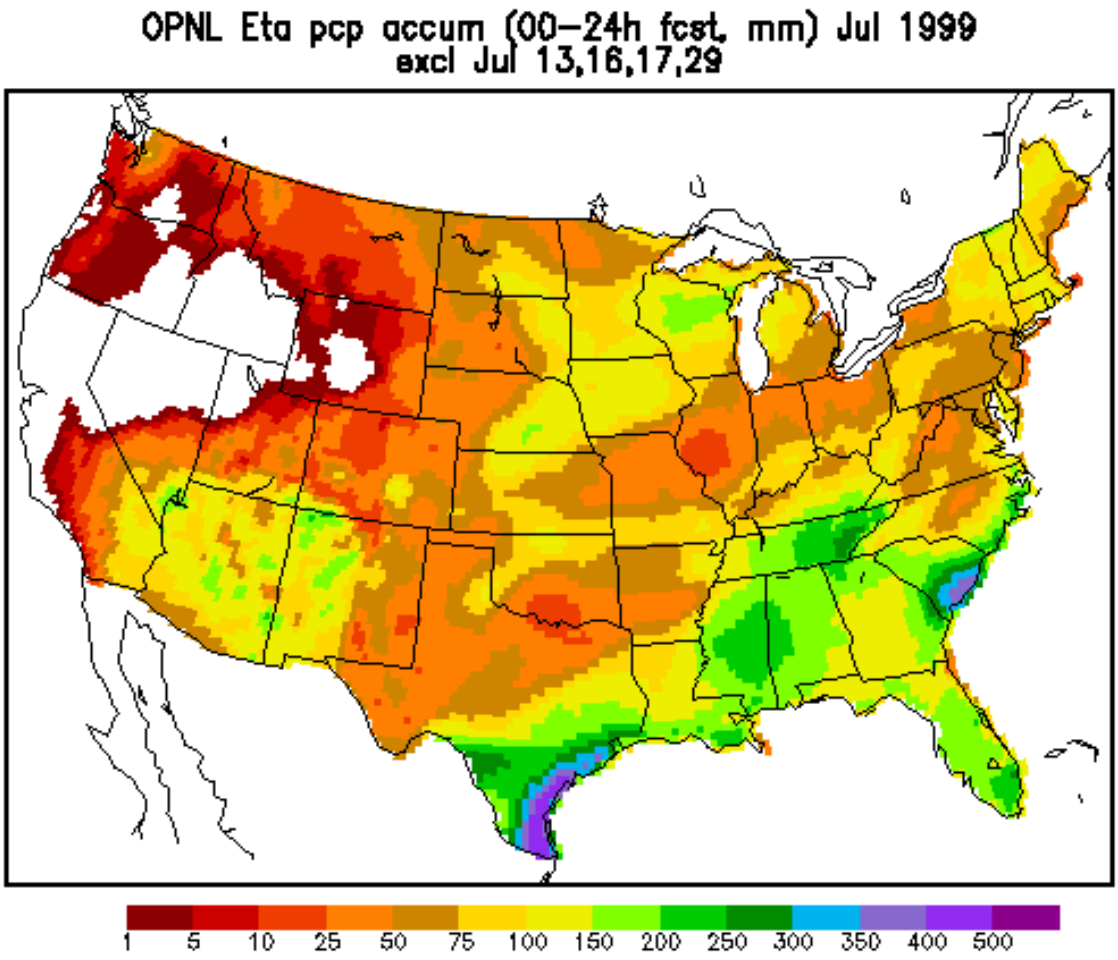
OPNL Eta pcp accum (00–24h fcst, mm) Jul 1999
excl Jul 13,16,17,29
1
5
10
25
50
75
100
150
200
250
300
350
400
500

Figure 21a

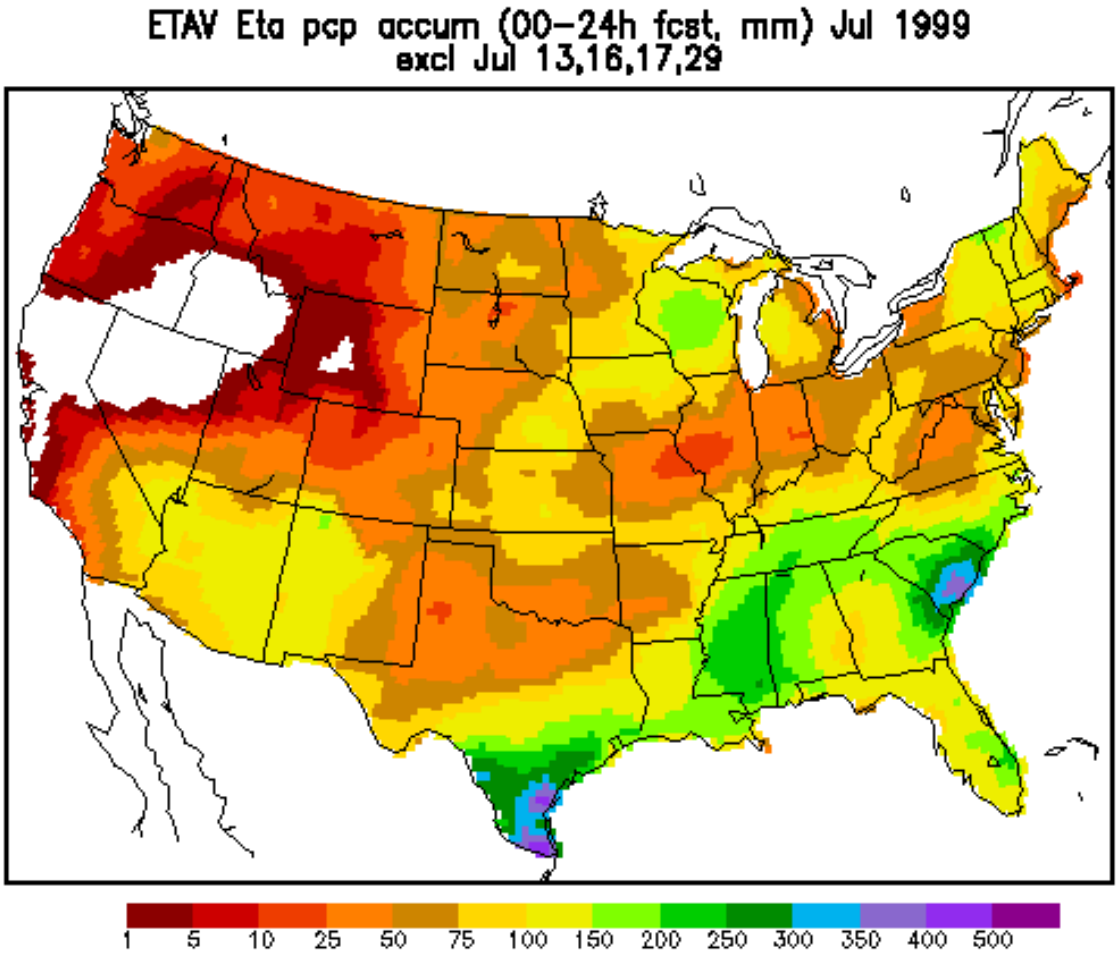
ETAV Eta pcp accum (00-24h fcst, mm) Jul 1999
excl Jul 13,16,17,29
1
5
10
25
50
75
100
150
200
250
300
350
400
500

Figure 21b

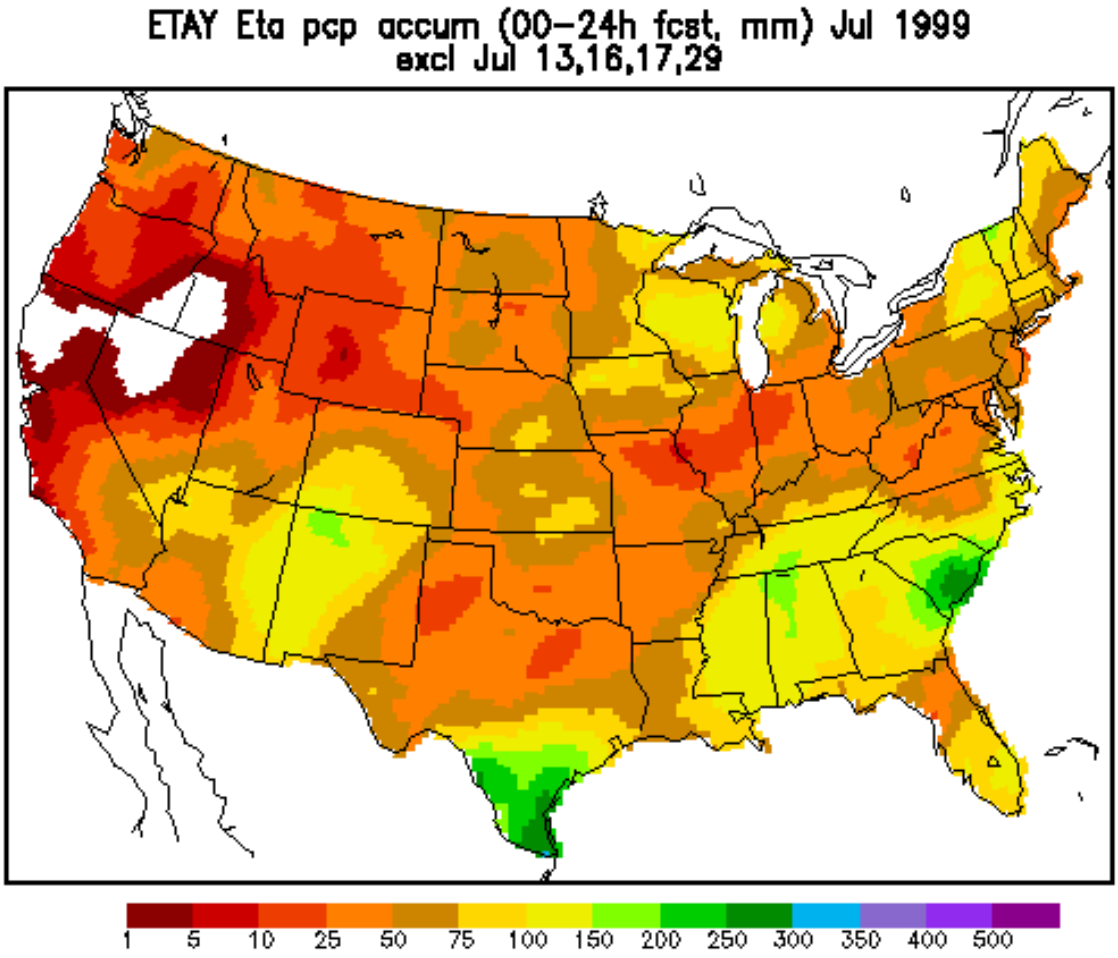
ETAY Eta pcp accum (00-24h fcst, mm) Jul 1999
excl Jul 13,16,17,29
1
5
10
25
50
75
100
150
200
250
300
350
400
500

Figure 21c

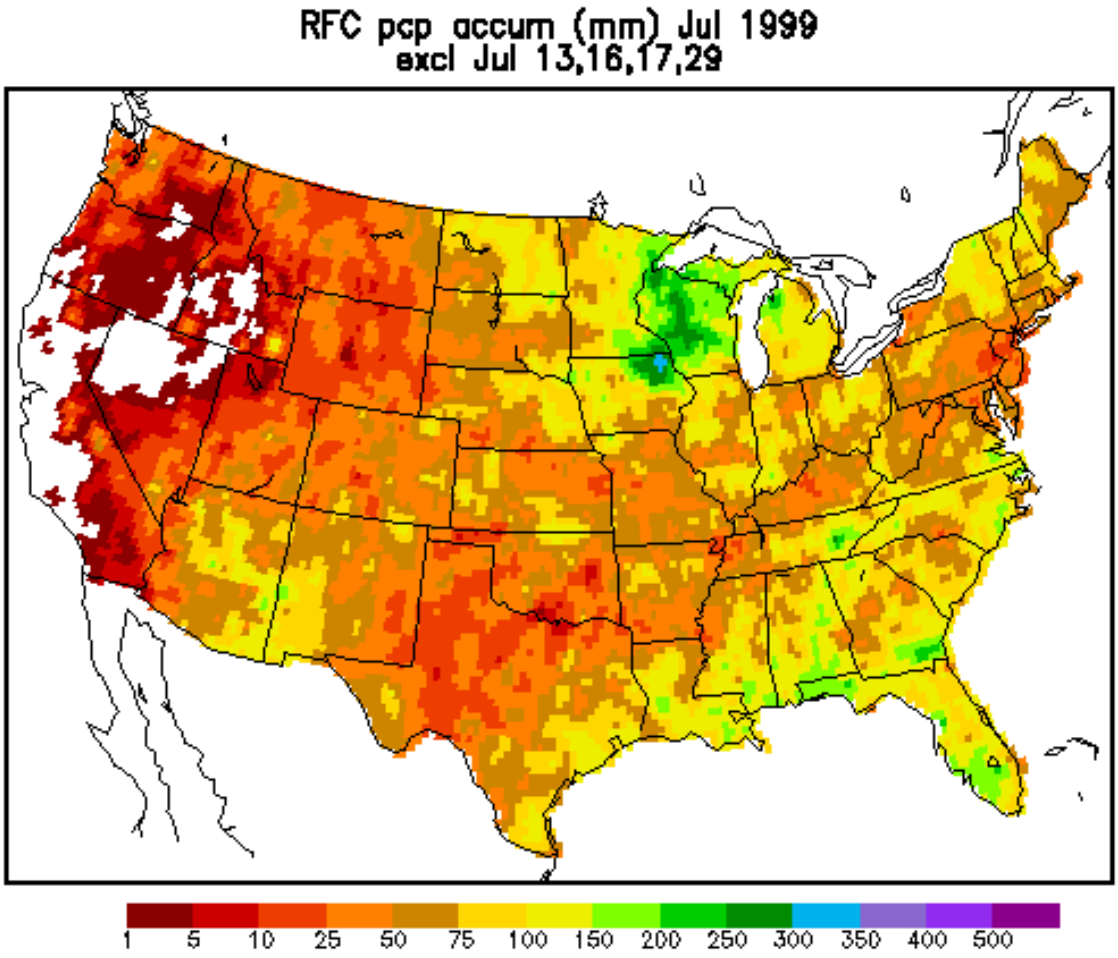
RFC pcp accum (mm) Jul 1999
excl Jul 13,16,17,29
1
5
10
25
50
75
100
150
200
250
300
350
400
500

Figure 21d

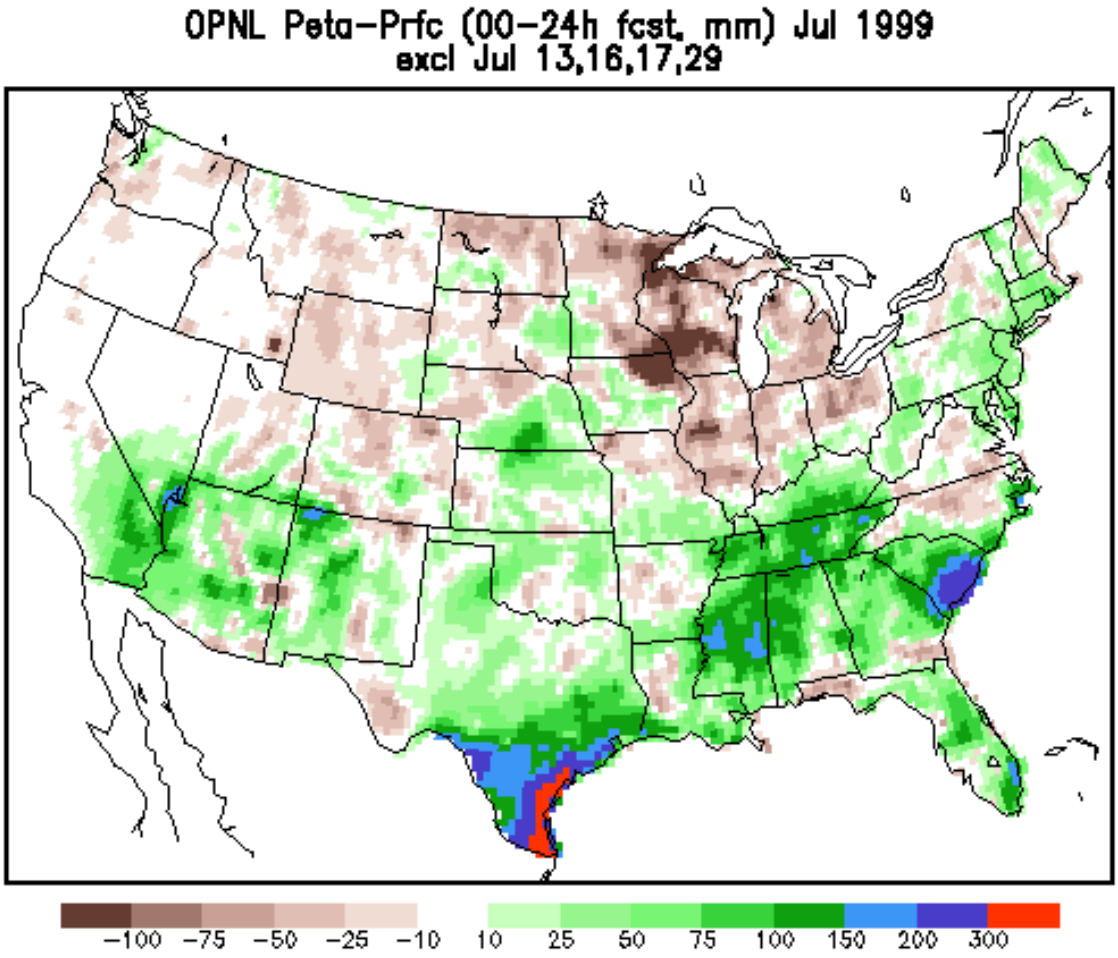
OPNL Peta-Prfc (00-24h fcst, mm) Jul 1999
excl Jul 13,16,17,29
-100 -75 -50 -25 -10 10 25 50 75 100 150 200 300

Figure 22a

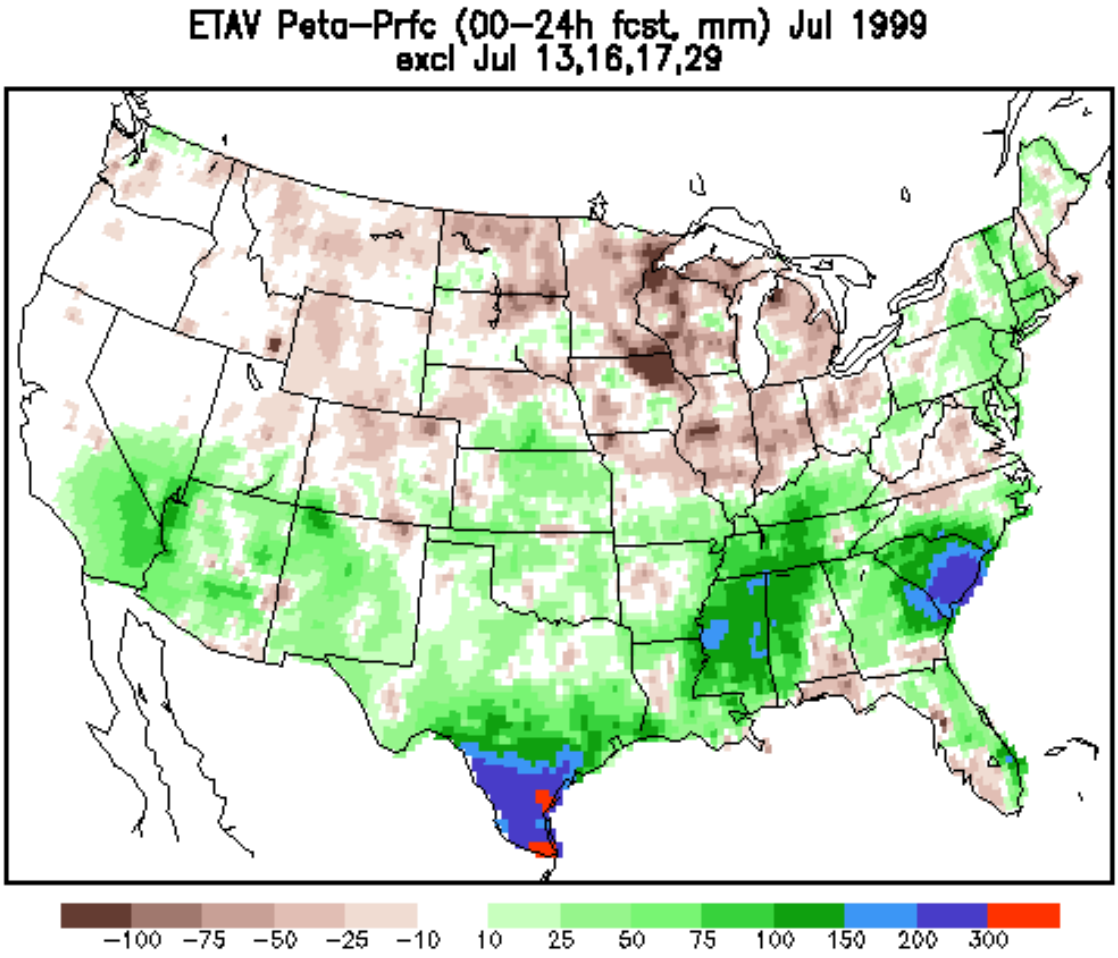
ETAV Peta–Prfc (00–24h fcst, mm) Jul 1999
excl Jul 13,16,17,29
–100 –75 –50 –25 –10 10 25 50 75 100 150 200 300

Figure 22b

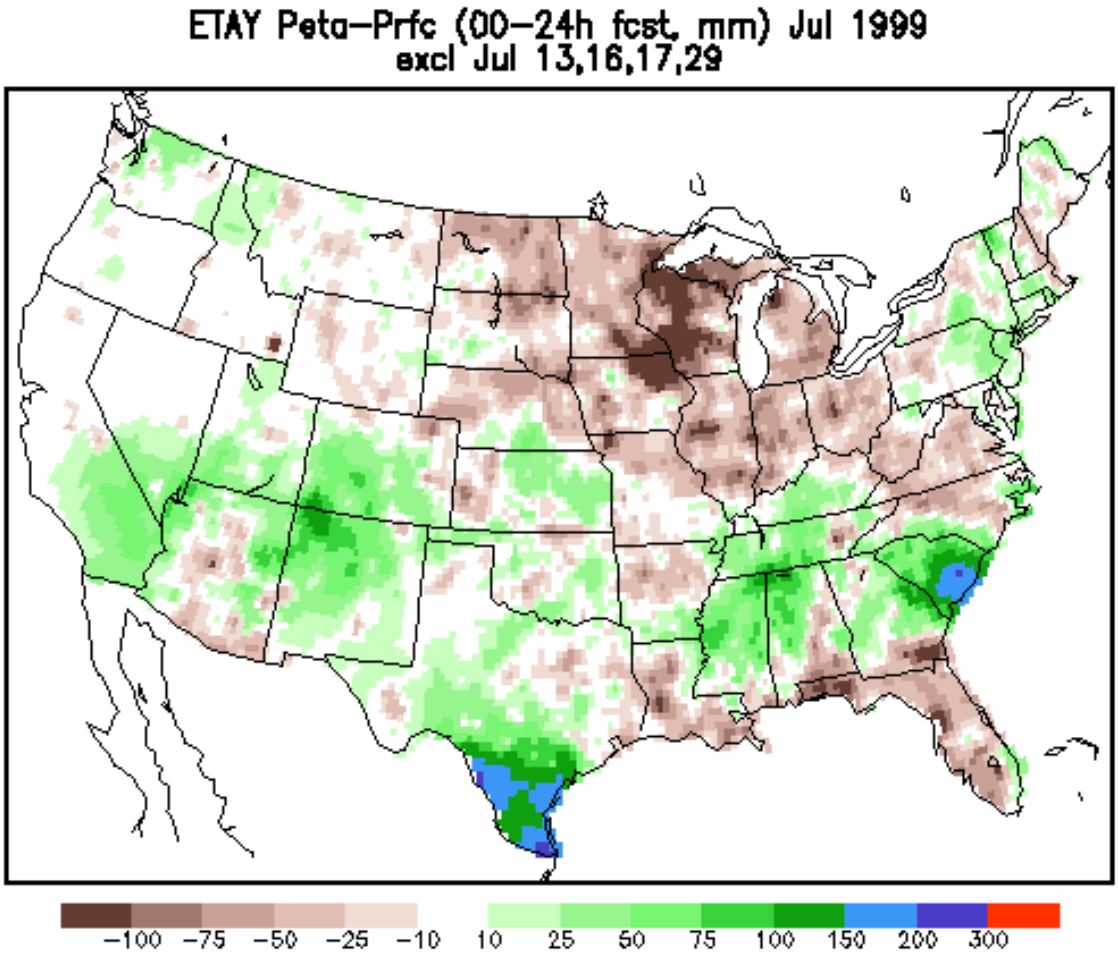
ETAY Peta-Prfc (00-24h fcst, mm) Jul 1999
excl Jul 13,16,17,29
-100 -75 -50 -25 -10 10 25 50 75 100 150 200 300

Figure 22c

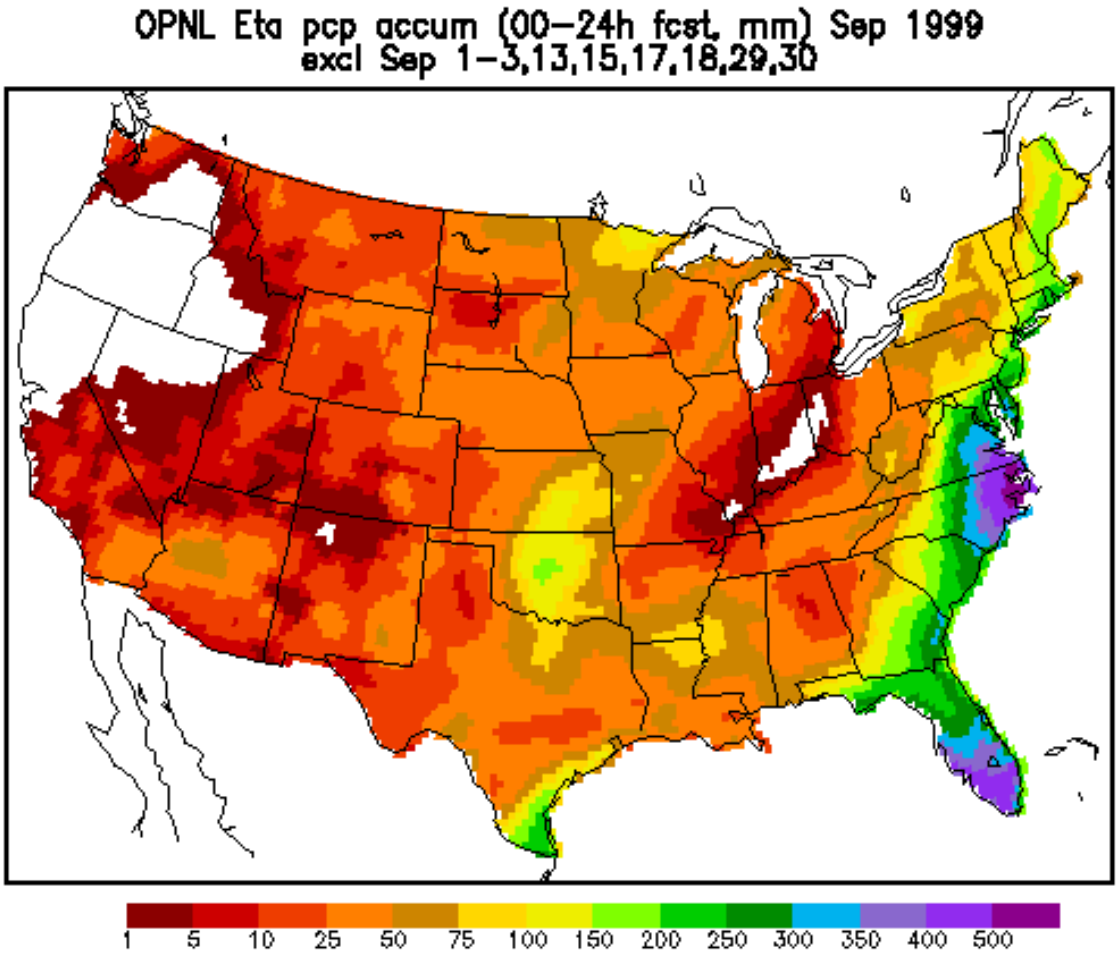
OPNL Eta pcp accum (00-24h fcst, mm) Sep 1999
excl Sep 1-3,13,15,17,18,29,30
1
5
10
25
50
75
100
150
200
250
300
350
400
500

Figure 23a

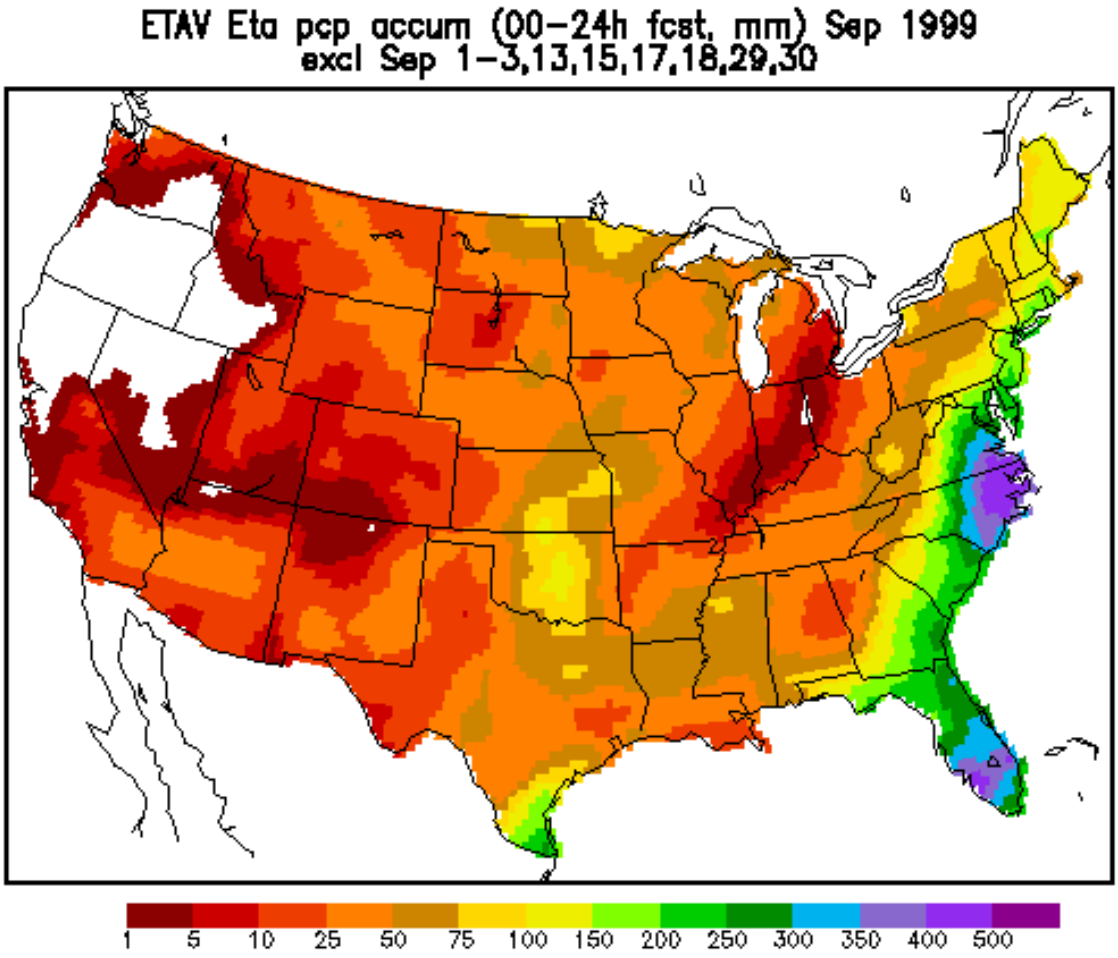
ETAV Eta pcp accum (00-24h fcst, mm) Sep 1999
excl Sep 1-3,13,15,17,18,29,30
1
5
10
25
50
75
100
150
200
250
300
350
400
500

Figure 23b

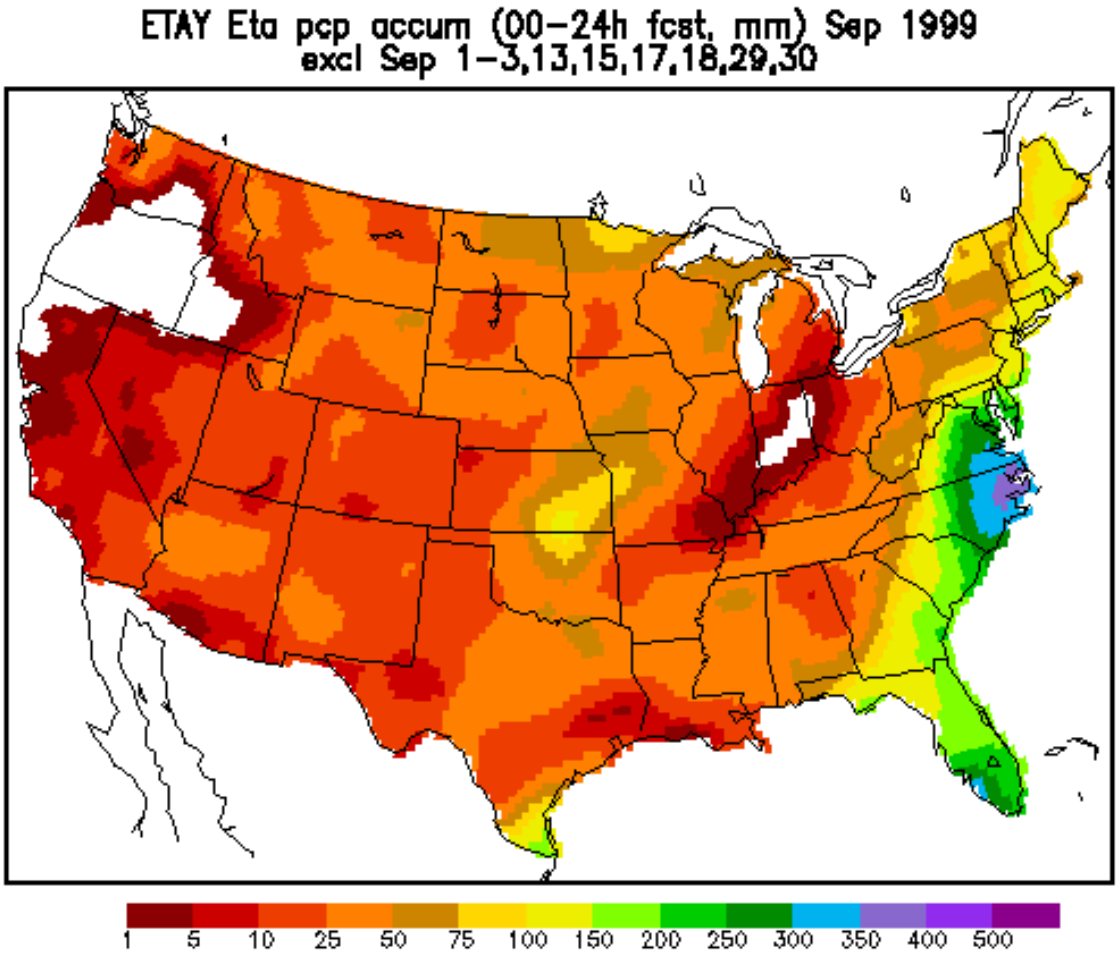
ETAY Eta pcp accum (00-24h fcst, mm) Sep 1999
excl Sep 1-3,13,15,17,18,29,30
1
5
10
25
50
75
100
150
200
250
300
350
400
500

Figure 23c

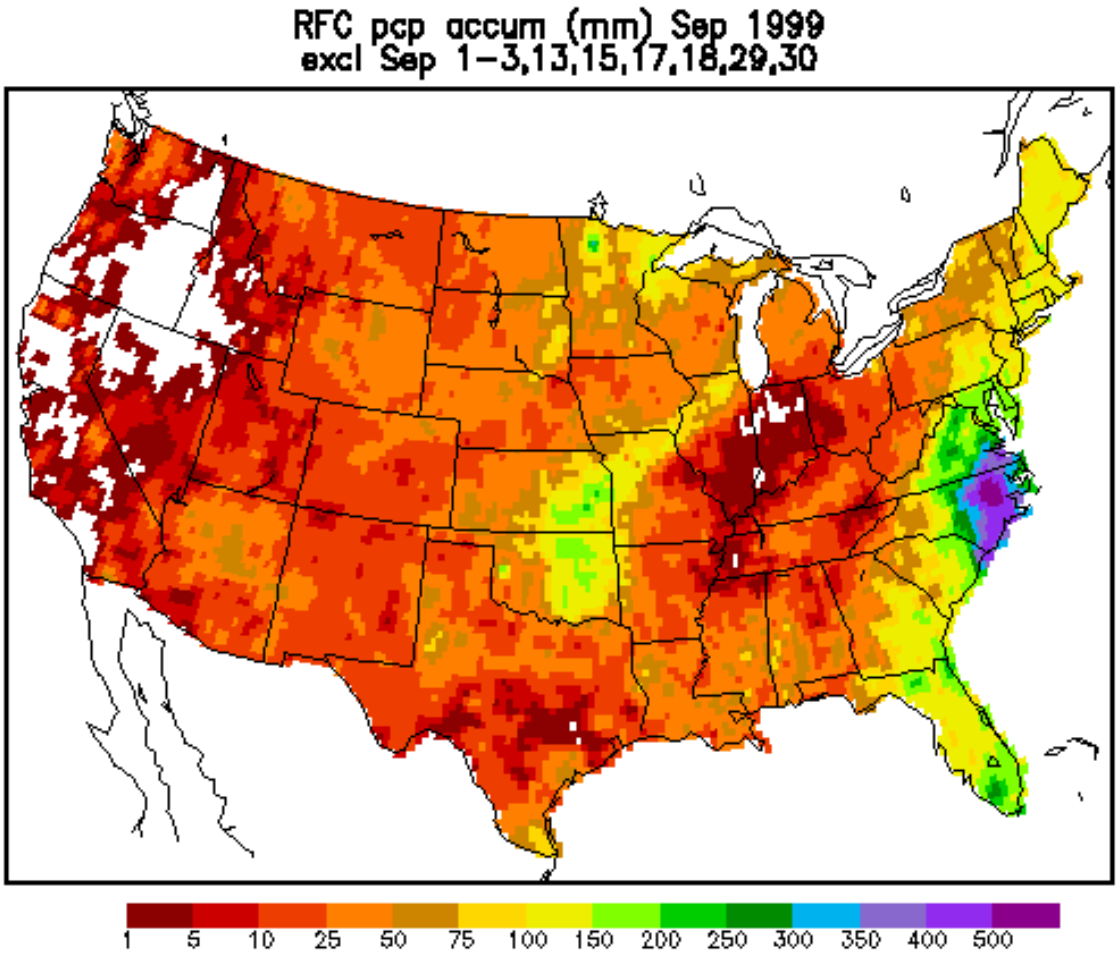
RFC pcp accum (mm) Sep 1999
excl Sep 1-3,13,15,17,18,29,30
1
5
10
25
50
75
100
150
200
250
300
350
400
500

Figure 23d

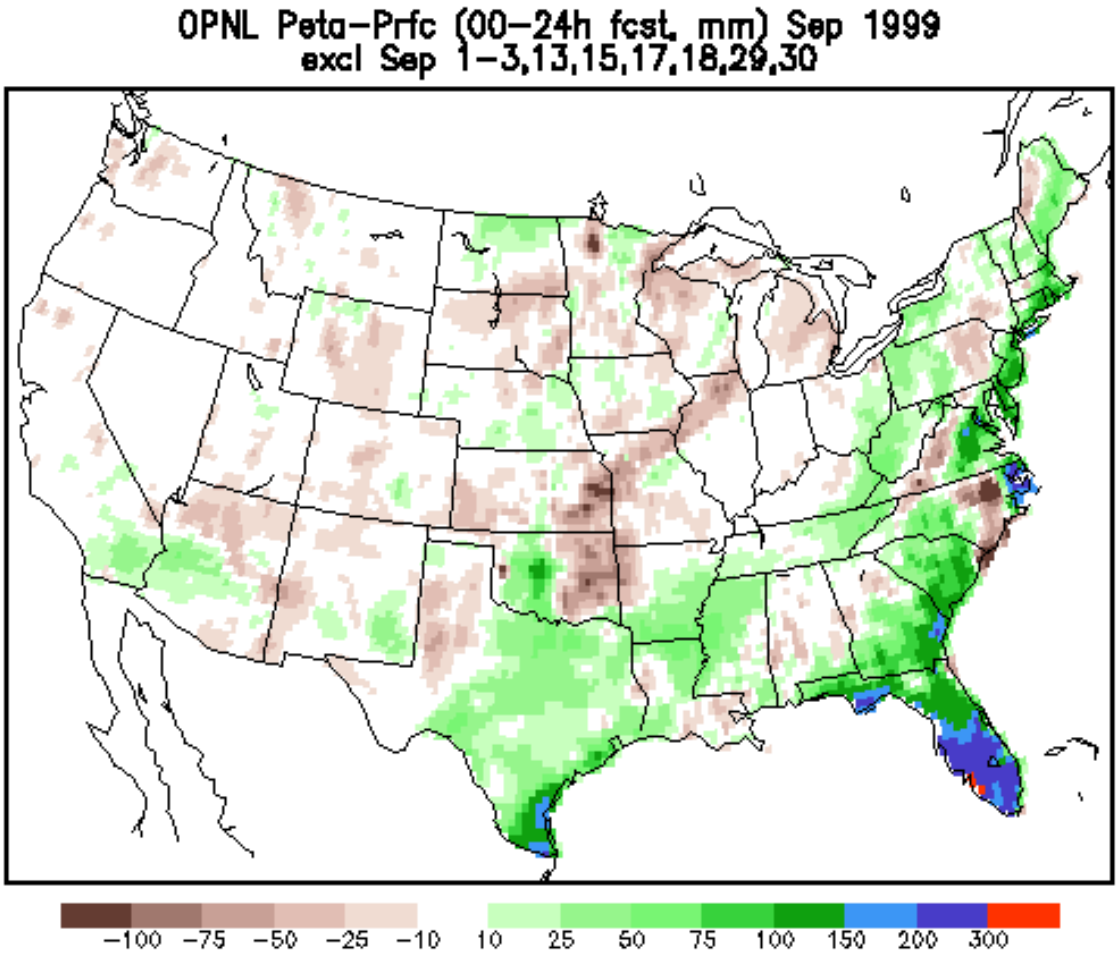
OPNL Peta-Prfc (00-24h fcst, mm) Sep 1999
excl Sep 1-3,13,15,17,18,29,30
-100 -75 -50 -25 -10 10 25 50 75 100 150 200 300

Figure 24a

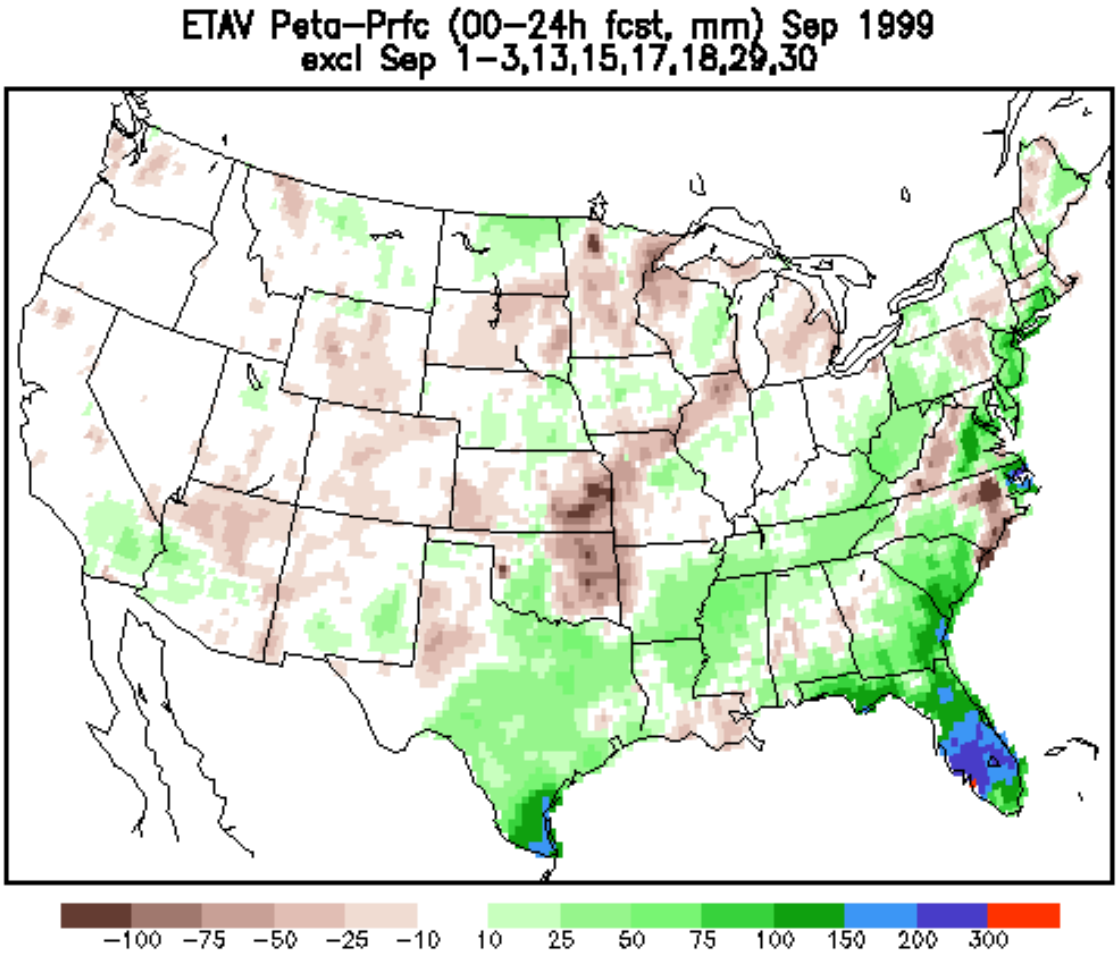
ETAV Peta-Prfc (00-24h fcst, mm) Sep 1999
excl Sep 1-3,13,15,17,18,29,30
-100 -75 -50 -25 -10 10 25 50 75 100 150 200 300

Figure 24b

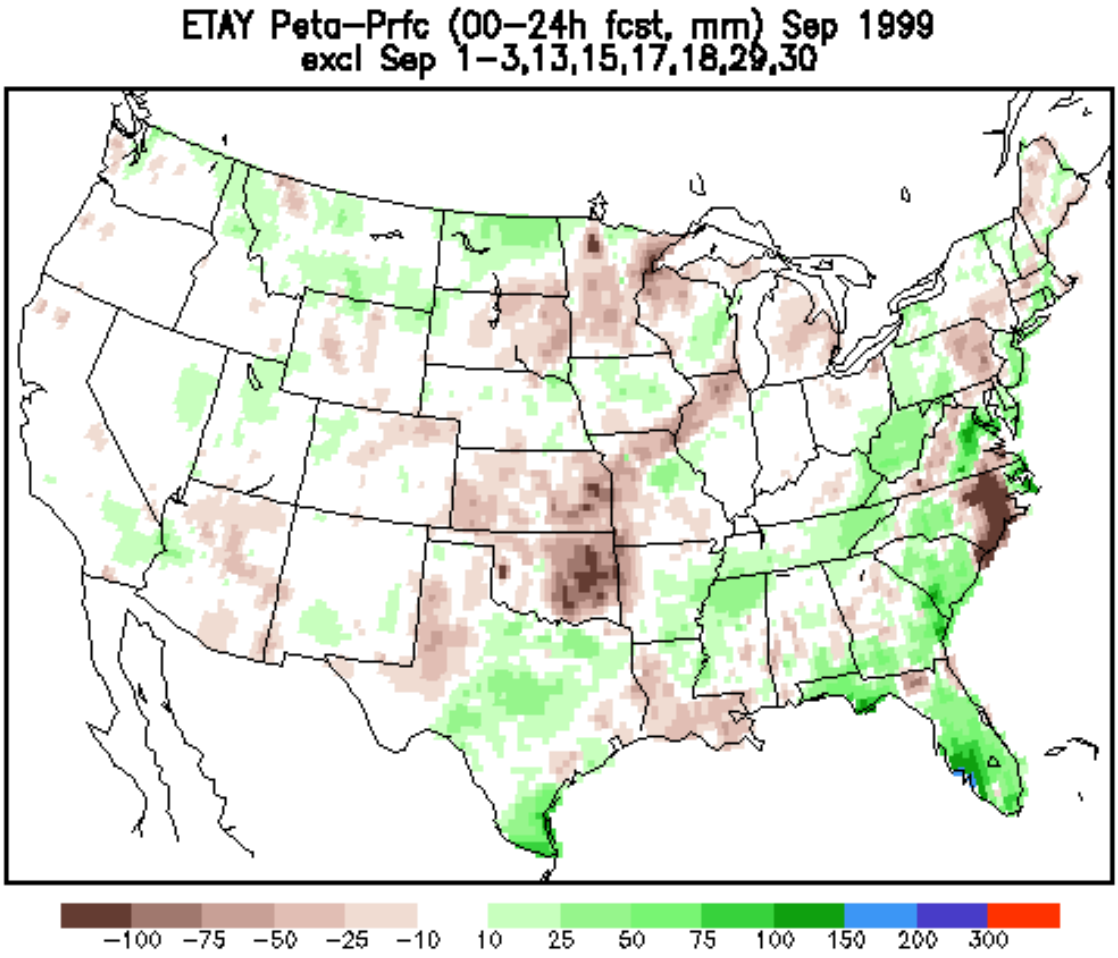
ETAY Peta-Prfc (00-24h fcst, mm) Sep 1999
excl Sep 1-3,13,15,17,18,29,30
-100 -75 -50 -25 -10 10 25 50 75 100 150 200 300

Figure 24c

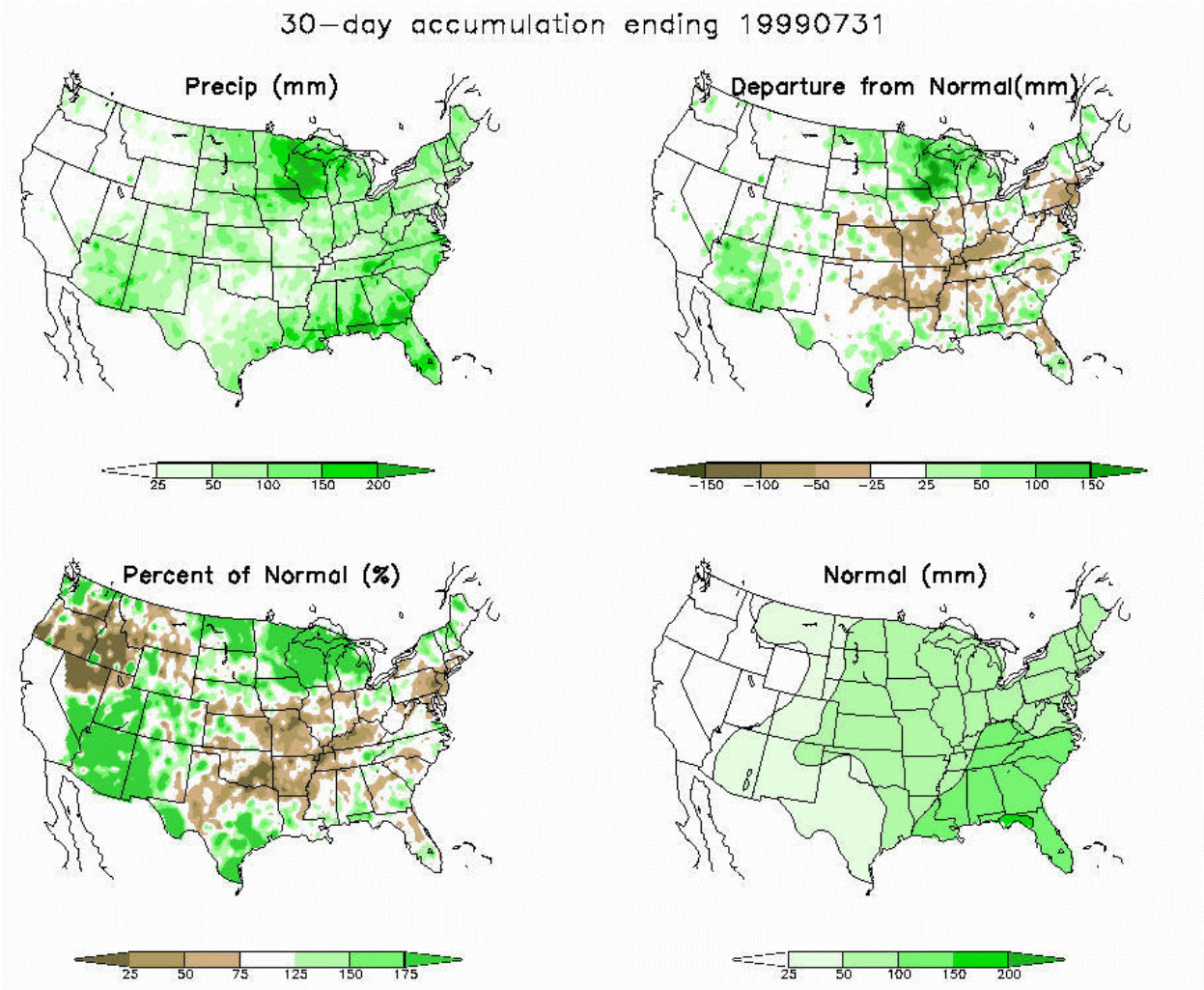
30-day accumulation ending 19990731
Precip (mm)
25 50 100 150 200
Departure from Normal(mm)
-150 -100 -50 -25 25 50 100 150
Percent of Normal (%)
25 50 75 125 150 175
Normal (mm)
25 50 100 150 200

Figure 25

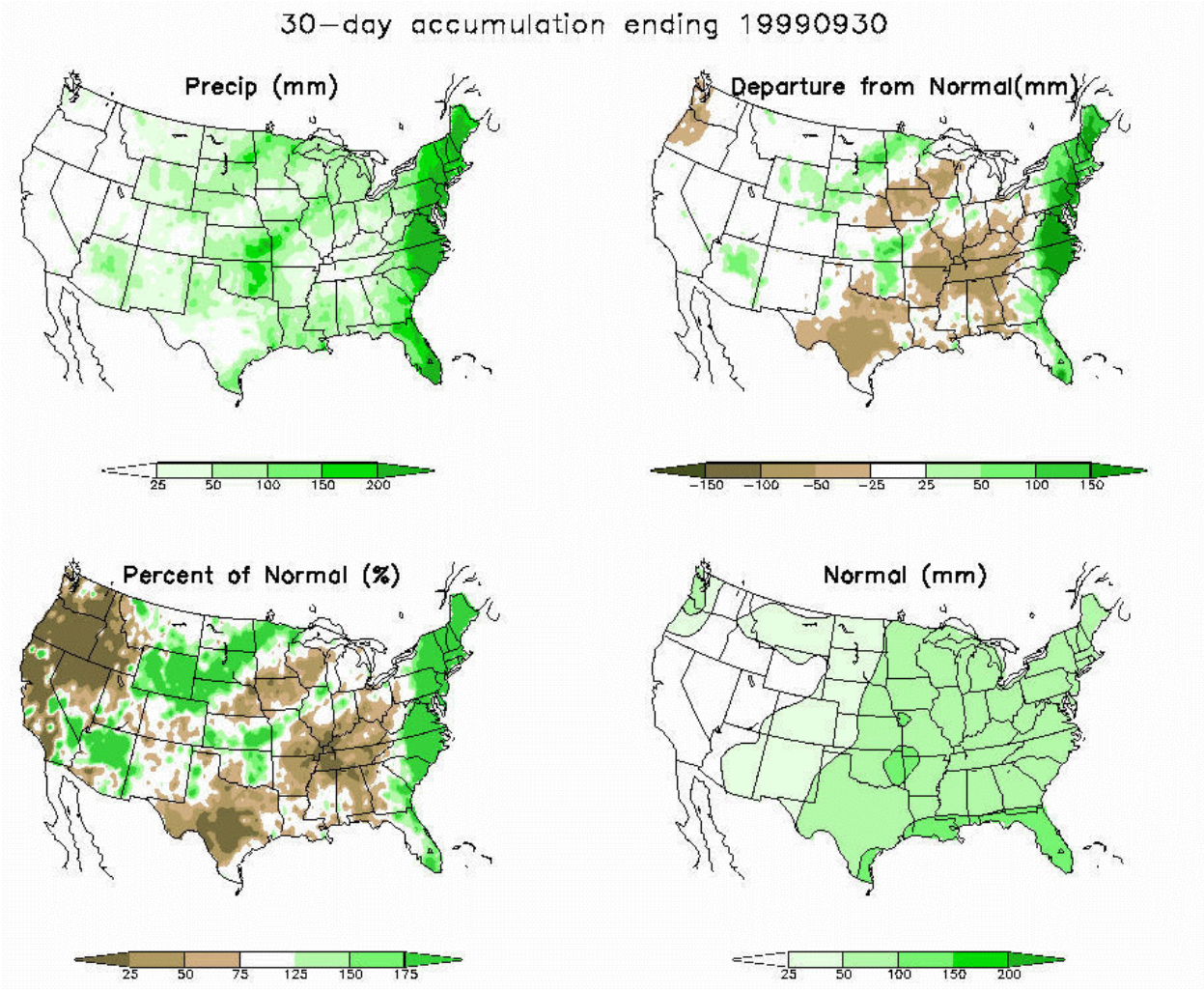
30-day accumulation ending 19990930
Precip (mm)
25 50 100 150 200
Departure from Normal(mm)
-150 -100 -50 -25 25 50 100 150
Percent of Normal (%)
25 50 75 125 150 175
Normal (mm)
25 50 100 150 200

Figure 26

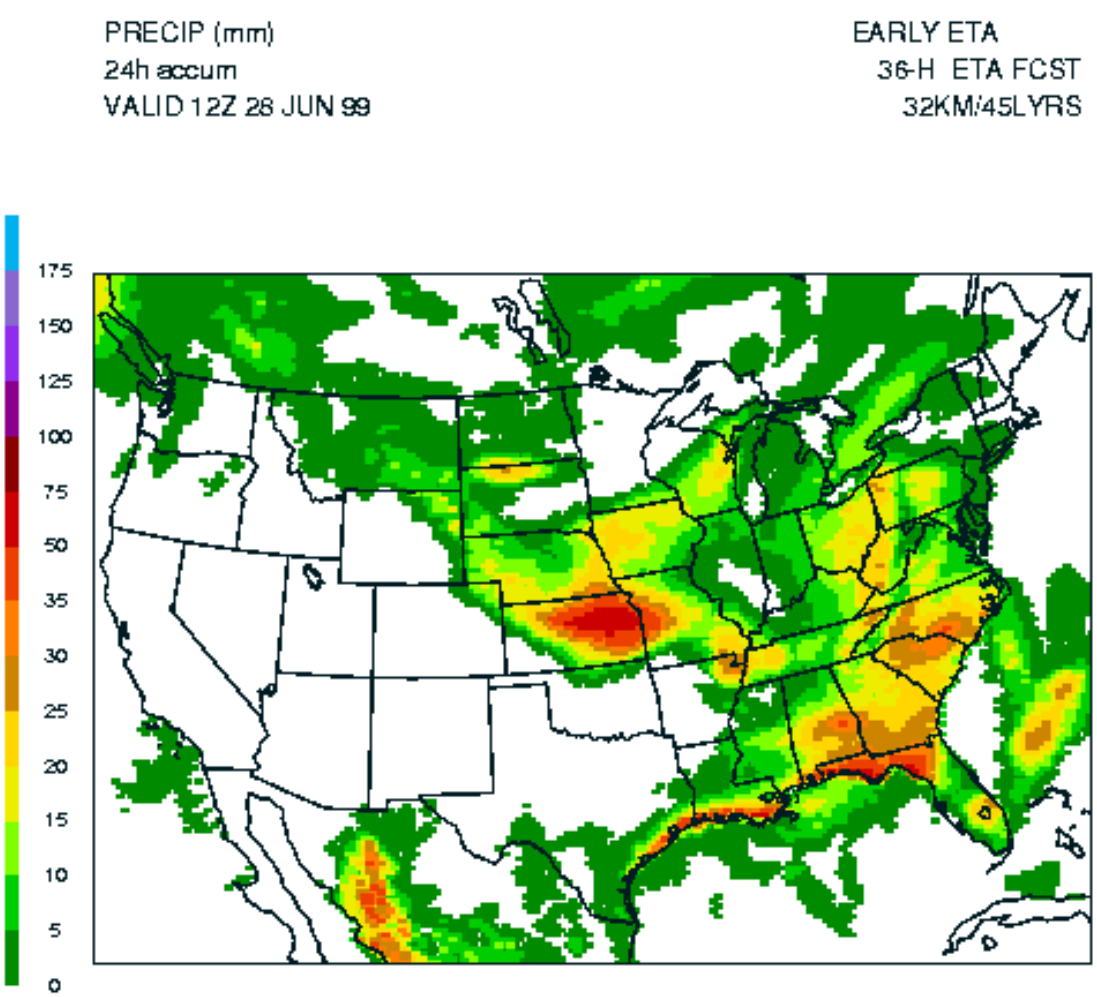
PRECIP (mm)
24h accum
VALID 12Z 28 JUN 99
EARLY ETA
36-H ETA FCST
32KM/45LYRS
175
150
125
100
75
50
35
30
25
20
15
10
5
0

Figure 27a

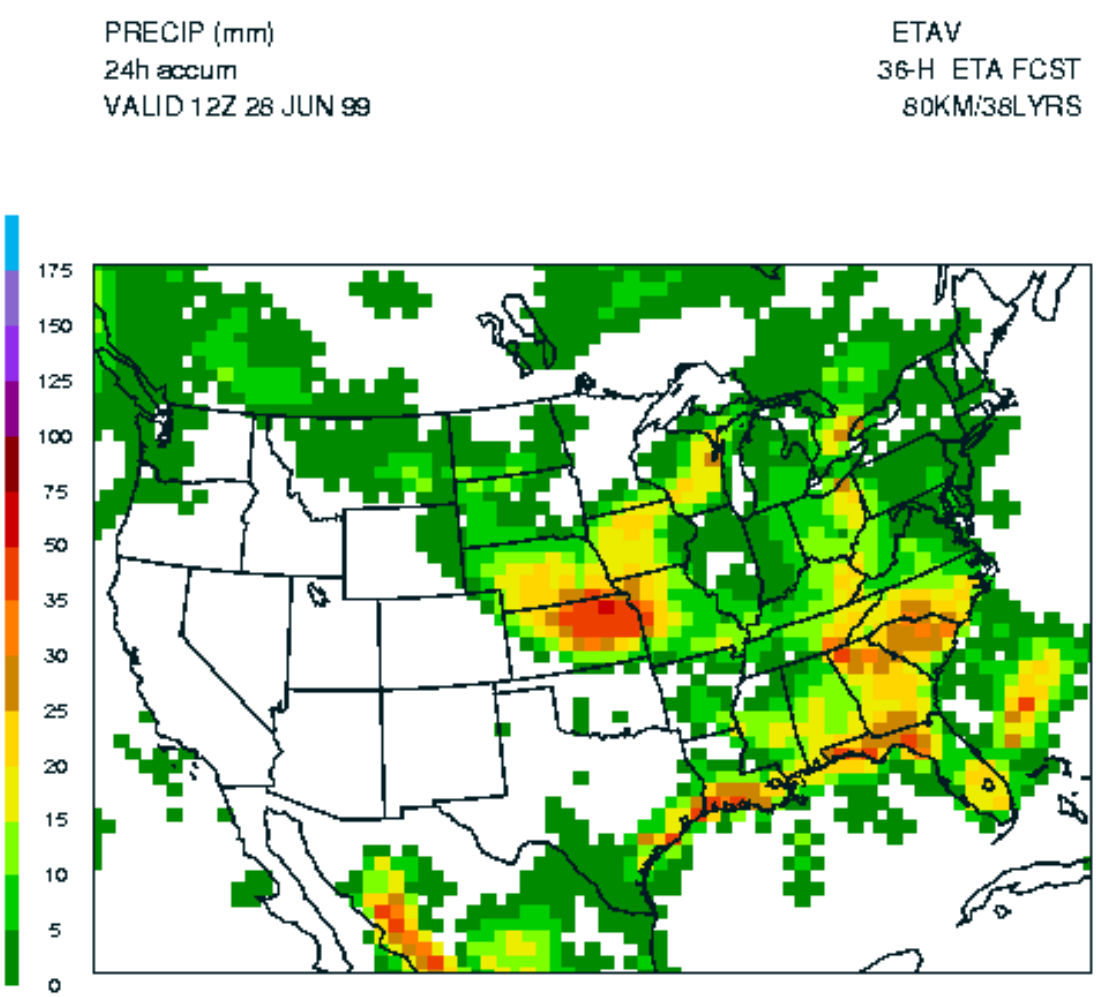
PRECIP (mm)
24h accum
VALID 12Z 28 JUN 99
ETAV
36-H ETA FCST
80KM/38LYRS
175
150
125
100
75
50
35
30
25
20
15
10
5
0

Figure 27b

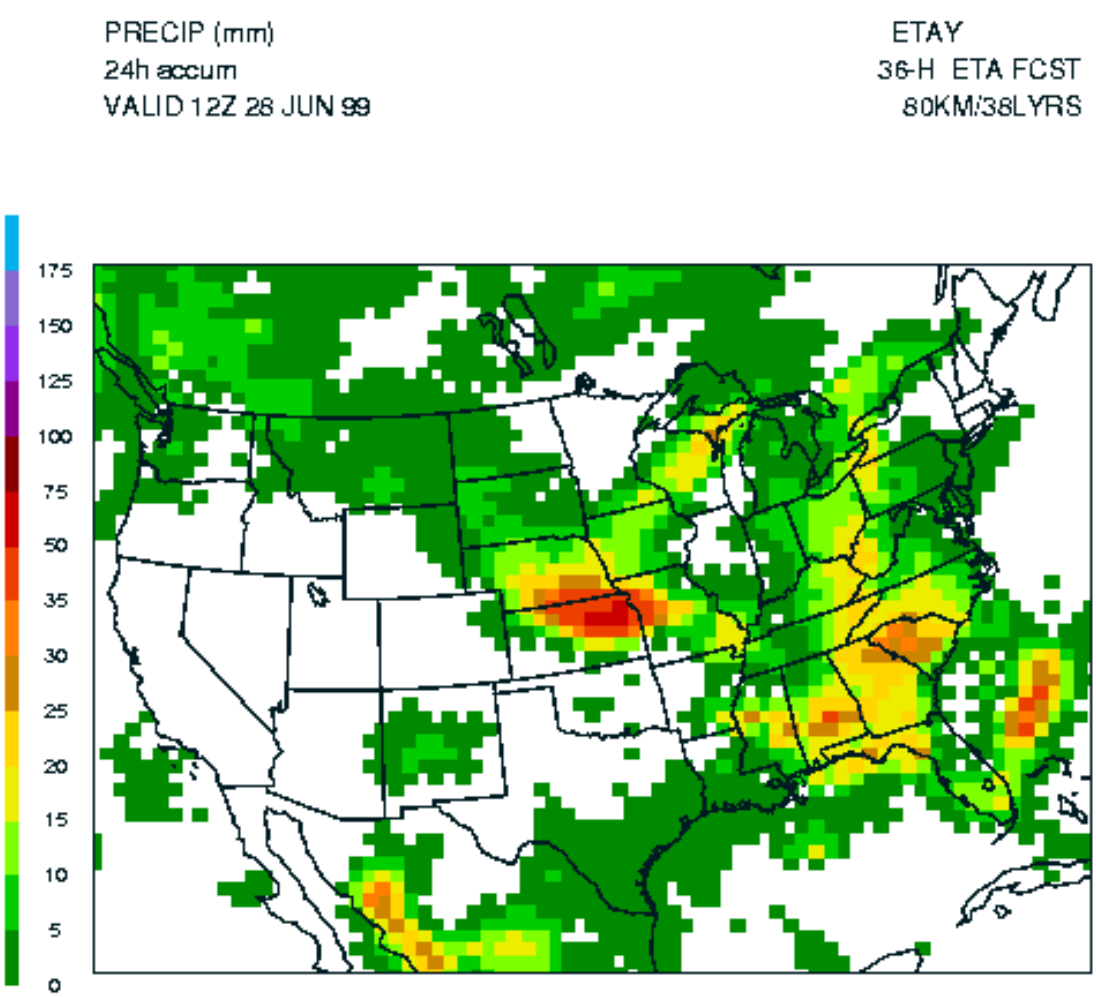
PRECIP (mm)
24h accum
VALID 12Z 28 JUN 99
ETAY
36-H ETA FCST
80KM/38LYRS
175
150
125
100
75
50
35
30
25
20
15
10
5
0

Figure 27c

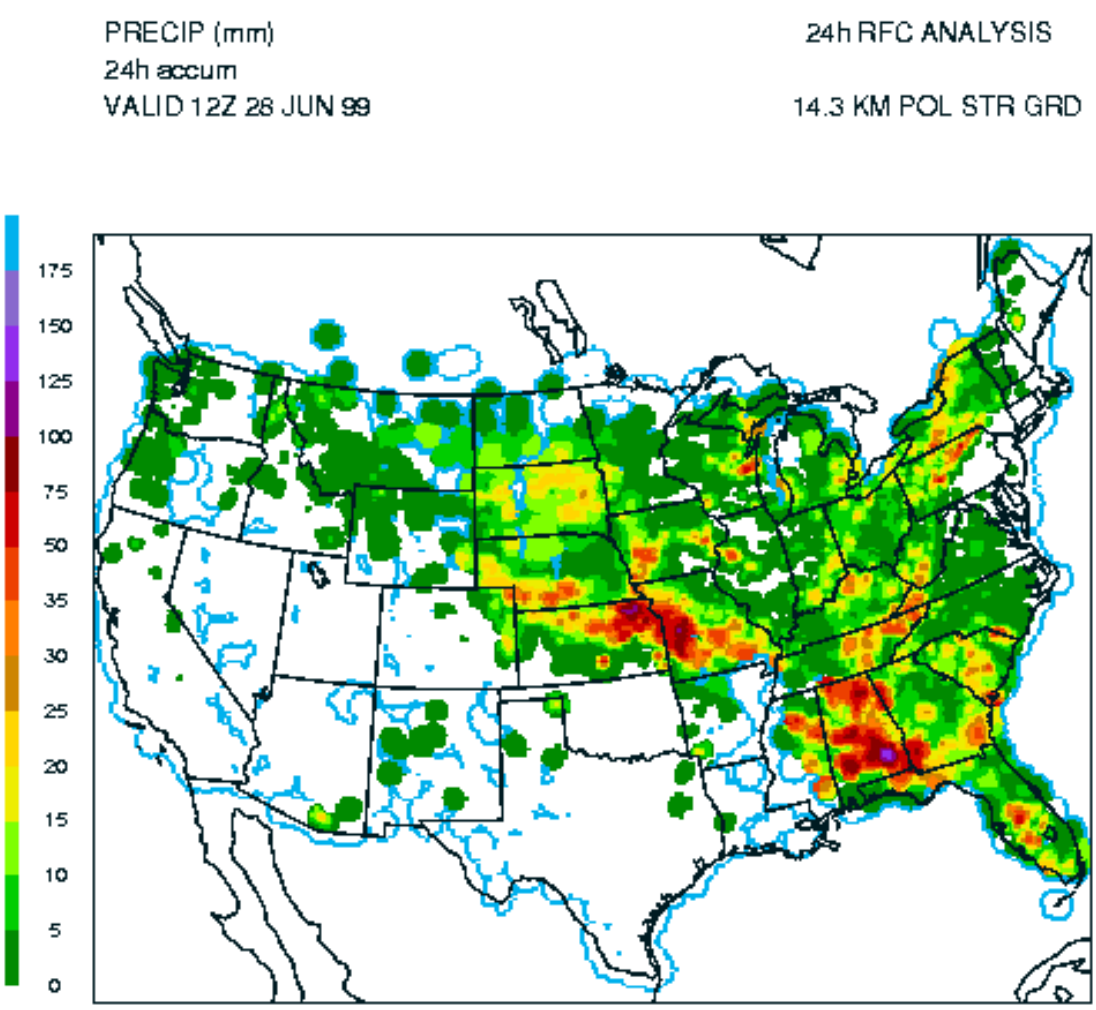
PRECIP (mm)
24h accum
VALID 12Z 28 JUN 99
24h RFC ANALYSIS
14.3 KM POL STR GRD
175
150
125
100
75
50
35
30
25
20
15
10
5
0

Figure 27d

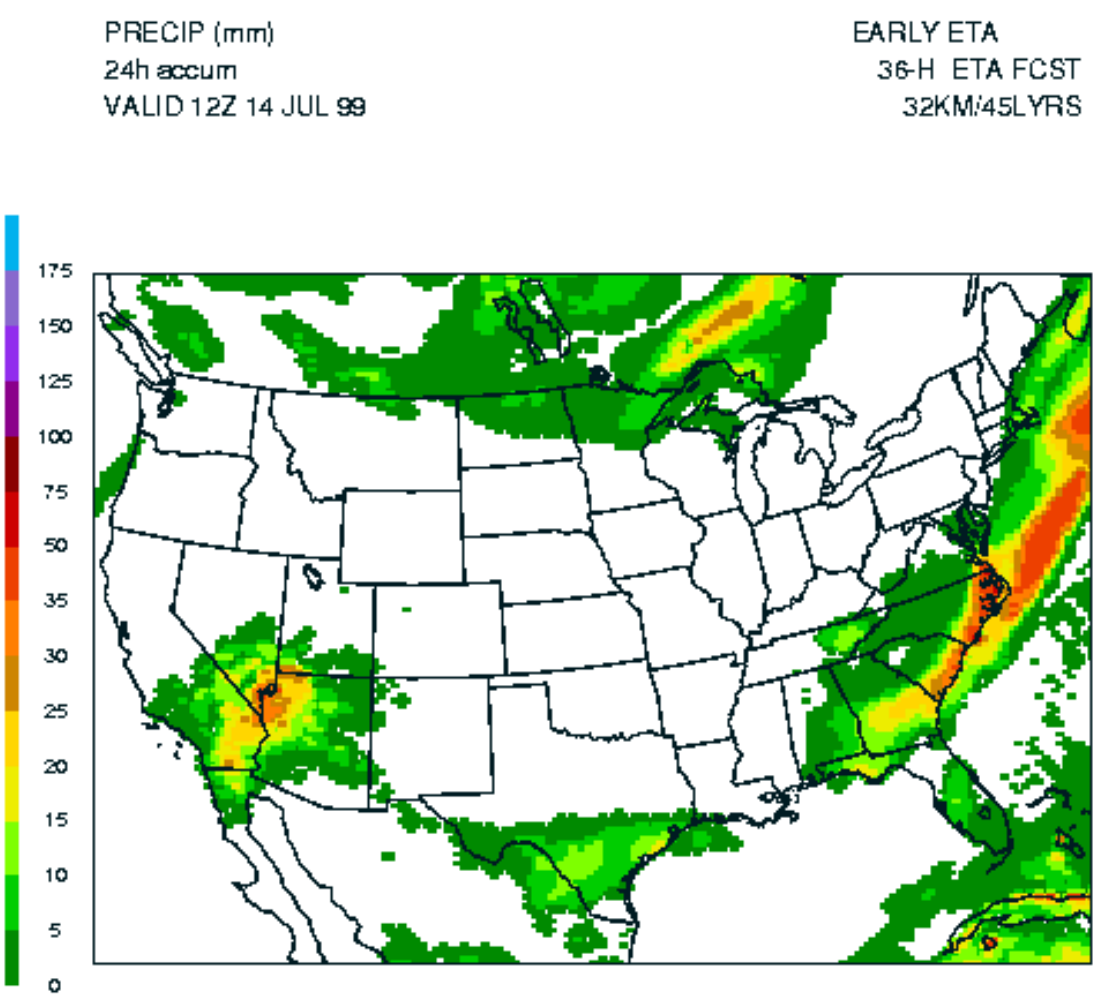
PRECIP (mm)
24h accum
VALID 12Z 14 JUL 99
EARLY ETA
36-H ETA FCST
32KM/45LYRS
175
150
125
100
75
50
35
30
25
20
15
10
5
0

Figure 28a

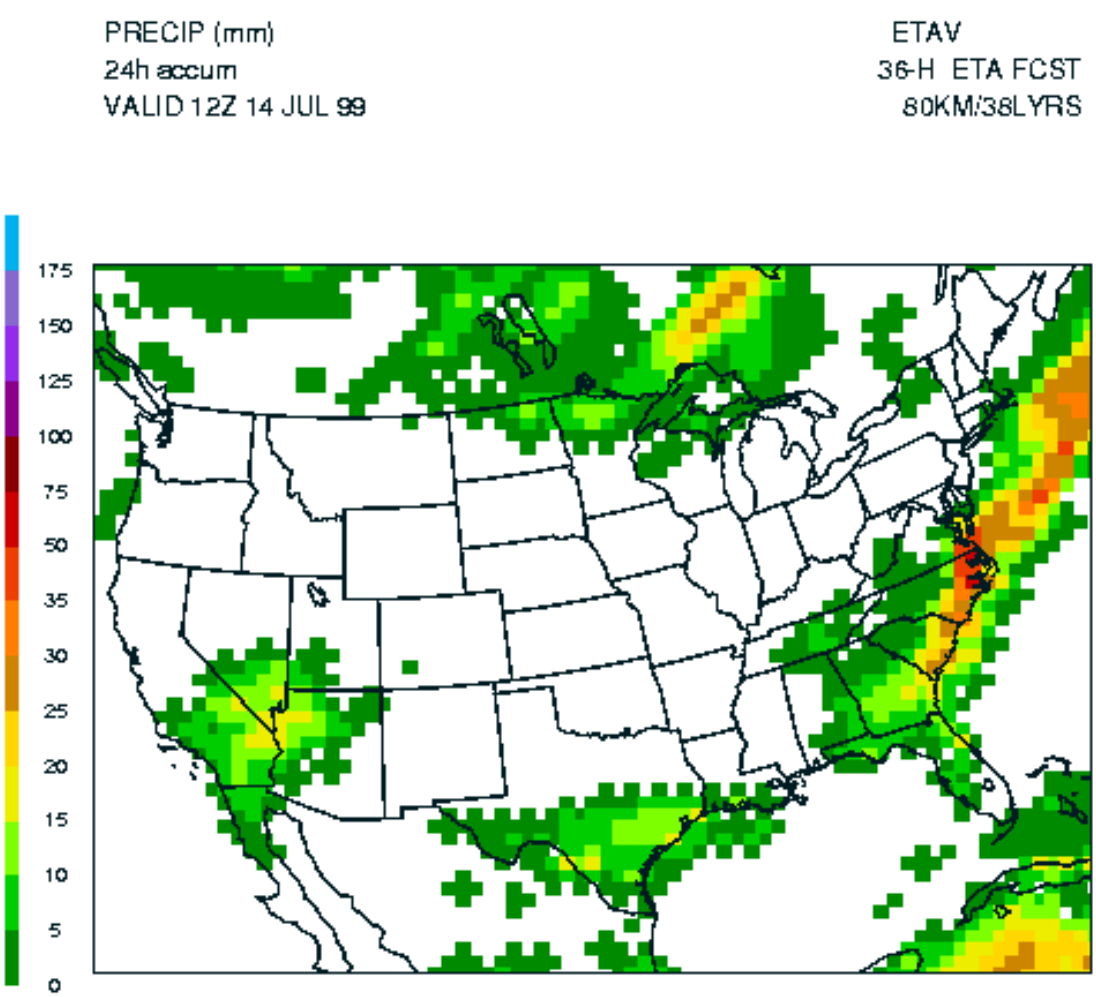
PRECIP (mm)
24h accum
VALID 12Z 14 JUL 99
ETAV
36-H ETA FCST
80KM/38LYRS
175
150
125
100
75
50
35
30
25
20
15
10
5
0

Figure 28b

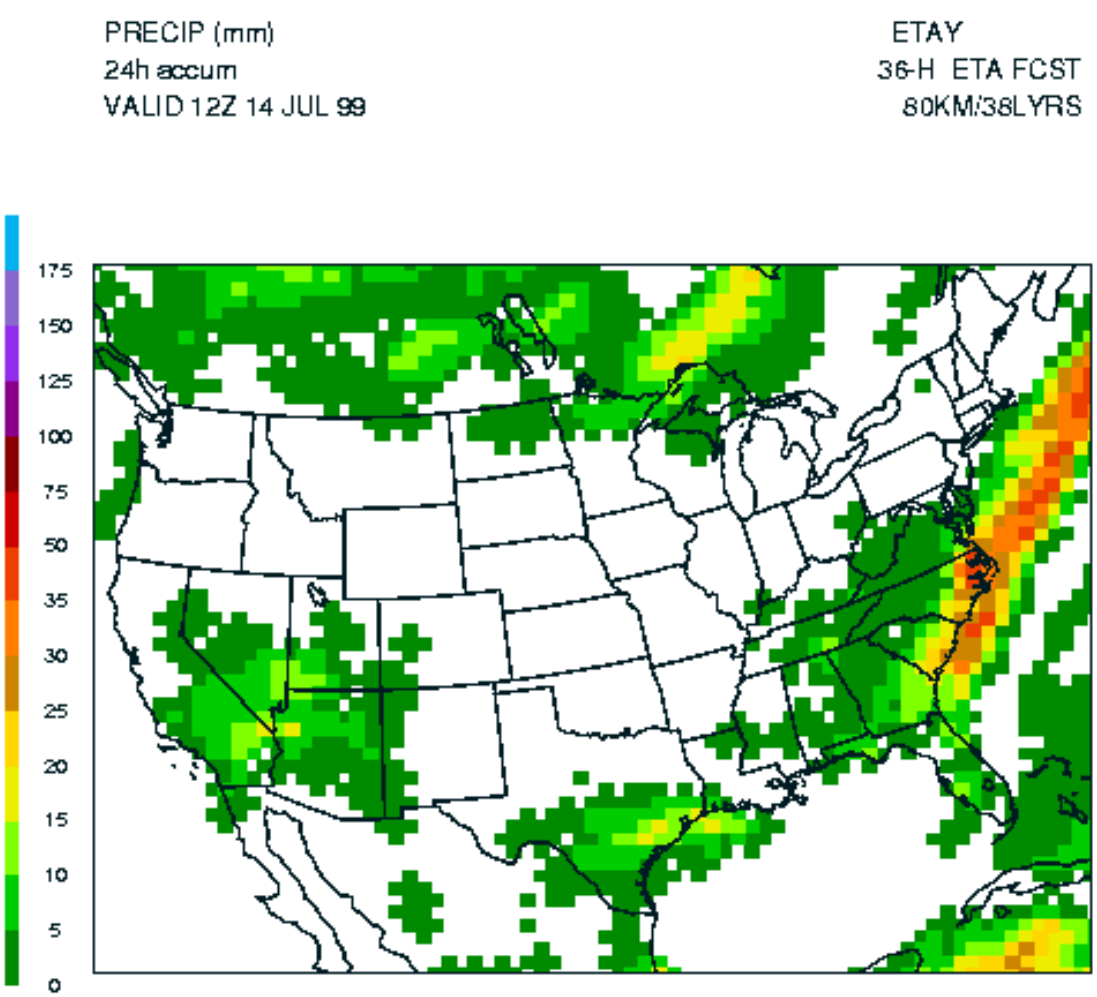
PRECIP (mm)
24h accum
VALID 12Z 14 JUL 99
ETAY
36-H ETA FCST
80KM/38LYRS
175
150
125
100
75
50
35
30
25
20
15
10
5
0

Figure 28c

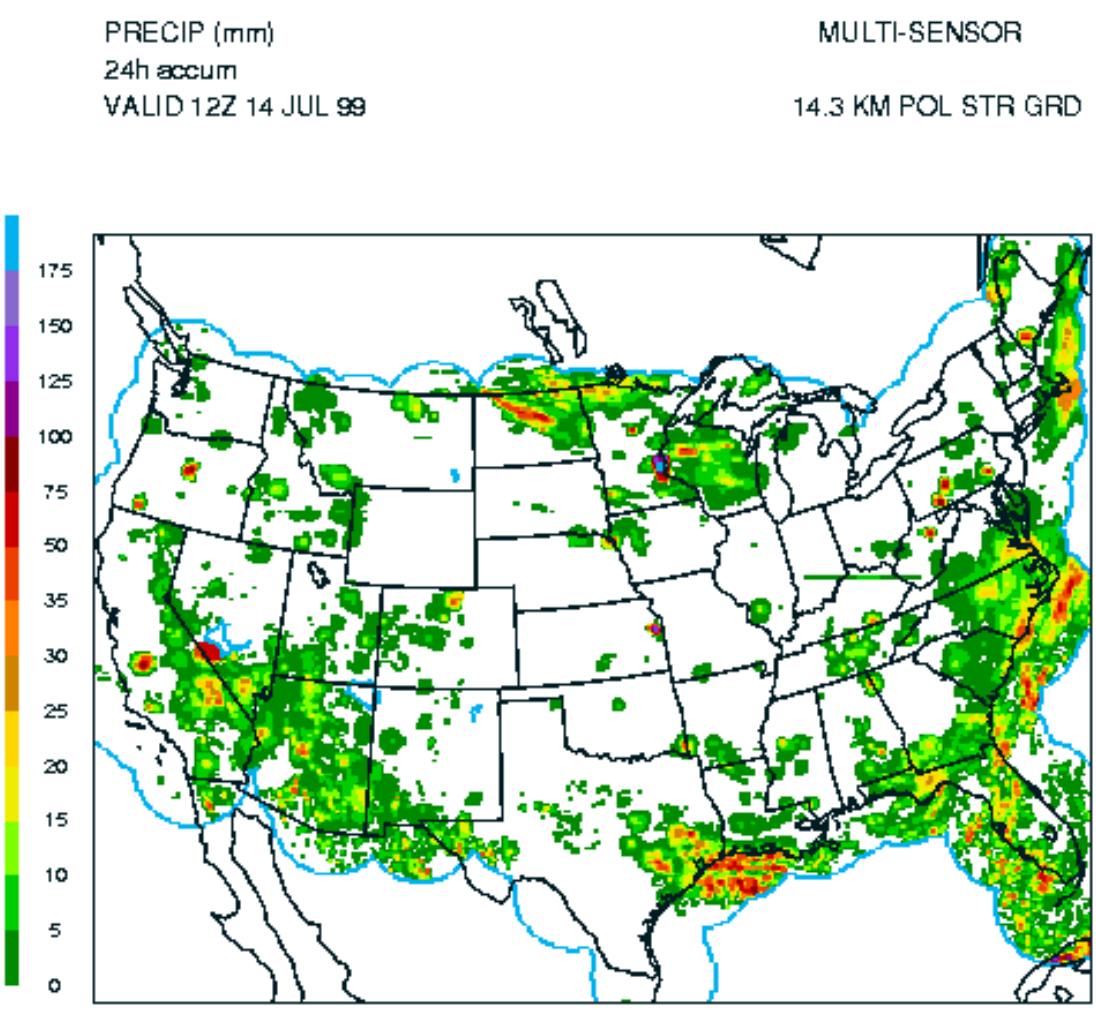
PRECIP (mm)
24h accum
VALID 12Z 14 JUL 99
MULTI-SENSOR
14.3 KM POL STR GRD
175
150
125
100
75
50
35
30
25
20
15
10
5
0

Figure 28d

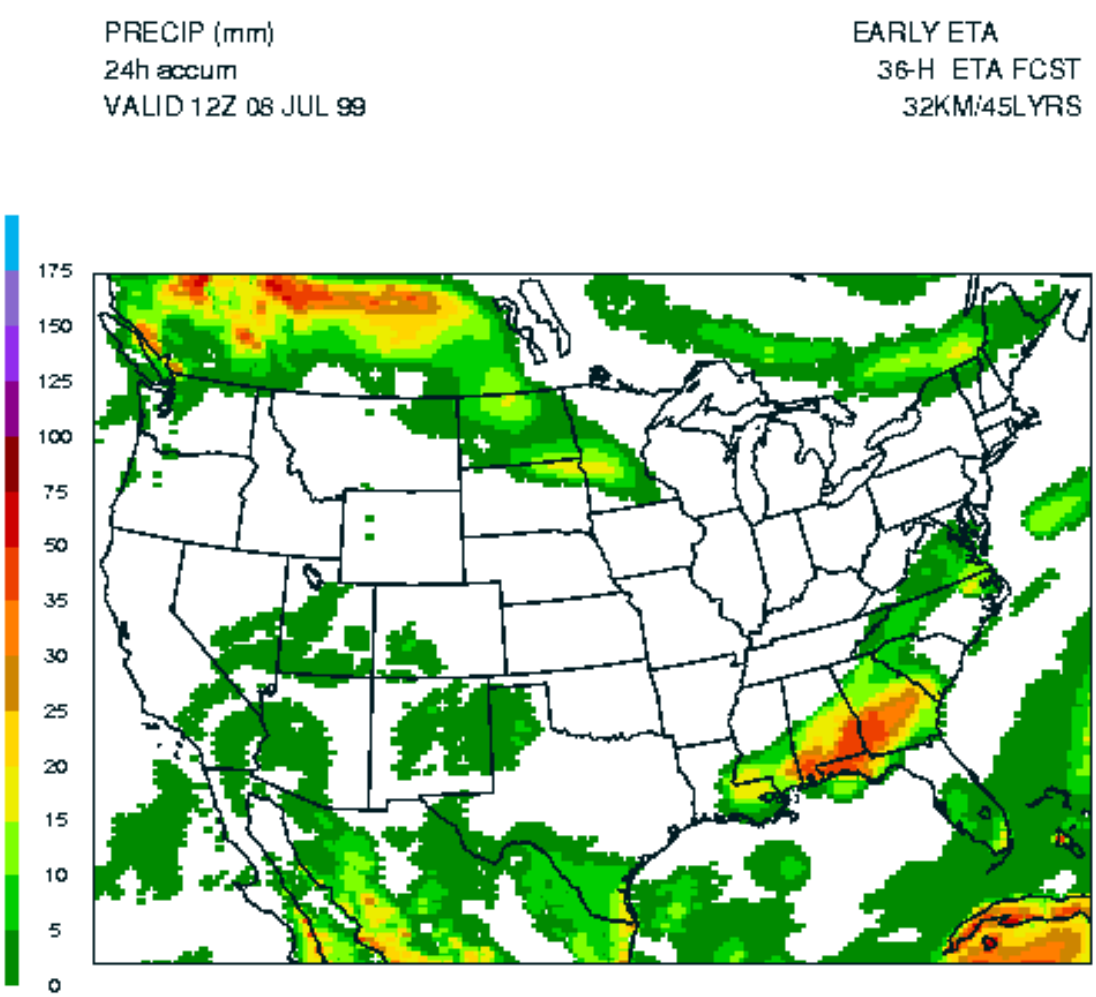
PRECIP (mm)
24h accum
VALID 12Z 08 JUL 99
EARLY ETA
36-H ETA FCST
32KM/45LYRS
175
150
125
100
75
50
35
30
25
20
15
10
5
0

Figure 29a

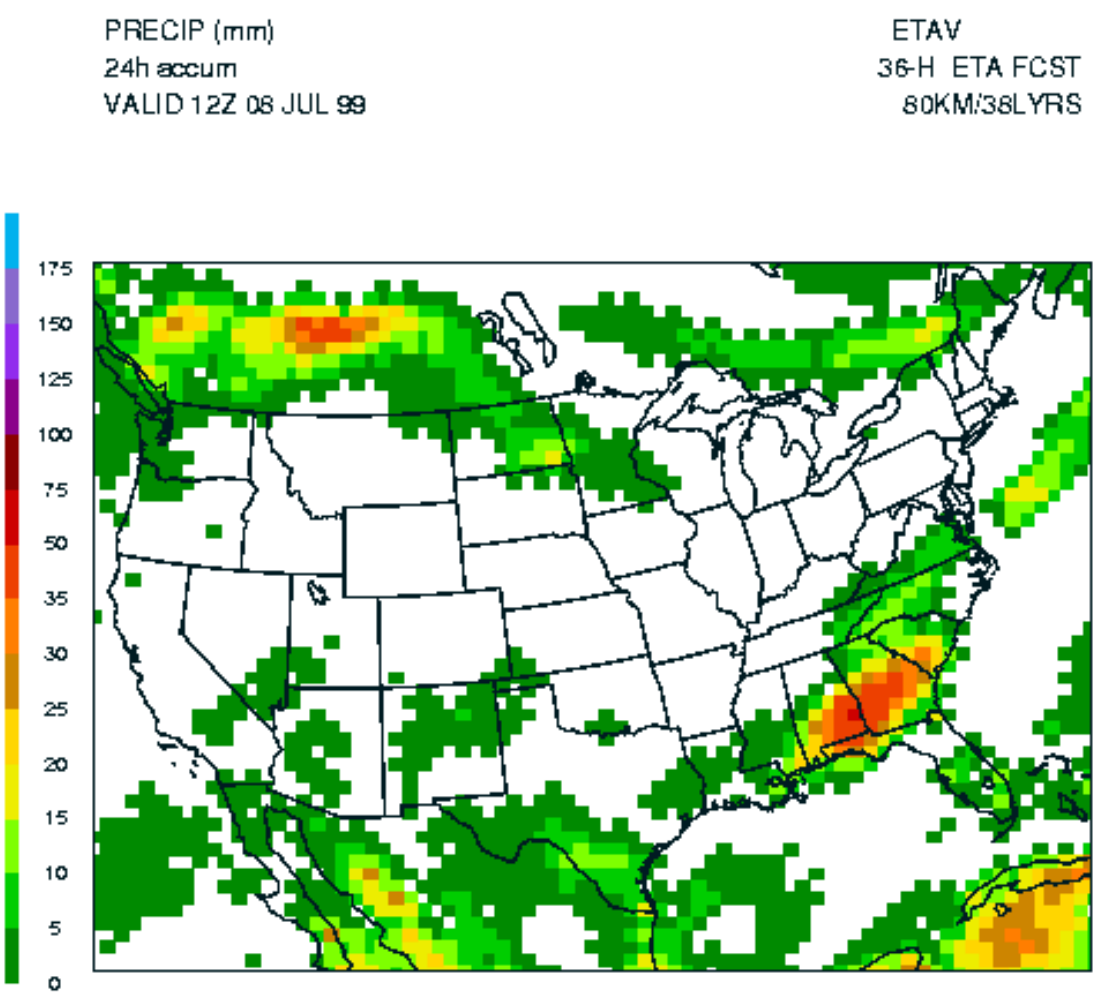
PRECIP (mm)
24h accum
VALID 12Z 08 JUL 99
ETAV
36-H ETA FCST
80KM/38LYRS
175
150
125
100
75
50
35
30
25
20
15
10
5
0

Figure 29b

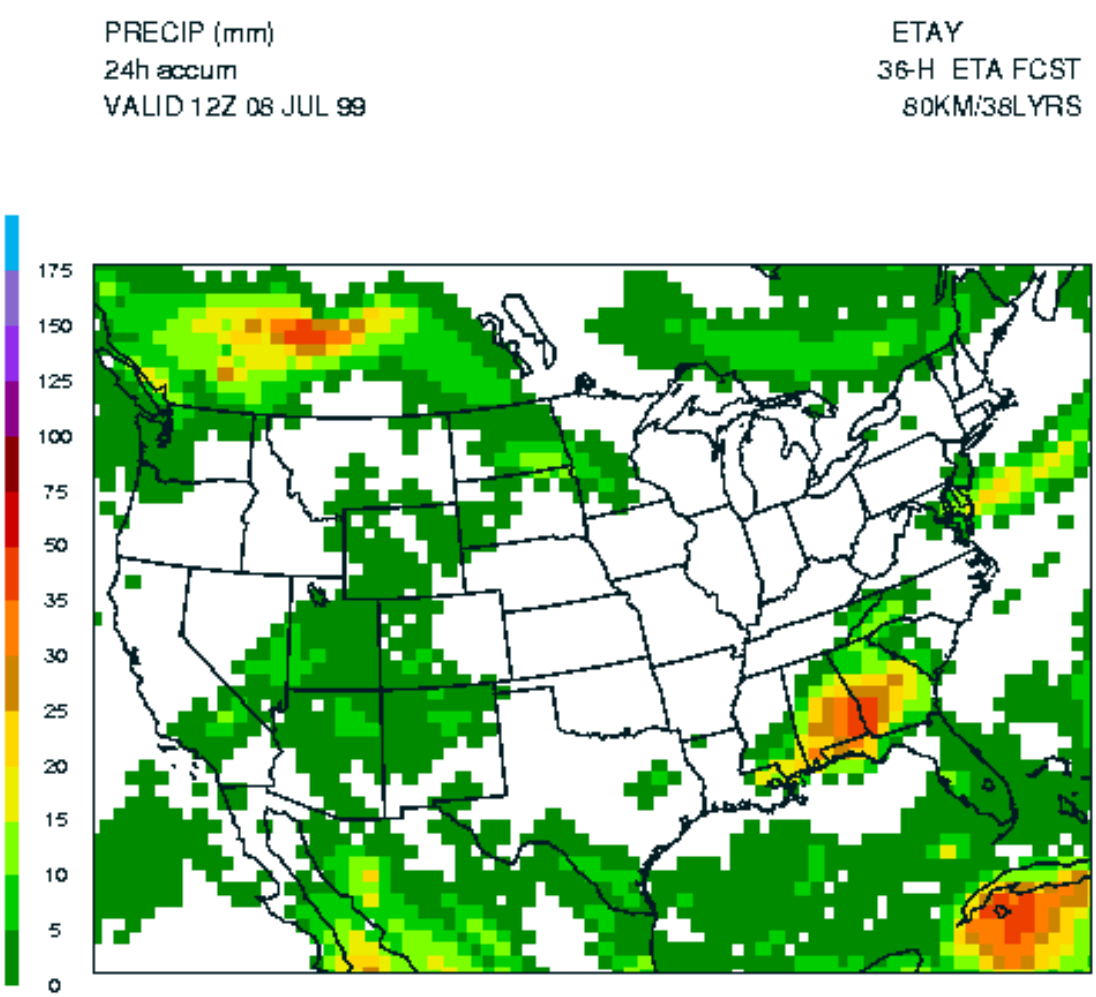
PRECIP (mm)
24h accum
VALID 12Z 08 JUL 99
ETAY
36-H ETA FCST
80KM/38LYRS
175
150
125
100
75
50
35
30
25
20
15
10
5
0

Figure 29c

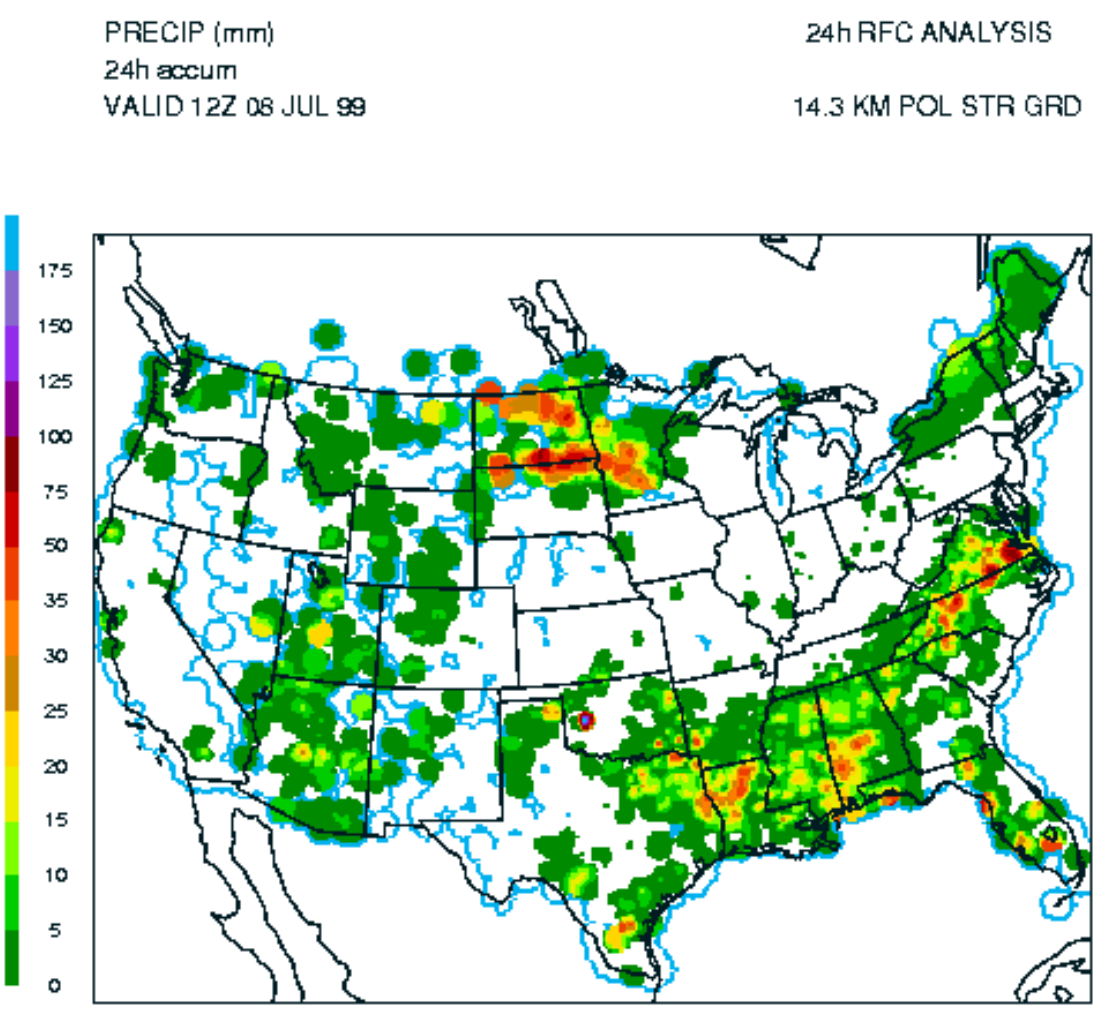
PRECIP (mm)
24h accum
VALID 12Z 08 JUL 99
24h RFC ANALYSIS
14.3 KM POL STR GRD
175
150
125
100
75
50
35
30
25
20
15
10
5
0

Figure 29d

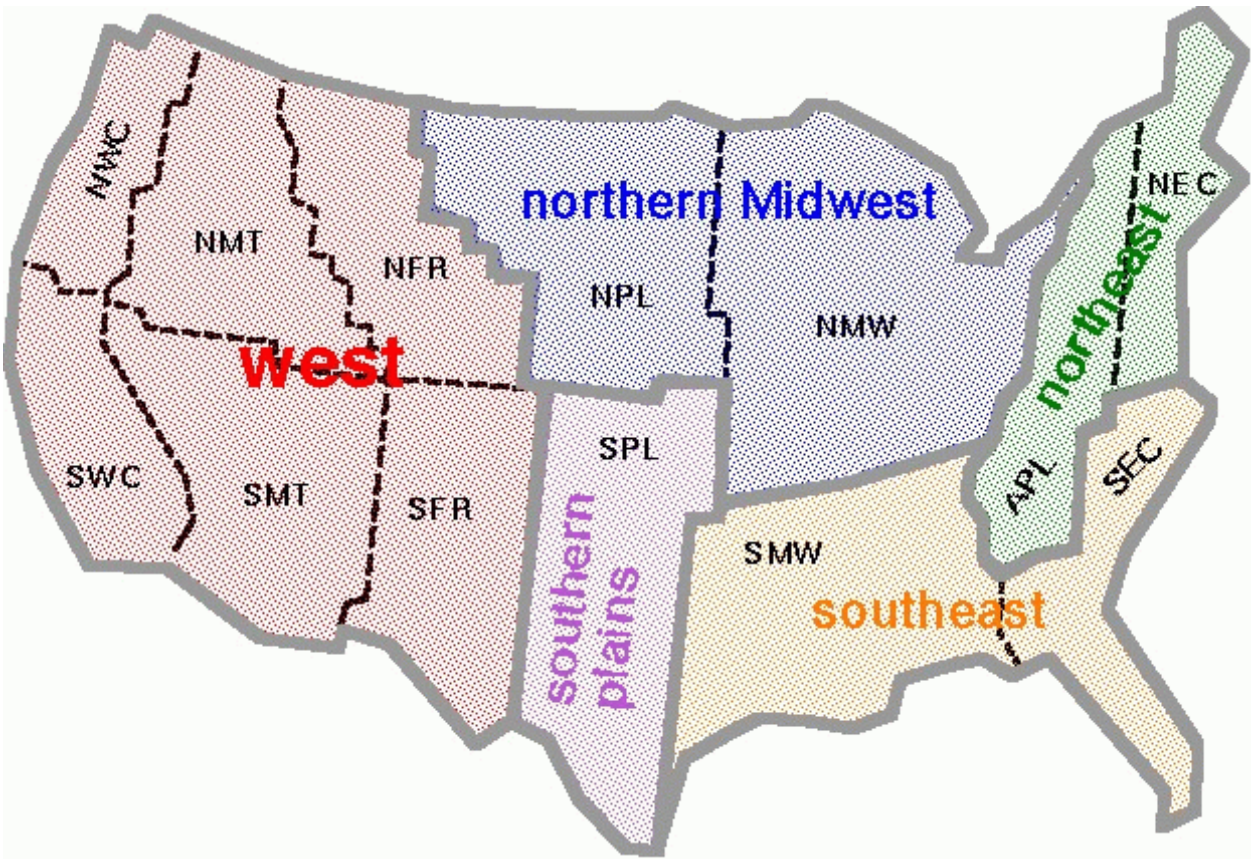
NWC
NMT
NFR
West
SWC
SMT
SFR
northern Midwest
NPL
NMW
SPL
southern plains
SMW
southeast
northeast
NEC
APL
SEC

Figure 30

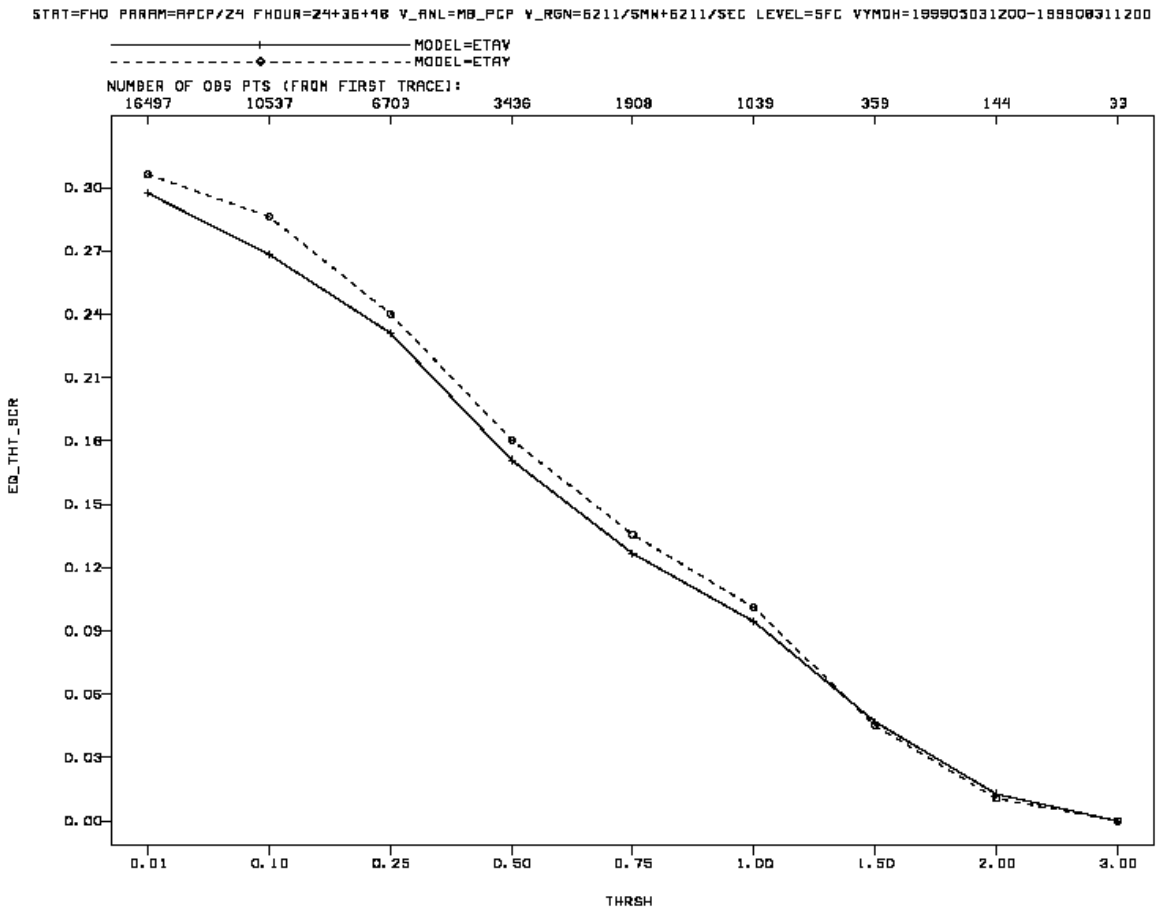
STAT=FHO PARAM=APCP/24 FHOUR=24+36+48 V_ANL=MB_PCP V_RGN=6211/SMN+6211/SEC LEVEL=SFC VYMDH=1999050312Z00-1999083112Z00
MODEL=ETAV
MODEL=ETAY
NUMBER OF OBS PTS (FROM FIRST TRACE):
16497
10537
6703
3436
1908
1039
359
144
33
EQ_THT_SCR
0.30
0.27
0.24
0.21
0.18
0.15
0.12
0.09
0.06
0.03
0.00
0.01
0.10
0.25
0.50
0.75
1.00
1.50
2.00
3.00
THRSH

Figure 31

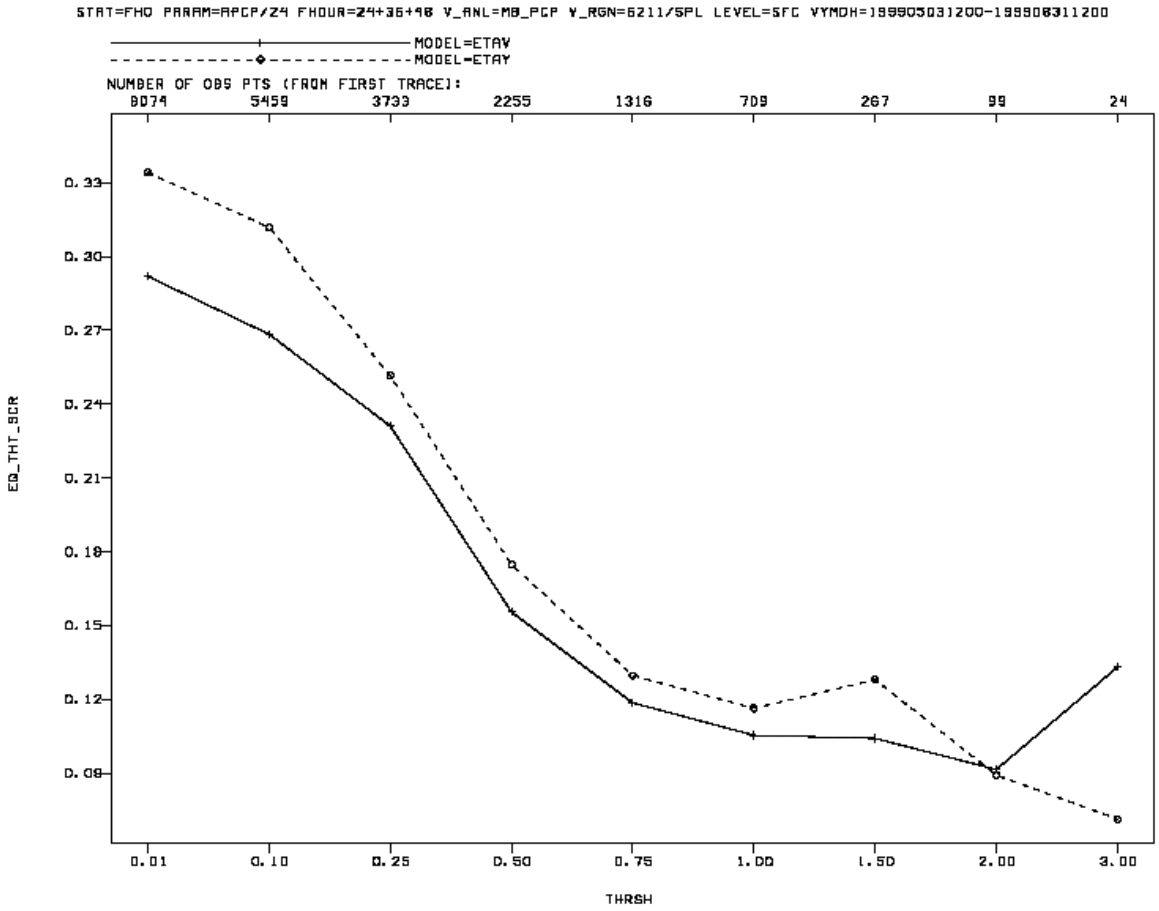
STAT=FHO PARAM=APCP/24 FHOUR=24+36+48 V_ANL=MB_PCP V_RGN=G211/SPL LEVEL=SFC YYMDH=1999050312DD-1999063112DD
MODEL=ETAV
MODEL=ETAY
NUMBER OF OBS PTS (FROM FIRST TRACE):
8074
5459
3733
2255
1316
709
267
99
24
0.33
0.30
0.27
0.24
0.21
0.18
0.15
0.12
0.09
EQ_THT_SCR
0.01
0.10
0.25
0.50
0.75
1.00
1.50
2.00
3.00
THRSH

Figure 32

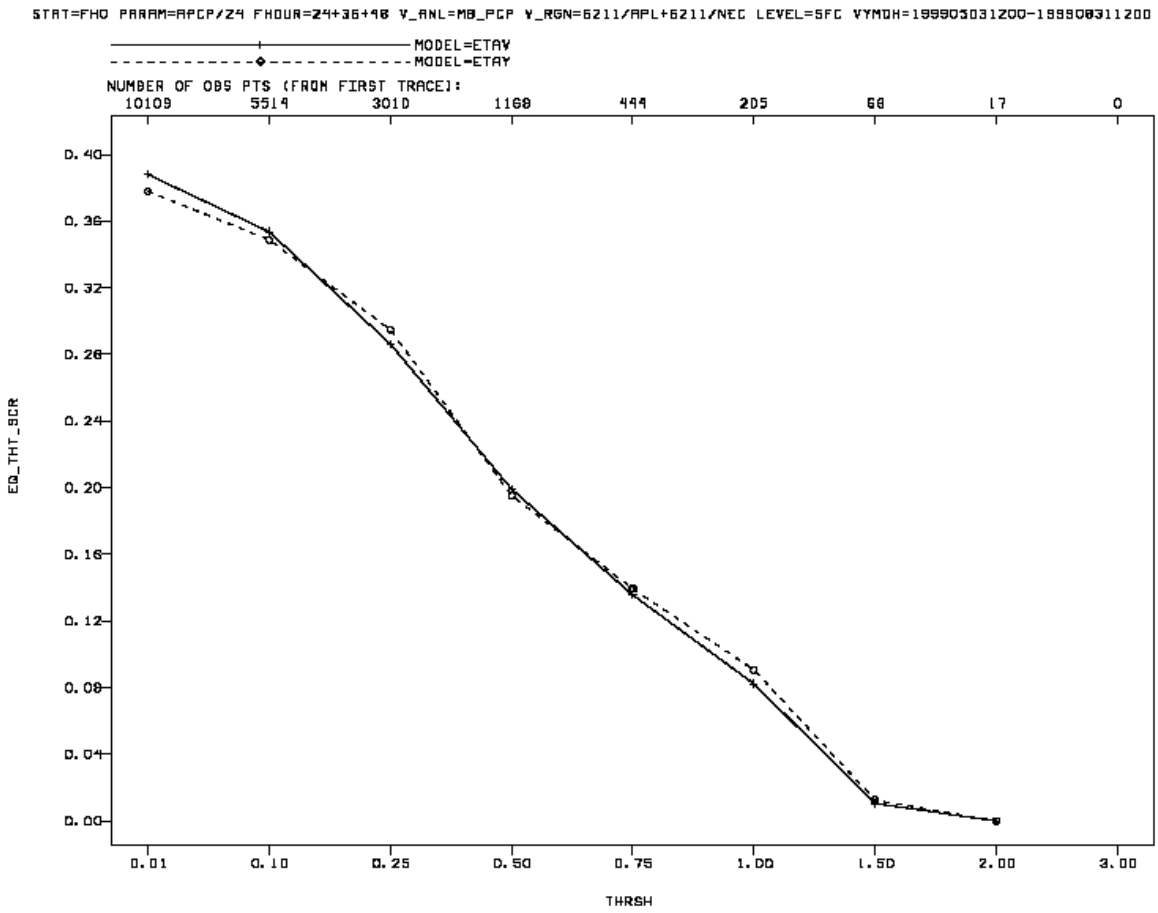
STAT=FHO PARAM=APCP/24 FHOUR=24+36+48 V_ANL=MB_PCP V_RGN=6211/APL+6211/NEC LEVEL=SFC YYMDH=1999050312Z00-1999083112Z00
MODEL=ETAV
MODEL=ETAY
NUMBER OF OBS PTS (FROM FIRST TRACE):
10109
5514
3010
1168
444
205
68
17
0
0.40
0.36
0.32
0.28
0.24
0.20
0.16
0.12
0.08
0.04
0.00
EQ_THT_SCR
0.01
0.10
0.25
0.50
0.75
1.00
1.50
2.00
3.00
THRSH

Figure 33

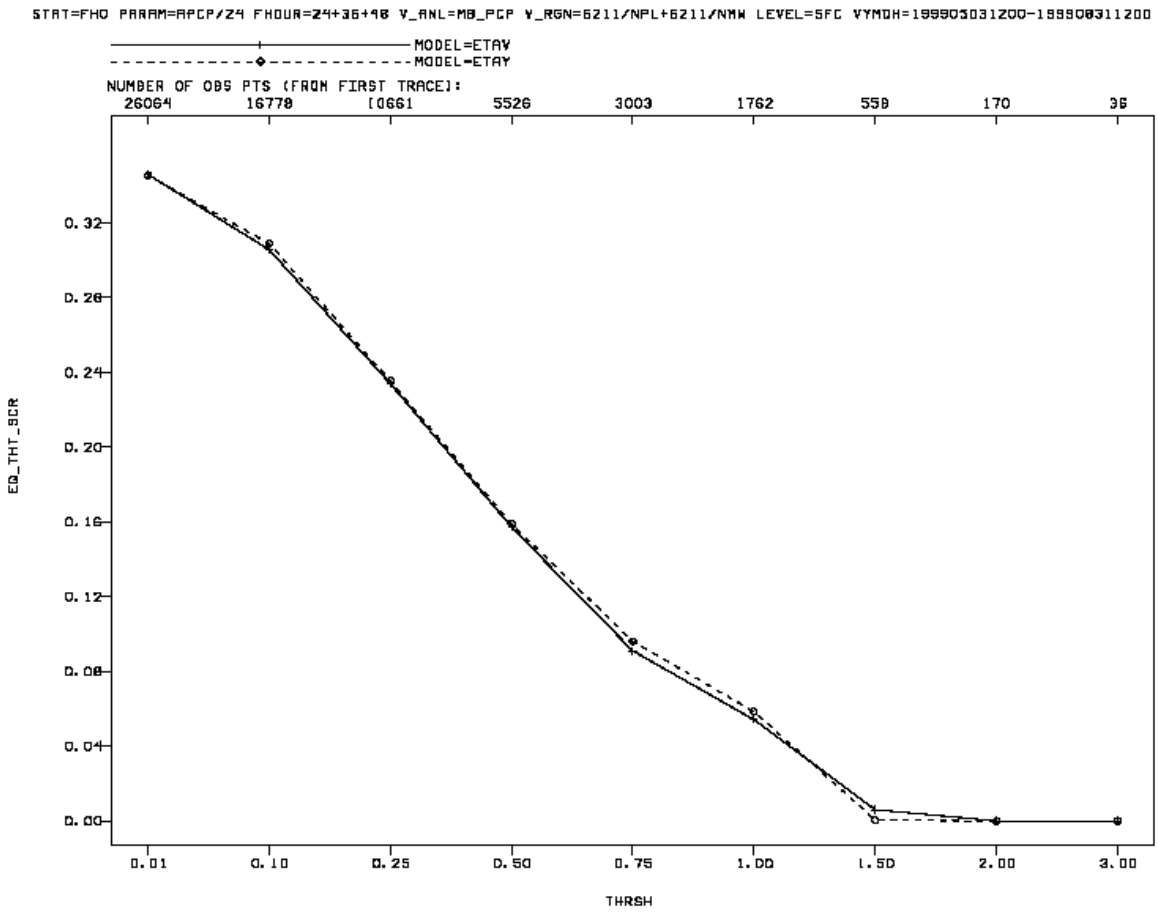
STAT=FHO PARAM=APCP/24 FHOUR=24+36+48 V_ANL=MB_PCP V_RGN=G211/NPL+G211/NMW LEVEL=SFC YYMDH=1999050312Z00-1999083112Z00
MODEL=ETAV
MODEL=ETAY
NUMBER OF OBS PTS (FROM FIRST TRACE):
26064
16778
10661
5526
3003
1762
558
170
35
EQ_THT_SCR
0.32
0.28
0.24
0.20
0.16
0.12
0.08
0.04
0.00
0.01
0.10
0.25
0.50
0.75
1.00
1.50
2.00
3.00
THRSH

Figure 34

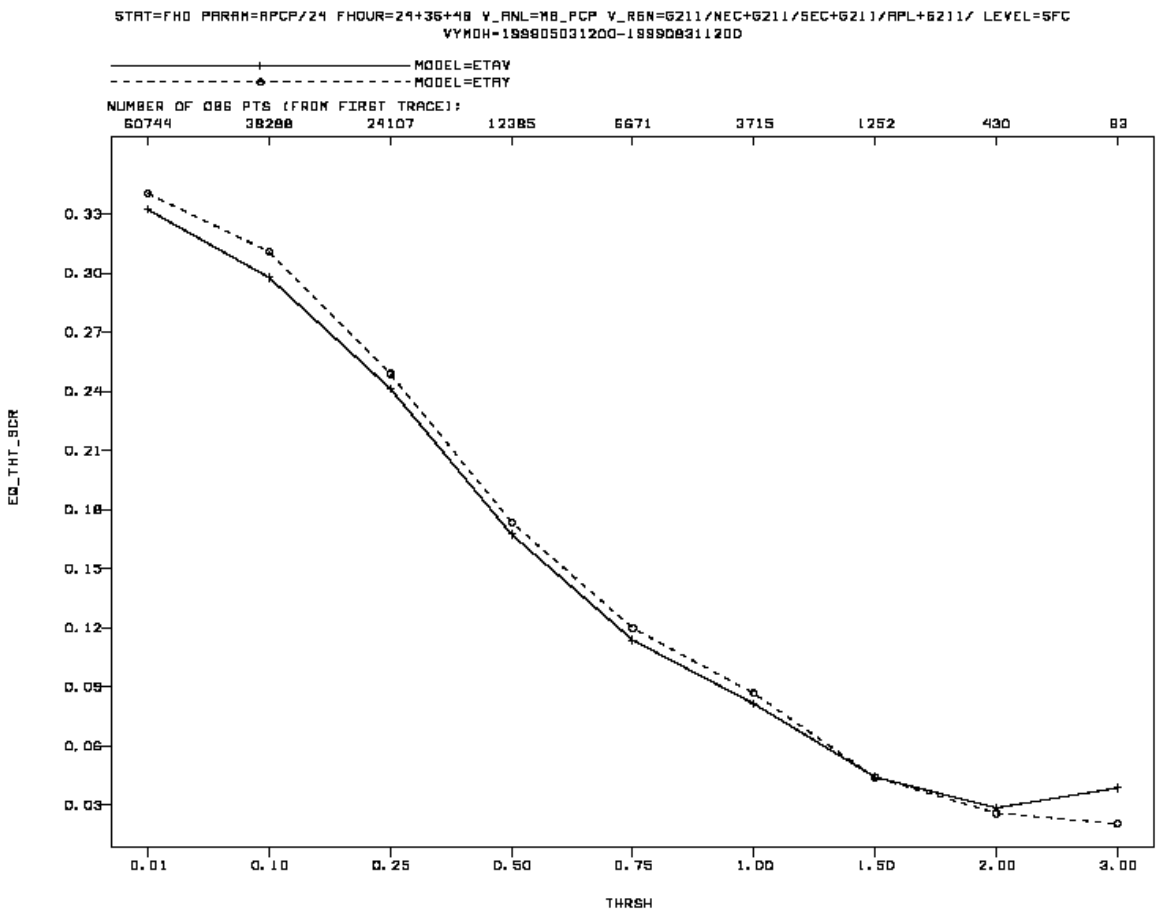
STAT=FHO PARAM=APCP/24 FHOUR=24+36+48 V_ANL=MB_PCP V_RGN=G211/NEC+G211/SEC+G211/APL+G211/ LEVEL=SFC
VYMDH=1998050312DD-1998083112DD
MODEL=ETAV
MODEL=ETAY
NUMBER OF OBS PTS (FROM FIRST TRACE):
60744
38288
24107
12385
6671
3715
1252
430
83
0.33
0.30
0.27
0.24
0.21
0.18
0.15
0.12
0.09
0.06
0.03
EQ_THT_SCR
0.01
0.10
0.25
0.50
0.75
1.00
1.50
2.00
3.00
THRSH

Figure 35

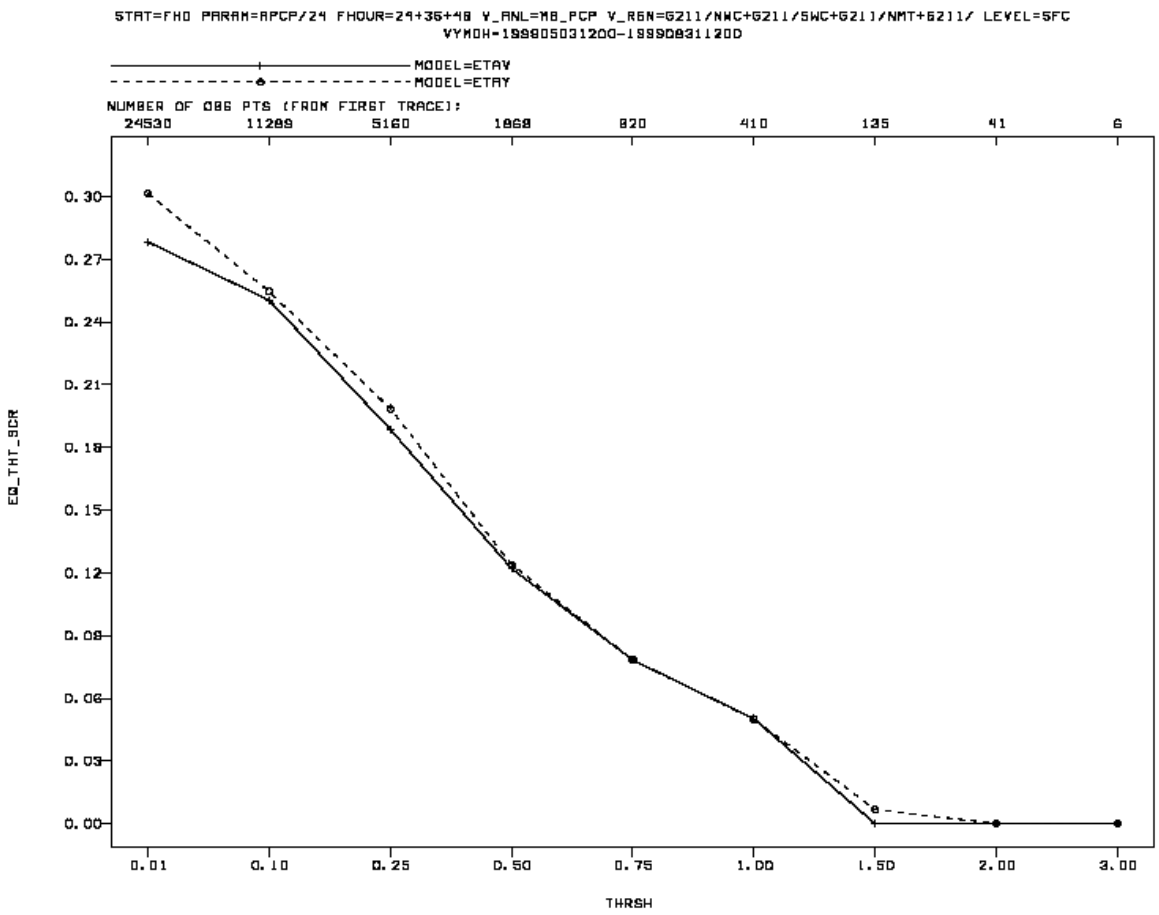
STAT=FHO PARAM=APCP/24 FHOUR=24+36+48 V_ANL=MB_PCP V_REGN=G211/NWC+G211/SWC+G211/NMT+G211/ LEVEL=SFC
VYMDH=1998050312DD-1998083112DD
MODEL=ETAV
MODEL=ETAY
NUMBER OF OBS PTS (FROM FIRST TRACE):
24530
11289
5160
1868
820
410
135
41
6
0.30
0.27
0.24
0.21
0.18
0.15
0.12
0.09
0.06
0.03
0.00
EQ_THT_SCR
0.01
0.10
0.25
0.50
0.75
1.00
1.50
2.00
3.00
THRSH

Figure 36